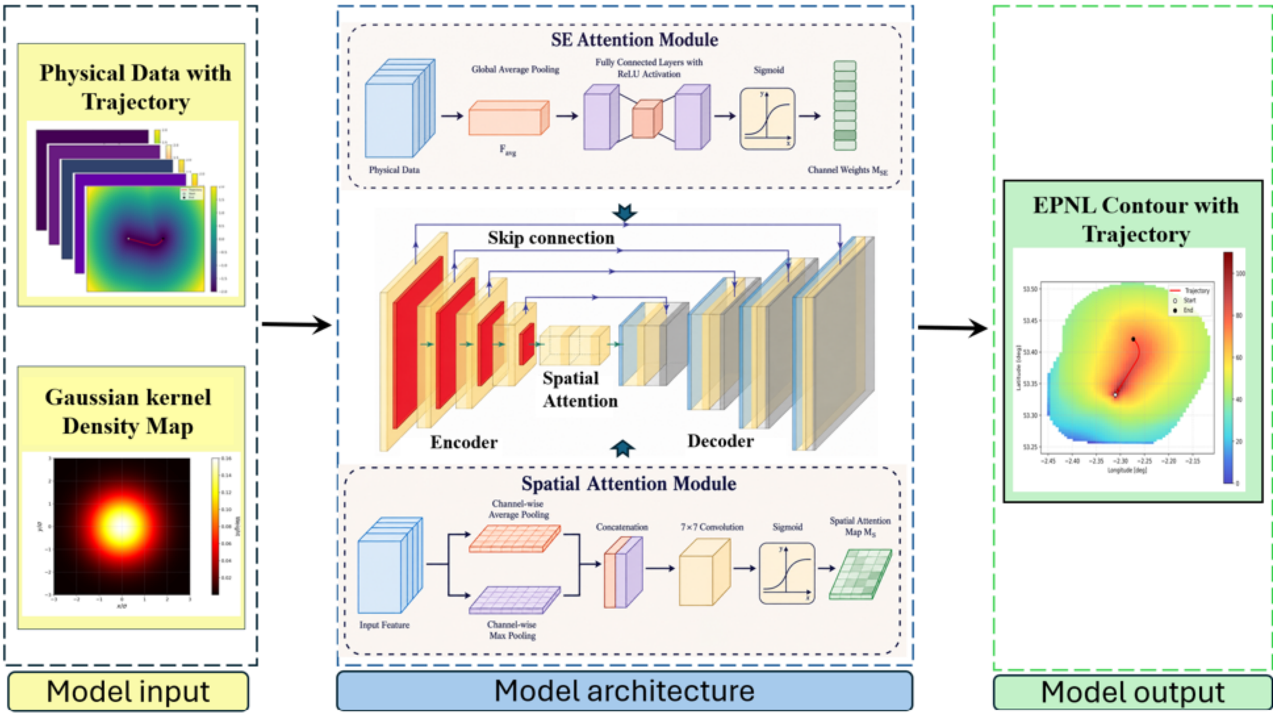

Data-Driven Aircraft Noise Modeling for Multidisciplinary Design and Trajectory Assessment

CHENZHAO LI

Department of Mechanical Engineering
CHALMERS UNIVERSITY OF TECHNOLOGY
Gothenburg, Sweden 2026

Thesis for the degree of Licentiate of Engineering

Data-Driven Aircraft Noise Modeling for Multidisciplinary Design and Trajectory Assessment

Chenzhao Li

Department of Mechanical Engineering
CHALMERS UNIVERSITY OF TECHNOLOGY
Göteborg, Sweden 2026

Data-Driven Aircraft Noise Modeling for Multidisciplinary Design and Trajectory Assessment
Chenzhao Li

Licentiatavhandlingar vid Chalmers tekniska högskola
Technical report No. 2026:08

Department of Mechanical Engineering
Chalmers University of Technology
SE–412 96 Göteborg, Sweden
Telephone + 46 (0) 31 – 772 1000

Chalmers Reproservice
Göteborg, Sweden 2026

Embrace the tide of change.

Abstract

Data-Driven Aircraft Noise Modeling for Multidisciplinary Design and Trajectory Assessment
Chenzhao Li
Mechanical engineering
Division of Fluid Dynamics
Chalmers University of Technology

Aircraft noise assessment is an important part of aircraft design and airport-operation planning. Conventional semi-empirical prediction tools can describe individual sources, propagation effects, and certification metrics with useful engineering fidelity, but their computational cost becomes restrictive when thousands of evaluations are required in multidisciplinary design optimization or large-scale studies of aircraft trajectories and operational procedures. This thesis investigates machine learning models for aircraft noise that reduce this cost while retaining high accuracy.

The study first focuses on the noise prediction model in the engine conceptual design phase. A database produced with the Chalmers Noise Code (CHOICE) is used to map different turbofan design-point and operating variables to the Effective Perceived Noise Level(EPNL) of engine components and the total engine. A deep neural network is compared with a local K-nearest-neighbor model and with a stacking architecture in which support-vector regression combines the two base learners. All evaluated models achieve root mean square errors(RMSE) below 0.3 dB for every source and total noise on the test set. The stacking model is particularly useful when compressor or turbine stage-count changes introduce local discontinuities that are difficult for a globally smooth neural approximation to reproduce. The second part of this study extends from the noise of the engine conceptual design to two-dimensional noise maps of a specific aircraft model under different flight conditions and trajectories. A Density-Guided Physics-Informed Attention U-Net (DGPIA U-Net) is trained on CHOICE-generated take-off cases for an A320 class aircraft. Sparse trajectory variables are converted to continuous influence fields through adaptive Gaussian diffusion, and channel and spatial attention are used to emphasize informative physical variables and locations. Once trained, the model produces noise fields on the millisecond scale, two to three orders of magnitude faster than the convention aircraft noise prediction method. Together, the studies establish a cross-scale strategy for data driven aircraft noise modeling: low dimensional surrogates accelerate design space exploration at engine component level, while physics-informed convolutional models reconstruct spatial exposure patterns for trajectory assessment.

Keywords: aircraft noise prediction, machine learning, physics-informed learning, attention U-Net.

Acknowledgments

This research was performed at the Division of Fluid Dynamics, Department of Mechanics Engineering at Chalmers University of Technology from January 2024 to September 2026. I would like to thank all the collaborators of Hydrogen Optimized multi-fuel Propulsion system for clean and silEnt aircraft (HOPE) project; Chalmers University of Technology, Bauhaus Luftfahrt, TU Delft, and the Manchester Metropolitan University, without whom this work would be impossible.

First and foremost, I would like to express my deepest gratitude to my supervisor, Xin Zhao, for his patient, detailed, and invaluable guidance throughout this research. He has provided me with tremendous support in every aspect of my work, ranging from theoretical discussions and scientific exploration to learning and implementing software tools and computer code. Beyond academic matters, Xin has also shown me great personal care and support. When I first moved abroad and arrived in Sweden, I experienced considerable cultural adjustment, and his kindness and understanding helped me greatly during this period.

Many thanks to Professor Tomas Grönstedt and all members of the turbomachinery research group for providing an excellent communication environment and academic atmosphere through weekly group meetings. I am also very grateful for the daily care and support from the group members. My sincere thanks also go to my examiner Niklas Andersson, as well as Malin Larsson and Srdjan Sasic for their supervision of my PhD progress at each follow-up meeting, and for their concern for my mental well-being.

I would also like to thank my officemate, Andhika Pratama, whose friendly and considerate nature helped create a calm, comfortable, and productive working environment. I am deeply grateful to Shuai Li and Henry Hudoyo for their kindness, support, and companionship in both my work and daily life. The wonderful times we shared playing badminton and table tennis greatly enriched my life beyond work.

Finally, I would like to express my deepest gratitude to my parents, whose unwavering and unconditional support has been a constant source of strength throughout my journey and has made it possible for me to reach this point.

Chenzhao Li
Göteborg, October 2026

List of Publications

This thesis is based on the following appended papers:

Paper I. Chenzhao Li, Evangelia Maria Thoma, and Xin Zhao

Adapting Turbofan Noise Modelling Tool Using Neural Networks

Paper II.(submitted manuscript) Chenzhao Li, Shuai Li, and Xin Zhao

Aircraft Trajectory Noise Modeling with Physics-Informed Multi-Channel Attention U-Net

Other Publications

The following publication is not included in this thesis:

Publication I. Xin Zhao, Albert Skegro, Kevin Jonathan Nesan Gnanaraj, Chenzhao Li, and Changfu Zou

Electric-powered air traffic network with integrated aircraft-battery modelling

The 12th Swedish Aerospace Technology Congress (FT2025), Stockholm

Contents

Part I

Introductory Chapters

Chapter 1

Introduction

1.1 Background

Global air transportation has experienced substantial long-term expansion, reflecting the increasing demand for mobility, tourism, international trade, and global economic integration. According to statistics reported by the International Civil Aviation Organization (ICAO), global scheduled passenger traffic, measured in revenue passenger-kilometres (RPK), increased from approximately 6.60 trillion RPK in 2015 to 8.69 trillion RPK in 2019, as shown in Fig. 1.1. This represents a cumulative increase of approximately 31.6% within four years, corresponding to an average annual growth rate of about 7%. The continuous increase observed during this period demonstrates that aviation had become one of the most rapidly developing components of the global transport system before the COVID-19 pandemic. Although the COVID-19 pandemic caused an exceptional and temporary disruption to aviation activity, global passenger demand subsequently recovered and exceeded its pre-pandemic level. In 2024, global passenger traffic measured in revenue passenger kilometres increased by approximately 10.4% compared with 2023 and was approximately 3.8% higher than the corresponding level in 2019. The growth of the aviation sector is expected to continue over the coming decades.

However, the development of economic and social benefits of aviation are accompanied by substantial environmental externalities. Aircraft noise is among the most direct and widely perceived environmental impacts that affect the health of populations living near airports and beneath frequently used flight paths [1–3].A substantial body of research has shown that aircraft noise has types of effects on both psychological and physiological human health [1]. Long-term exposure to high levels of aircraft noise may lead to sleep disturbance, high risk hypertension, reduced attention, and impaired learning efficiency [2–4]. These effects are often more obvious in vulnerable populations, including children, older adults, individuals susceptible to cardiovascular disease and pregnant women leading to low birth weight [5–7]. Aircraft noise management is therefore critical for lowering noise exposure in communities near the airport.

Aircraft noise reduction has been driven primarily by increasingly stringent regulations established by the ICAO and other regulatory bodies in response to growing concerns among communities exposed to aviation noise. In developing these regulatory frameworks, ICAO considered a broad range of technical, operational, environmental, and economic factors beyond noise emissions alone. These efforts led to the adoption of the aircraft environmental protection standards contained in Annex 16 to the Convention on International Civil Aviation, whose initial noise-related provisions entered into force in 1971. The ICAO regulations underwent a series of major updates and enforcements called Chapters. The transition from Chapter 3 to Chapter 4 and subsequently to Chapter 14 represents a progressive tightening of aircraft-noise certification standards. The current regulations, at the date of this contribution, are represented by Chapter 14, as shown in Fig. 1.2. The purpose of these regulations is to encourage aircraft manufacturers and operators to reduce noise as far as technically and economically practicable. To include noise pollution related public health concerns in the development of sustainable airport operations, the assessment and prediction of aircraft noise from departures and arrivals is essential.

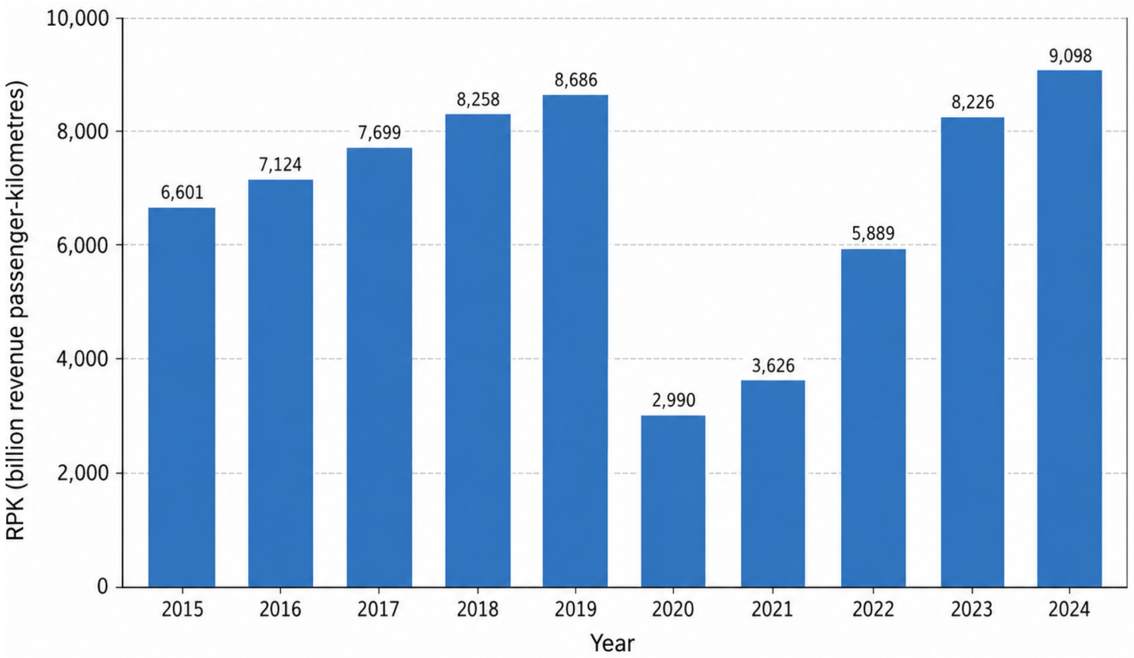

Figure 1.1: Changes in billion revenue passenger-kilometres from 2015 to 2024[8].

1.2 Conventional Methods for Aircraft Noise Prediction

Noise prediction method based on flight trajectories and aircraft performance makes it possible to estimate, prior to flight execution, the local airport noise impacts associated with different operations. Such predictive capability is valuable for trajectory optimization, for example by avoiding flying over densely populated areas [10], designing continuous descent operations to reduce thrust requirement and noise [11], and customizing optimized noise abatement departure procedures [12].

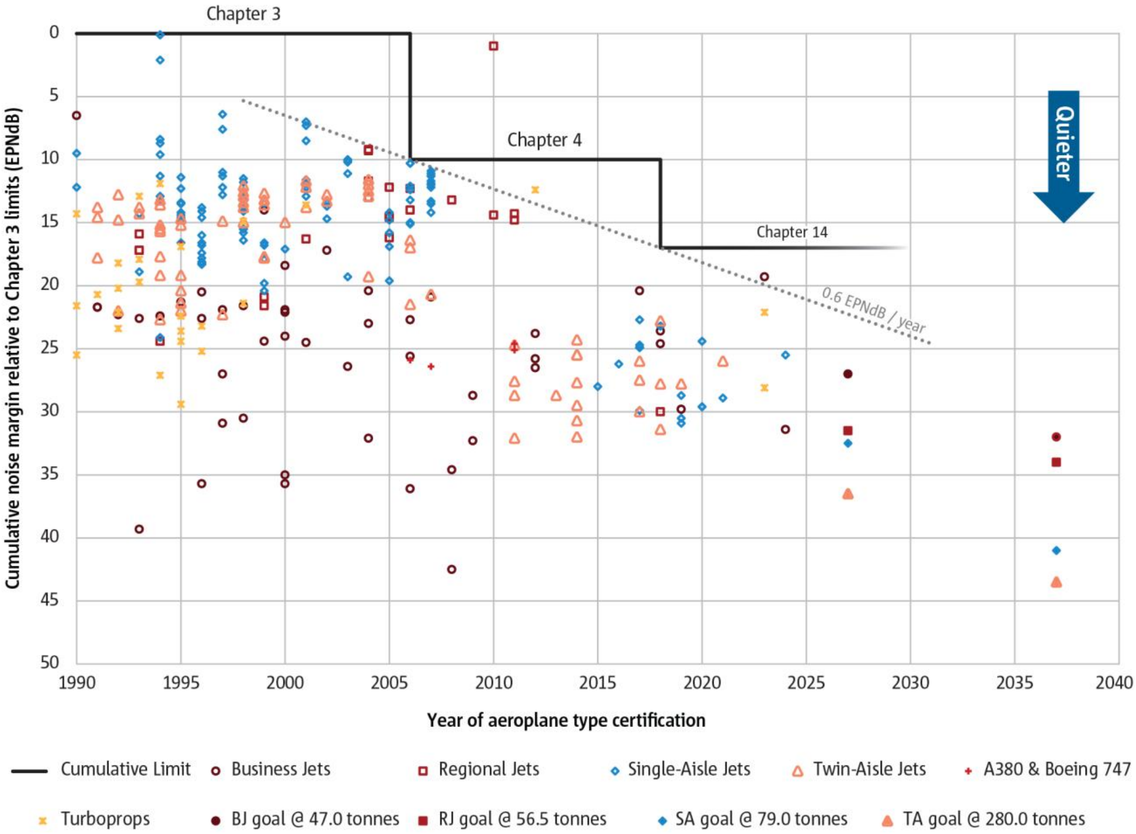

Figure 1.2: Evolution in certified aircraft noise levels over time[9].

This provides a foundation for multi-objective flight optimization that simultaneously accounts for operational efficiency and environmental impacts. Research on aircraft noise prediction methods can generally be classified into two major categories: (1) best practice methods and (2) theoretical methods [13].

The best practice approach can be traced back to 1978, when the Federal Aviation Administration (FAA) introduced the Integrated Noise Model (INM) [14], a program that has since been widely used by airports and regulatory authorities around the world. This computational tool provides a relatively simple framework for estimating aircraft noise in the vicinity of airports and assessing its impact on surrounding communities with only a small set of input parameters. Specifically, the method relies on extensive empirical formulations, such as flyover measurement data and other experimental observations, to calculate the noise level at a given receiver location based on noise–power–distance (NPD) data, engine thrust and atmospheric conditions. Similar approaches have also been adopted in several other countries, including the ANCON model in the United Kingdom [15], FLULA in Switzerland [16], and the SIMUL and AzB codes in Germany [17, 18]. These models are based on NPD databases combined with different sound-propagation attenuation models or statistical approaches to perform noise prediction. The IMPACT developed by EURONCONTROL used aircraft noise and performance (ANP) database for noise modelling purposes. ANP was collected by EUROCONTROL and the U.S. Federal Aviation Administration (FAA) and then verified by the FAA/U. S. The NPD/ANP databases themselves benefit from large volumes of historical data, including radar trajectory records and real-time ground microphone measurements of noise exposure levels. Consequently, best practice methods are inherently constrained by the substantial financial and logistical resources required to establish and maintain a comprehensive database infrastructure. Theoretical methods build physical modeling of noise generation and propagation. The development of theoretical aircraft noise prediction can be traced back to the early 1970s, when FAA and NASA started to predict the noise generated by single flyover events. One of the earliest computational tools developed for this purpose was Aircraft Noise Prediction Program (ANOPP), established at NASA Langley [19, 20]. In this framework, aircraft flight dynamics were coupled with semi-empirical models describing the generation and propagation of noise from various sources, including the fan, compressor, jet exhaust, wings, and landing gear. The propagation module accounted for physical effects on the received noise, such as spherical spreading, atmospheric attenuation, and ground reflection. Subsequently, the second-generation framework, ANOPP2, introduced substantial advancements, partially incorporating computationally intensive high-fidelity methods [21, 22]. Most source and propagation models have since been investigated and developed independently. Correspondingly, each model typically requires a large number of input parameters and huge computational source to ensure adequate computational accuracy. This approach, which predicts aircraft noise by combining individual discrete noise sources with empirical or semi-empirical formulations, has subsequently achieved substantial progress. Filippone, Marily etc. developed integrated aircraft noise-prediction frameworks FLIGHT and CHOICE that require moderate computational demand while maintaining relatively high predictive accuracy, based on publicly available semi-empirical methods [23–25]. Nevertheless, the prediction of trajectory-dependent aircraft noise still requires considerable computational resources, including the time for computing detailed aircraft and engine performance data input. In addition, the German Aerospace Center (DLR) developed the PANAM code as a tool for aircraft noise design and assessment, with a particular emphasis on comparative noise evaluation across different aircraft configurations [26]. To provide rapid solutions and efficient analysis capability, PANAM accounts only for the dominant noise contributions in the overall aircraft noise prediction. Engine noise is represented solely by jet and fan noise components. As a result, the computational efficiency is improved, but at the expense of prediction accuracy.

1.3 Machine Learning-Based Methods for Aircraft Noise Prediction

In recent years, with the rapid advancement of artificial intelligence, many people have focused on the application of machine learning to aircraft noise prediction. This technique applies such as artificial neural networks, random forests, and convolutional neural networks (CNN), machine-learning-based methods to extract informative physical features, achieving fast and accurate prediction. As the first to apply machine learning to aeroacoustic prediction, Tenney et al. quantified the effects of feature space, learning rate, and network architecture on model performance, demonstrated the high prediction accuracy of a deep neural network (DNN) predicting jet noise for far-field overall sound pressure level [27]. Subsequently, an increasing number of researchers have attempted to integrate physical information with machine-learning models, establishing new methodologies for aircraft noise study. Based on experimental measurements, Zhang et al. developed a noise spectral deep learning (NSDL) approach to predict landing gear aerodynamic noise [28]. In this framework, an encoder was used to extract the dominant characteristics of the noise spectrum, while a multi-layer perception (MLP) was employed to establish the mapping between these features and flow parameters such as velocity and angle of attack. In a series of subsequent studies, Zhang and co-workers used high-fidelity computational fluid dynamics (CFD) results as the database for machine learning, and achieved accurate prediction of airfoil aerodynamic noise by means of random forest and compressed sensing algorithms [29, 30]. These studies focus on applying machine learning techniques in the prediction of component level noise sources from high fidelity simulations and experiments, to reduce the demand of large number of simulations and tests. At overall aircraft level, Wu and Redonnet extracted a wide range of aircraft airframe structural and flight performance parameters as inputs and developed a simplified whole-aircraft noise prediction model using a multivariate linear regression-based machine learning approach. The model demonstrated high predictive accuracy; however, its outputs were limited to two specific noise monitoring locations [31]. Suat Toraman and co-workers employed random forest and long short-term memory (LSTM) approaches to develop aircraft noise prediction models at the approach, sideline, and cutback certification points [32]. Using publicly available noise databases for Airbus and Boeing aircraft, they extracted practical operational parameters, such as aircraft weight and engine thrust, as model inputs. Although the model demonstrated relatively high predictive accuracy, its outputs were limited to noise estimates at only three certification points, and lack of noise impact over the area covered by the flight trajectory which is more crucial for realistic flight operation.

1.4 Thesis outline and scope

In summary, the integration of machine learning with physical information has achieved promising progress in the prediction of individual aircraft noise sources, such as jet noise, airfoil noise, and landing gear noise. However, noise prediction methods for conceptual aircraft engine design and whole-aircraft trajectory analysis are still lacking. Significant limitations exist in traditional best practice methods and theoretical methods that highly detailed aircraft and propulsion data input are required as well as relatively high computational cost. Even minutes of computation for noise, in multidisciplinary integrated design of future aircraft and air traffic system combining hundreds of aircraft and near-airport operational procedures, is a bottle neck for real-time and large-scale air traffic applications. Therefore, this research aims to develop a physics-informed machine learning framework capable of predicting overall engine noise and aircraft trajectory noise within milliseconds.

Chapter 2 provides a detailed description of the principal noise-source components and their underlying generation mechanisms considered in conventional aircraft noise prediction methods. It then discusses the propagation of aircraft noise from the source to the observer and concludes by introducing the acoustic metrics used to quantify aircraft noise. Chapters 3 and 4 present the application of different machine learning approaches to conceptual engine noise prediction and whole-aircraft trajectory-noise prediction, respectively. Each chapter provides a detailed description of the generation and preprocessing of the corresponding datasets, machine learning models employed, associated training strategies, and the evaluation metrics used to assess model performance. Chapter 5 briefly summarises the work conducted and the main findings presented in the two appended papers. Finally, Chapter 6 provides an overall synthesis of the contributions of this thesis, and outlines directions for future research.

Chapter 2

Aircraft Noise Prediction

All datasets used to train and test the machine-learning models in this thesis were generated using the Chalmers Noise Code(CHOICE) model. Therefore, before introducing the machine-learning methodologies, the noise-prediction approach implemented in CHOICE and the general metrics used for aircraft noise assessment are first presented.

CHOICE is an open-source framework for estimating aircraft source noise and its propagation along a trajectory [25]. Individual airframe and propulsion sources are modeled using published empirical and semi-empirical relations, and the framework produces frequency- and directivity-dependent source levels before calculating observer metrics. Engine performance and geometry needed by the source models can be supplied by the in-house GESTPAN system[33].

2.1 Engine noise

Engine noise, or propulsion noise, encompasses the acoustic contributions from all major components of the propulsion system. In a turbofan engine, the primary noise sources include the fan, compressor, combustor, turbine, and exhaust jet. Figure 2.1illustrates the relative contributions and directivity characteristics of these individual sources [34]. In the forward direction, fan noise is generally dominant, whereas the contribution from the compressor is comparatively small. In the aft direction, the fan and jet typically represent the two major noise sources. Although their overall noise levels may be comparable, they exhibit different directivity patterns. The turbine and combustor also contribute to aft-radiated noise, but their contributions are generally lower.

Fan noise is the major contributor to overall aircraft noise under most flight conditions. It represents the dominant engine noise source during final approach and primary contributor with jet noise at take-off.At subsonic blade tip speeds, broadband fan noise is generated from random unsteady fluctuations due to turbulence in the flow passing the blades. This unsteadiness can be caused by turbulence in the wall and blade boundary layers, in the blade wakes and vortices, or in the freestream inlet flow [35, 36]. Tonal noise is caused by periodic lift fluctuations due to inlet flow turbulence or interaction between rotors and stators.The resulting tones occur at the

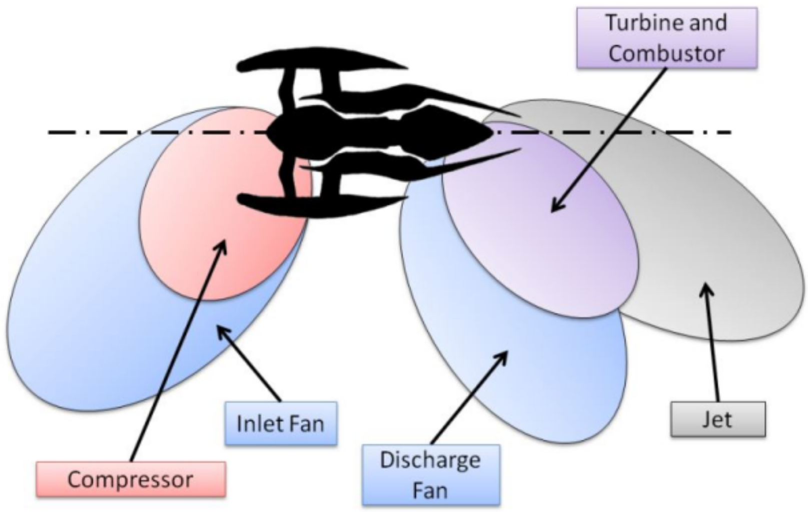

Figure 2.1: Noise contribution and directivity of high bypass ratio turbofan engine components[34].

blade-passing frequency (BPF) and its integer harmonics. At supersonic blade-tip speeds, shock waves form near the rotor leading edges, generating multiple pure tones at harmonics of the shaft rotational frequency which could be typically observed during takeoff.Based on the experimental data, Heidmann, etc developed an empirical model for predicting noise generated by fan and compressor components [36]. The model mentions that fan or compressor noise at the inlet duct is a combination of broadband, discrete-tone and, possibly, multiple pure tone noise. At the discharge duct, only fan broadband and discrete tone noise are present. The predicted noise is in 1/3 octave band frequencies of the free field noise pattern and the required parameters for the prediction are the mass flow rate, the total temperature rise for a fan or compressor stage and the design and operating point values of the rotor tip relative inlet Mach number.

Although combustor noise is generally not a dominant source, it can contribute appreciably to overall engine noise, particularly in the low- and mid-frequency ranges. Combustion noise is generated through two physically distinct mechanisms: direct and indirect combustion noise [37]. Direct combustion noise arises from unsteady heat release associated with chemical reactions, which generates acoustic pressure fluctuations within the combustion chamber. Indirect combustion noise originates from entropy and velocity perturbations produced by the unsteady combustion process. As these disturbances are convected downstream and accelerated through the turbine stages, they interact with the mean flow and generate acoustic waves [38, 39].

According to the semi-empirical framework developed by Dunn and Peart, aircraft-engine turbine noise is generated by aerodynamic interactions within the turbine stages and is generally decomposed into broadband and discrete-tone components [40]. The underlying mechanisms are assumed to be broadly similar to those responsible for fan and compressor noise. Discrete-tone noise is primarily associated with periodic aerodynamic interactions between rotors and stators. The flow leaving an upstream stator contains circumferentially nonuniform velocity distributions caused by the stator wakes. As the downstream rotor blades pass through these wakes, they experience periodic fluctuations in incidence angle and aerodynamic loading. Conversely, the wakes shed by a rotor interact with the downstream stator vanes and generate periodic fluctuating forces on the vane surfaces. These coherent loading fluctuations produce acoustic tones at the blade-passing frequency.Broadband turbine noise, by contrast, results from random fluctuations in the aerodynamic loading of the rotor blades and stator vanes. These fluctuations are caused mainly by turbulent velocity disturbances convected through the turbine. The relevant disturbances may originate from blade and end-wall boundary layers, turbulent wakes generated by upstream blade rows, tip-clearance flows, and other nonuniform flow structures. When such turbulent disturbances interact with a blade surface, they produce stochastic lift fluctuations over a broad range of frequencies. The resulting acoustic spectrum is therefore continuous rather than concentrated at individual harmonics [40, 41].

Jet noise is generated primarily by the turbulent mixing between the high-velocity exhaust flow and the surrounding atmosphere. In a turbofan engine, the hot core jet and the relatively cold bypass stream form several shear layers, within which large velocity, temperature, and density gradients lead to hydrodynamic instability and turbulence. These initially organized disturbances develop into vortical structures, interact with one another, and eventually break down into smaller-scale turbulence [38, 42]. A small fraction of the associated turbulent kinetic energy is converted into acoustic energy and radiated into the far field.The fundamental theoretical description of turbulent jet noise was established by Lighthill, who reformulated the compressible-flow equations as an inhomogeneous acoustic wave equation [43]. In this acoustic analogy, turbulence within a free jet behaves approximately as a distribution of quadrupole sources. For an ideal cold subsonic jet, the total acoustic power is approximately proportional to the eighth power of the characteristic jet velocity. Although this scaling is not universally applicable to heated or non-ideal jets, it demonstrates why reducing exhaust velocity is particularly effective in lowering aircraft noise. This principle partly explains the noise advantage of modern high-bypass-ratio turbofan engines, which produce thrust by accelerating a larger mass flow through a smaller velocity increment. Later, Jet noise was modeled as presented by Russel [42]. This method can be used to estimate source noise both from circular and coaxial jets, and it is based on extensive test data. The sound pressure levels from the test data are curve fitted, as a function of frequency and directivity, using bicubic splines and a third order Taylor series. The component noise levels are then defined for all frequencies and longitudinal directivities.

2.2 Airframe noise

Airframe noise is commonly defined as the aerodynamic noise generated by an aircraft in the absence of an operating propulsion system [44]. It primarily results from turbulent airflow interacting with the aircraft surfaces and structural components.

The principal airframe noise sources include the trailing edges of the wings and tail surfaces, high-lift devices such as flaps and slats, and the landing gear. Depending on the aircraft configuration, additional structural features may also contribute to the overall airframe noise. Examples include landing-gear cavities and wing cavities associated with fuel overpressure relief ports [45, 46]. During most phases of flight, airframe noise is generally less significant because engine noise remains dominant or because the aircraft is sufficiently far from the ground. However, during final approach and landing, airframe noise can become a major, and in some cases dominant, contributor as propulsion noise continues to be reduced through advances in engine technology.

According to Fink's component-based airframe-noise model, the noise generated by an aircraft in its clean configuration is primarily attributed to turbulent-boundary-layer trailing-edge noise [47, 48]. When the turbulent boundary layer developing over a wing or tail surface passes over a sharp trailing edge, the hydrodynamic pressure fluctuations embedded in the boundary layer are scattered into propagating acoustic waves. The trailing edge therefore acts as an efficient conversion mechanism between otherwise non-radiating turbulent disturbances and far-field sound. Fink's formulation is based partly on the half-plane scattering theory of Ffowcs Williams and Hall, which predicts that the corresponding acoustic intensity scales approximately with the fifth power of the flow velocity and exhibits a dipole-like directivity.The deployment of high-lift devices introduces additional noise sources. For trailing-edge flaps, Fink assumes that the flap panels are immersed in the turbulent wake of the main wing and, for multi-element systems, in the wakes of upstream flap elements. The incident turbulence produces unsteady lift fluctuations on the deflected flap surfaces, which radiate as an aerodynamic dipole.Leading-edge slat noise is represented more simply. Fink identifies two contributions: the increase in main-wing trailing-edge noise caused by the slat-induced modification of the wing boundary layer, and the trailing-edge noise generated by the slat itself.The total high-lift-system noise is obtained by summing the mean-square acoustic pressures of the individual components, which are assumed to be mutually incoherent. This approach provides an efficient engineering model requiring only basic geometric and operating parameters.

Landing gear noise is predominantly broadband and is mainly generated through two mechanisms: turbulent flow separation around bluff-body components, including struts, joints, and tires, and the subsequent interaction of the resulting turbulent wakes with downstream aircraft structures, particularly high-lift devices [13, 49]. In both mechanisms, a small fraction of the turbulent kinetic energy is converted into acoustic energy and radiated as propagating sound waves. In addition to broadband noise, tonal components may be produced by coherent vortex shedding from smaller structural elements, such as wires and equipment dressings [49], as well as by flow interactions with cavities within the landing gear assembly [50–52]. Among these mechanisms, semi-empirical prediction methods generally account only for noise generated by turbulent flow separation around the primary landing gear components , since this mechanism is typically regarded as the dominant contributor to overall landing gear noise.

2.3 Sound propagation

The aircraft noise received by a ground-based microphone or observer is influenced by several physical effects that occur between sound emission and reception. These effects can be broadly classified into source-motion effects and atmospheric propagation effects. Source-motion effects arise from the relative motion between the aircraft and the observer and primarily include retarded-time effects, convective amplification, and Doppler frequency shift[53, 54]. As the acoustic waves propagate through the atmosphere, their amplitude, spectral content, and propagation direction may be further modified before reaching the observer. The principal propagation mechanisms include atmospheric absorption, spherical spreading, variations in the characteristic acoustic impedance of the atmosphere, and reflection from the ground surface[55, 56]. Accurately accounting for these effects is essential for predicting the noise levels and spectra received at ground-based observer locations. no subsection, short the part of efforts

2.3.1 Source motion effects

Aircraft motion modifies the acoustic signal received by a stationary ground-based observer, even when atmospheric absorption, ground reflection, and other propagation effects are neglected. In particular, the received sound may differ from the emitted sound in both frequency and amplitude. The frequency variation is associated with the Doppler effect, whereas the change in acoustic amplitude is commonly described by convective amplification. These moving-source effects must be considered when noise models developed under static test conditions are applied to aircraft operating in flight.

The Doppler effect describes the frequency shift caused by the relative motion between the sound source and the observer. When an aircraft moves toward a stationary observer, successive acoustic wavefronts arrive at shorter time intervals, resulting in a received frequency that is higher than the emitted frequency[54]. Conversely, as the aircraft moves away from the observer, the wavefronts become more widely separated in time, and the received frequency decreases.

Convective amplification refers to the modification of the received acoustic amplitude and directivity caused by source motion. As the aircraft travels through the surrounding medium, acoustic energy is effectively concentrated in some radiation directions and reduced in others. For a compact moving source, this effect is commonly represented by a convective factor involving the term $(1 - M\cos\theta)$[53].

Aircraft motion also introduces a distinction between the time at which sound is emitted and the time at which it is received. Consider a simplified case in which sound propagates along a straight path without refraction or reflection. A sound wave emitted by the aircraft at the emission time (t_e), when the source is located at a distance (R_e) from the observer, reaches the observer at the reception time (t_o). During the propagation interval, the aircraft continues to move and may therefore be located at a different distance (R_o) when the sound is received, as illustrated in Figure 2.2. The propagation time is determined by the source–observer distance at the instant of emission and is given by (R_e/c). The reception and emission times are therefore related by

$$t_o = t_e + \frac{R_e(t_e)}{c}.$$

The emission time (t_e), also referred to as the retarded time, represents the earlier source time corresponding to the acoustic signal received at (t_o).

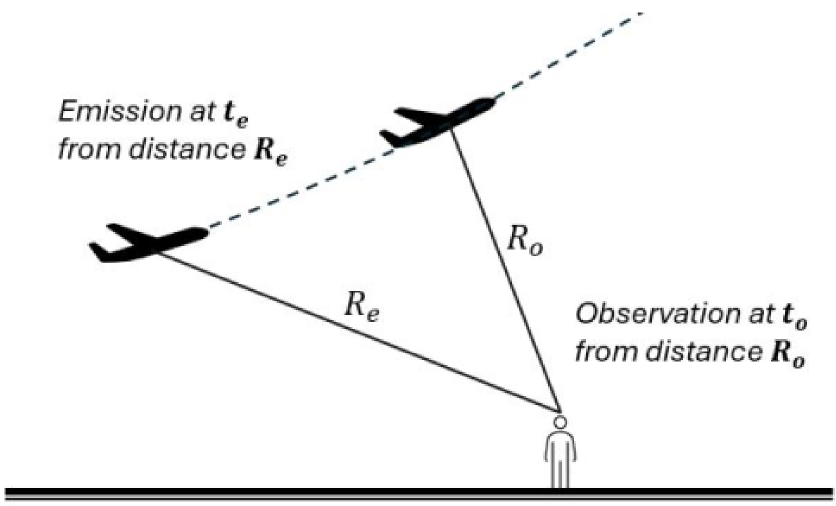

Figure 2.2: Retarded time effect for a moving source[25].

2.3.2 Atmospheric propagation effects

Spherical spreading describes the reduction in sound intensity as acoustic energy propagates away from a point source. Assuming that the source radiates uniformly in all directions and that the total acoustic power remains constant, the emitted energy is distributed over an increasingly large spherical surface. Since the surface area increases with the square of the propagation distance, the acoustic intensity decreases according to $1/R^2$, where R is the distance between the source and the observer[55]. Consequently, aircraft noise levels measured on the ground are strongly influenced by the source–observer distance.

During propagation through the atmosphere, an aircraft-generated sound wave experiences additional attenuation due to atmospheric absorption. This attenuation is mainly associated with classical absorption caused by viscous and thermal-conduction losses, together with molecular absorption resulting from the rotational and vibrational relaxation processes of oxygen and nitrogen. The magnitude of atmospheric absorption depends on several factors, particularly sound frequency, propagation distance, temperature, humidity, and atmospheric pressure[56].

Ground reflection arises when part of the acoustic energy emitted by a source reaches an observer after being reflected from the ground, in addition to the sound travelling along the direct propagation path. The superposition of the direct and reflected waves may lead to either constructive or destructive interference, thereby increasing or reducing the received sound level depending on their relative phase. The strength of the reflected wave is governed by the acoustic properties of the ground surface, which may vary considerably between soft surfaces, such as snow and grass, and hard surfaces, such as concrete and asphalt. These properties are commonly characterised by the acoustic impedance, which represents the resistance of the ground surface to acoustic particle motion and determines the proportions of incident sound energy that are absorbed and reflected.

2.4 Noise metrics

Several acoustic metrics may be used to quantify aircraft noise at ground-level observer locations, depending on the specific objective and application of the analysis. For comparison with the aircraft noise certification limits established by the International Civil Aviation Organization (ICAO), the effective perceived noise level (EPNL) is commonly adopted . EPNL is specifically designed for aircraft noise certification and accounts for the perceived noisiness, tonal characteristics, and duration of an individual aircraft noise event. By contrast, comparisons with flyover measurements are generally based on the sound pressure level (SPL) or L_p) or the A-weighted sound pressure level (L_{pA}). Aircraft noise contours and spatial noise maps are typically expressed in terms of the sound exposure level (SEL), although the maximum A-weighted sound pressure level ($L_{A,\max}$) may also be used for specific applications. The following sections provide a brief overview of these metrics.

2.4.1 Effective perceived noise level

The effective perceived noise level (EPNL) is a noise metric that accounts for the human perception of the spectral characteristics and duration of an aircraft noise event. It is primarily used to evaluate individual aircraft events at a specified measurement location, particularly for aircraft noise certification, and is expressed in (EPN dB). The EPNL is not measured directly but is derived from the perceived noise level (PNL) by applying corrections for spectral irregularities, such as prominent tonal components, and for the duration of the event. The PNL is calculated from the measured or predicted sound pressure level spectrum using frequency-dependent weighting functions that represent the frequency sensitivity of human hearing.

2.4.2 Maximum A-weighted sound pressure level

The maximum A-weighted sound pressure level, denoted by $L_{A,\max}$, represents the highest A-weighted sound pressure level recorded during a specified noise event and is expressed in dB(A). A-weighting is applied to approximate the frequency-dependent sensitivity of the human auditory system and therefore provides an indication of the maximum perceived loudness during the event. Since $L_{A,\max}$ describes only the highest instantaneous noise level and does not account for the duration or cumulative exposure of the event, it is commonly used together with complementary noise metrics, such as the sound exposure level.

2.4.3 Sound exposure level

The sound exposure level (SEL) quantifies the total acoustic energy received during a noise event by accounting for both the sound level and the event duration. It is expressed in dB or dB(A) and represents the constant sound level that would contain the same total acoustic energy if it were maintained for a reference duration of one second. The SEL is therefore particularly suitable for comparing individual aircraft noise events with different durations. It is determined by integrating the squared sound pressure over the duration of the event and normalising the result to the one-second reference period.

Chapter 3

Turbofan Engine Noise Modeling with Machine Learning

This chapter presents a machine learning framework for accelerating component-level turbofan noise prediction. Reference data are generated by coupling the engine performance code GESTPAN with CHOICE for an A320 class aircraft during approach. Deep neural network (DNN) and K-nearest-neighbor (KNN) models are trained to predict the EPNL of the principal engine noise components and the total engine noise. Their predictions are subsequently combined through a support-vector-regression stacking model. The framework is designed to represent both smooth nonlinear trends and discrete changes introduced by the engine sizing process.

3.1 Data generation and process

The engine noise datasets used for machine learning model training were generated using the CHOICE. The engine-noise source estimation in CHOICE requires detailed engine-performance parameters, which are calculated using the in-house engine-performance code GESTPAN. GESTPAN takes thrust, airspeed, altitude, and ambient conditions as inputs and generates the performance data required for each engine component. The performance and dimension files for the engine were then input to CHOICE together with a trajectory file, and the engine noise was calculated for every point in the trajectory. The output from CHOICE was a sound pressure level matrix for every frequency and longitudinal directivity and for every trajectory point. This matrix was generated for every component separately, and the total noise was calculated by summing all the individual sources. A reference case involving an A320 class aircraft was established. Turbofan design point parameters - Fan pressure ratio (FPR), Low-Pressure Compressor Pressure ratio (LPC PR), specific thrust, thrust, Mach number, deviation from International Standard Atmosphere (ΔISA), and altitude as listed in Table 3.1, have been varied around the nominal value within the specified range for this study.

Meanwhile, the overall pressure ratio, combustor-outlet temperature, and cooling-flow fractions were fixed at their respective design-point values. The design-point specific thrust was maintained at its nominal value for all cases except those in

Table 3.1: Turbofan engine noise sensitivity parameters

Parameter	***Nominal Value***	***Range***
FPR	**1.37** [-]	-2.5% **to** $+2.5\%$
LPC PR	**2.8** [-]	-15% **to** $+15\%$
Specific Thrust	**244.5** [kg/s]	-7% **to** $+7\%$
Thrust	**21000** [N]	-20% **to** $+20\%$
Mach	**0.78** [-]	-10% **to** $+10\%$
Altitude	**10668** [m]	-10% **to** $+10\%$
ΔISA	**10.0** [K]	-10 K **to** $+10$ K

** Design-point data are used if not otherwise specified.*

which specific thrust was the parameter being varied. Similarly, the design-point thrust remained at its nominal value except for cases involving thrust variation. A single key parameter was changed at a time, and changes in engine components and overall noise levels were stored and used as a dataset for subsequent machine learning training. The parameter ranges were selected to produce noticeable changes in noise levels while maintaining physically reasonable engine-design conditions. For example, a variation of only 2.5% in the design-point FPR is relatively small compared with the variations applied to the other parameters. Nevertheless, this variation can produce a difference of approximately 1 dB in the total engine EPNL because of the strong influence of FPR on jet noise. In contrast, varying the LPC PR from -15% to $+15\%$ does not produce a clear change in the total engine-noise level. However, this variation can trigger a change in the number of low-pressure-compressor stages and was therefore initially considered a suitable test case for the K-nearest-neighbours (KNN) model. After completing the data-generation process, it was observed that variations in most parameters caused a change in the stage count of either the low-pressure compressor (LPC) or the low-pressure turbine (LPT). The variation in the design-point value of ΔISA was the only case that exhibited an approximately linear relationship with the predicted noise levels. It was therefore used as a useful comparison case when evaluating the ability of different machine-learning models to represent both smooth and discontinuous noise-response behaviour.

3.2 Machine learning models

3.2.1 Deep neural network

Deep Neural Network (DNN) is a machine learning model with multiple hidden layers between input and output. It processes data through interconnected neurons, applying activation functions and backpropagation to adjust weights, enabling complex pattern recognition and decision making [57]. DNNs excel at handling complex data, recognizing patterns, and making accurate predictions. They improve with more data, support feature extraction, and perform well in regression tasks. Fig 3.1 shows the configuration of the DNN model for predicting engine component noise and total noise. A three layer neural network model was used, with each hidden layer consisting of 64 nodes. The output includes six predicted engine component noise and total noise. The intermediate and output layers are fully connected.

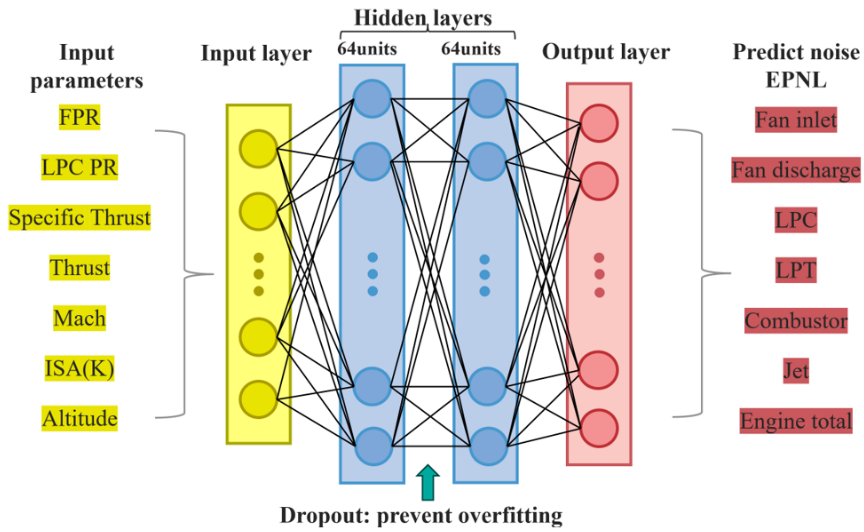

Figure 3.1: Schematic of Deep Learning Model.

The rectified linear unit (ReLU) was used as the activation function. Dropout was applied to the output values of the first intermediate layer with a dropout rate of 0.3. Dropout is one of the most effective methods for preventing overfitting in neural networks [58].Twenty percent of the 705 cases, corresponding to 141 cases, are reserved as an independent test set. It is important to note that the raw database used here for training and testing the DNN is relatively small, compared to typical neural network applications. To minimize potential bias from the limited dataset, a 5-fold cross validation method is employed. This technique ensures proper convergence during the training phase while using all data points to estimate network loss. The entire dataset is first divided into two subsets according to the prescribed train-test split ratio. The first subset is used for model training, while the second is reserved for testing, following standard practice. However, the training subset is further divided into five non-overlapping sub-subsets. Four sub-subsets are used to train a specific model, which is then evaluated using the fifth sub-subset. This process results in five independently trained and tested models, each following an 80%-20% train-test ratio. The best performing fold is retained as the final model and subsequently benchmarked against the unseen testing subset.The NN is trained to minimize the loss function $\mathrm{RMSE}_{\mathrm{total}}$ by using the Adam algorithm to update the weights [59]. The backpropagation algorithm is used to calculate the gradient required by Adam. The number of epochs is 2000. The model described above is implemented in Python with Keras library7 in Tensorflow backend [60]

For N test cases, the RMSE of one acoustic output is

$$\mathrm{RMSE} = \sqrt{\frac{1}{N}\sum_{i=1}^{N}(y_i - \hat{y}_i)^2}. \tag{3.1}$$

RMSE is reported in decibels and measures the average magnitude of the prediction error. Component-level errors are evaluated separately because averaging over the total-noise output alone could conceal a poorly represented source. The numerical values reported below are held-out estimates for interpolation within the sampled simulation domain.

3.2.2 Stacking Algorithm

K-nearest neighbours (KNN) is a commonly used supervised-learning algorithm [61]. Its primary purpose is to calculate the distance between an object and neighbouring samples with known labels. The general Minkowski distance is defined as

$$d(\mathbf{x}, \mathbf{y}) = \left(\sum_{i=1}^{q} |x_i - y_i|^p \right)^{1/p}, \tag{3.2}$$

where $\mathbf{x}$ denotes the query object, $\mathbf{y}$ denotes a neighbouring sample with a known label, and q is the number of input features. When $p = 1$, Equation (3.2) represents the Manhattan distance, whereas $p = 2$ gives the Euclidean distance.

Based on the calculated distances, the algorithm identifies the k nearest neighbours, where k is a user-defined hyperparameter that can significantly influence model performance. For conventional KNN regression, the prediction is obtained by averaging the target values of the selected neighbours. For weighted KNN, a distance-based weighting scheme assigns greater influence to samples located closer to the query point, which can improve prediction accuracy in certain cases. One of the principal advantages of KNN regression is its simplicity and its ability to represent nonlinear relationships without requiring complex feature transformations. It is also well suited to datasets containing local patterns because its predictions are derived directly from neighbouring samples. In this study, the number of neighbours is set to $k = 3$, a distance-based weighting method is employed, and $p = 2$ is used in Equation (3.2). Consequently, the neighbours are selected according to Euclidean distance. Ensemble learning can improve the generalisation performance of individual models by combining multiple learners. According to their combination strategies, ensemble-learning methods can generally be classified as stacking [62], bagging [63], and boosting [64]. Bagging and boosting combine several weak learners to construct a stronger learner. The final output is commonly determined by averaging or voting over the predictions generated by the individual weak learners. Unlike bagging and boosting, stacking employs a meta-learner to combine a group of base learners. The central concept of stacking is to construct a multi-level learning framework in which predictions generated by multiple base learners are treated as new input features. These features are then combined by a meta-learner to improve the generalisation performance of the overall model.

The stacking procedure generally consists of two principal stages. In the first stage, different base learners are trained independently using the same dataset, and each learner generates its own predictions. The base learners may have different bias–variance characteristics and can include decision trees, support-vector machines, neural networks, and other regression algorithms. In the second stage, the predictions generated by the trained base learners are treated as new features and supplied to the meta-learner. The meta-learner subsequently combines the outputs of the base models to produce a final prediction that more accurately represents the target variable.

In the present study, DNN and KNN are selected as the two base learners. Their predictions can be expressed as

$$\mathbf{z} = \begin{bmatrix} \widehat{y}_{\mathrm{DNN}} \\ \widehat{y}_{\mathrm{KNN}} \end{bmatrix}, \tag{3.3}$$

where $\widehat{y}_{\mathrm{DNN}}$ and $\widehat{y}_{\mathrm{KNN}}$ are the predictions generated by the DNN and KNN base models, respectively. The combined prediction is then obtained from the meta-model according to

$$\widehat{y}_{\mathrm{stack}} = f_{\mathrm{SVR}}\left(\mathbf{z}\right), \tag{3.4}$$

where f_{SVR} represents the support-vector-regression meta-model.

Support vector regression (SVR) with a Gaussian kernel is a nonlinear regression technique suitable for representing complex relationships between input features and target variables. Through the kernel function, the input data are implicitly mapped into a higher-dimensional feature space, in which linear regression can be used to approximate nonlinear patterns in the original input space. This approach offers strong generalisation capability and is particularly suitable for high-dimensional problems with relatively small datasets. In this study, SVR is employed as the stacking meta-model. The penalty parameter is set to $C = 2000$, while the width of the epsilon-insensitive loss function is set to $\varepsilon = 0.01$. A Gaussian radial basis function kernel is selected as the kernel function. The complete DNN–KNN stacking process is illustrated in Figure 3.2. The principal advantage of the stacking model is its ability to reduce the bias and variance of the individual base models, thereby improving the robustness and generalisation capability of the combined prediction model.

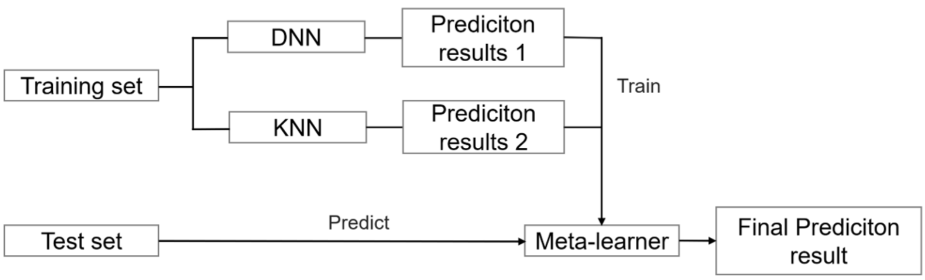

Figure 3.2: Workflow of the DNN–KNN stacking model.

Chapter 4

Aircraft Trajectory Noise Modeling With Machine Learning

This chapter proposes a Density-Guided Physics-Informed Attention U-Net (DGPIA U-Net) for rapid predicting two dimensional aircraft noise fields. The proposed framework uses U-Net architecture as its backbone and introduces density-guided physics-informed maps generated through adaptive Gaussian kernel diffusion to transform sparse trajectory information into continuous spatial influence fields. Furthermore, squeeze-and-excitation channel attention and bottleneck spatial attention are incorporated to enhance the weighting of heterogeneous physical variables and improve spatial feature representation.

4.1 Data generation and process

The trajectory aircraft noise mapping datasets used for machine learning model training were generated by the CHOICE. The departure procedure of an A320 class aircraft from Runway 05R at Manchester Airport was selected as study case. By varying the post-liftoff horizontal flight trajectory and the vertical climb profiles associated with different departure procedures, a noise database covering a range of flight trajectories was established. In the vertical plane, two different noise abatement departure procedures (NADP)[12], NADP1 and NADP2 were adopted. The main difference between them lies in their noise control objectives. NADP1 is primarily intended to mitigate noise in areas close to the airport, as the aircraft usually maintain a steeper climb for a longer period and low air speed after takeoff, thereby reducing noise exposure near the runway. In contrast, NADP2 is mainly aimed at reducing noise in areas farther from the airport, as it generally initiates acceleration and configuration cleanup earlier, which helps lower the noise impact in regions located farther along the departure path. In accordance with the official guidance, the flight altitude was constrained to 5,000 ft. In the horizontal plane, three officially published departure procedures for Runway 05R at Manchester Airport—ASMIM, LISTO2Z, and DESIG1Z—were considered, and the flight heading after liftoff was changed. The heading deviation ranged from $-25°$ to $+25°$, with an increment of $0.5°$ for each variation, The variation in the aircraft take-off trajectory in the horizontal plane and with the corresponding three-dimensional trajectories incorporating the vertical profiles of NADP1 and NADP2 shown in Fig 4.1. the parameter variations as shown in Table 4.1.

Table 4.1: Summary of datasets

Parameter	Value
Runway 05R take off procedure	ASMIM, LISTO2S, DESIG1S
NADP operation	NADP1, NADP2
Heading deviation angle α	$-25° \sim +25°$, $\Delta\alpha = 0.5°$
Total take off procedure cases	606

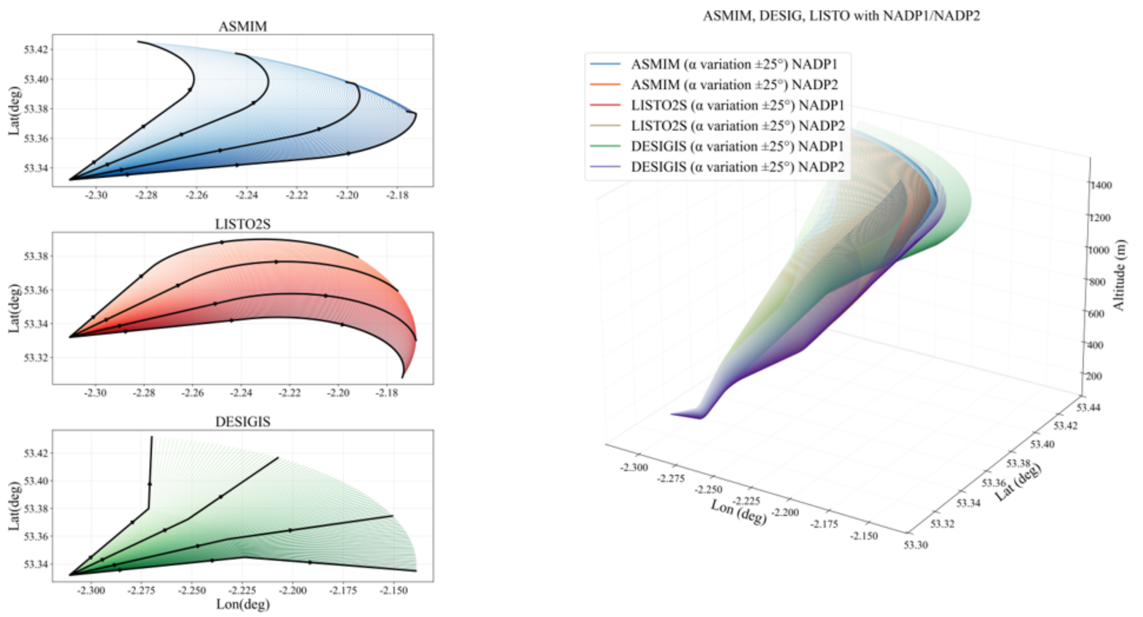

Figure 4.1: 3D diagram of trajectories database.

For each flight case, the raw trajectory data and the corresponding EPNL results were first converted into a trajectory-aligned two-dimensional computational grid. The grid was constructed using the first and last trajectory points as the longitudinal reference axis, while the transverse direction was defined as the normal direction to the flight path, and the grid extent was adaptively determined to cover the effective EPNL results field. Because of the differences in each takeoff route, the noise mapping size generated by CHOICE varies. Therefore, before training begins, padding was used to unify all labeled results to the maximum noise mapping size. The two-dimensional field size of the input and output is 115×172. The model input consisted of heterogeneous physical and spatial feature maps. Eleven trajectory-related physics variables were used as input channel, including time, true air speed, ground speed, Mach number, height, distance, flaps angle, slats angle, landing gear state, airfoil angle of attack and aircraft climb rate. Before being passed to the neural network, each continuous input channel was standardized using training-set statistics.

For a given channel c, the global mean μ_c and standard deviation σ_c were computed by aggregating all valid grid values from the training cases. The normalized input was then obtained as Eq. (4.1):

$$\widehat{X}_c(i,j) = \frac{X_c(i,j) - \mu_c}{\sigma_c} \tag{4.1}$$

This operation maps heterogeneous physical quantities, such as trajectory-referenced distance, speed, Mach number, altitude and aircraft configuration variables, onto a comparable dimensionless scale. Signed Distance Functions (SDF) provide spatial distance field with trajectory and computational grid, as shown in Fig. 4.2. The trajectory was first projected from geographic coordinates into a local Cartesian coordinate system. The flight path was then represented as a two-dimensional polyline composed of consecutive trajectory points. For each grid cell, the SDF value was computed as the shortest Euclidean distance from the grid point to the trajectory polyline:

$$D_{\mathrm{SDF}(i,j)} = \min_k \|G(i,j) - Q_k\| \tag{4.2}$$

Where $G(i,j)$ denotes the Cartesian coordinate of the grid cell (i,j), and Q_k is the closest projected point on the k-th trajectory segment. In the current model, the unsigned form of the SDF is used. Therefore, $D_{\mathrm{SDF}(i,j)} \geq 0$, and the channel encodes the distance magnitude from each grid cell to the nearest point on the flight trajectory. In addition, a binary mask map indicates whether a grid point is valid targe or padding. Providing this mask as an input to the model facilitates the construction of the loss function, enabling the model to focus more on the valid regions.

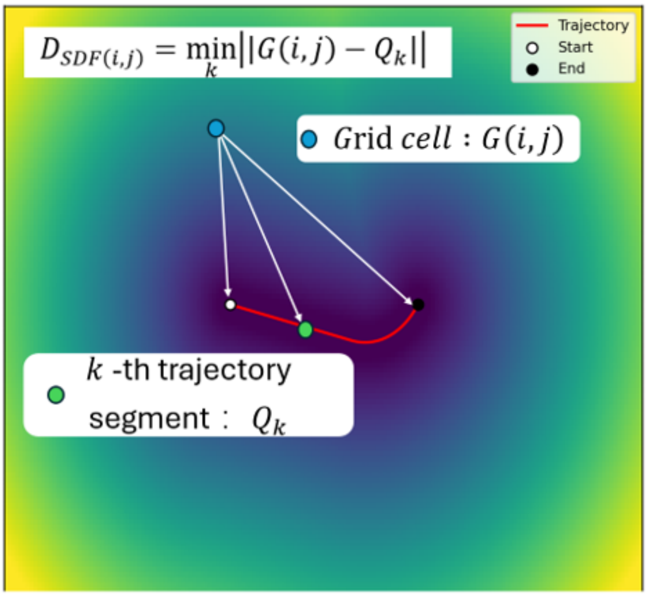

Figure 4.2: The schematic diagram of SDF on the computational grid

4.2 Density-Guided Physics-Informed Attention U-Net

As shown in Fig 4.3, Density-Guided Physics-Informed Attention U-Net (DGPIA U-Net) model is designed to reconstruct the two-dimensional distribution of effective perceived noise level (EPNL) from multi-channel input features. Model comprises two key components: a) multi density guided map, b) the U-Net network with attention mechanisms. Density-guided maps are introduced as physics-informed spatial prior inputs by using adaptive Gaussian kernels. Multi-scale density maps are generated by projecting trajectory points onto the grid using adaptive Gaussian kernels modulated by flight height, speed, and their interaction. They provide physics-informed spatial priors that indicate where trajectory-induced noise influence is stronger. The standard U-Net is used as the main encoder-decoder architecture for EPNL field reconstruction. The encoder progressively extracts multi-level features from the channels input feature maps through convolutional blocks and downsampling operations. Then the decoder restores the spatial resolution through upsampling layers and skip connections. The final 1×1 convolution maps the decoded feature representation to a single-channel EPNL prediction. Attention mechanisms include channel SE attention, Bottleneck spatial attention. They help the model focus on important physical variables, feature channels, and spatial regions relevant to EPNL prediction.

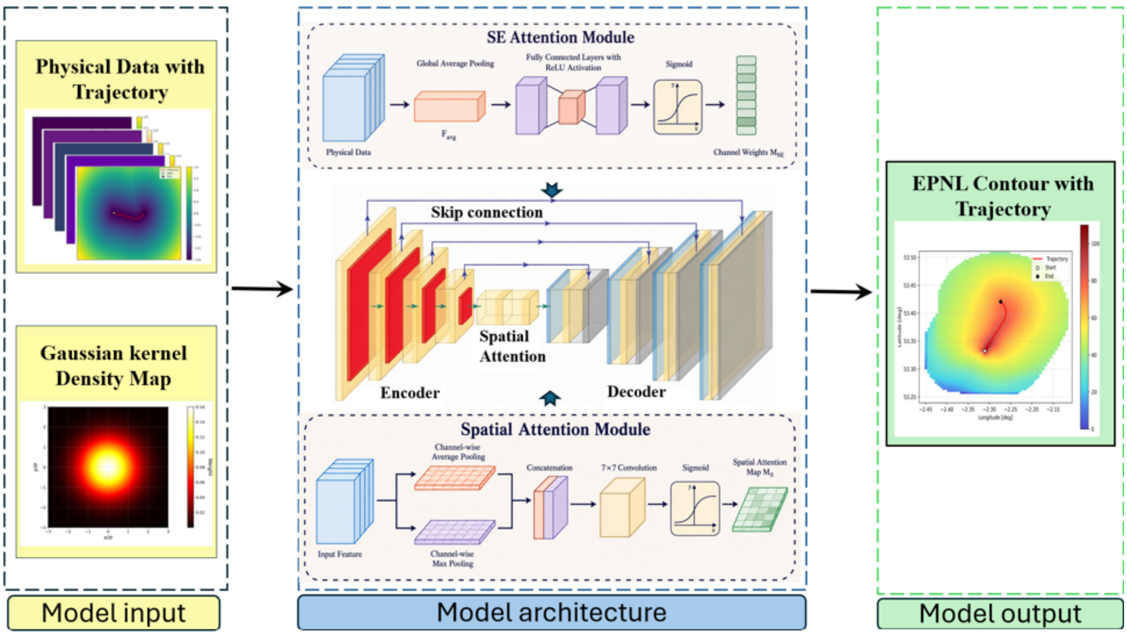

Figure 4.3: Density-Guided Physics-Informed Attention U-Net (DGPIA U-Net) model framework

4.2.1 Density guided map based on Gaussian kernel diffusion and physical information

In the present model, the density map used as a physics-informed prior input that transforms discrete flight-trajectory points into a continuous two-dimensional influence field. The original trajectory consists of a sequence of discrete points, each point containing the aircraft physical state at a given time instant, including altitude, speed and other variables. Compared with the output of a two-dimensional noise field, the original trajectory physical information serve as model input is sparse. Therefore, the density guide map was applied to construct a continuous spatial influence map through Gaussian diffusion. Specifically, for a trajectory point $p_i = (x_i, y_i)$ and a grid cell $g_{m,n} = (x_{m,n}, y_{m,n})$, their Euclidean distance is defined as Eq. (4.3):

$$d_{i,m,n} = \|g_{m,n} - p_i\|_2 \tag{4.3}$$

The Gaussian contribution from the i-th trajectory point to the grid cell (m, n) is calculated as Eq. (4.4):

$$w_{i,m,n} = \exp\left[-\frac{1}{2}\left(\frac{d_{i,m,n}}{\sigma}\right)^2\right], \qquad d_{i,m,n} \le R \tag{4.4}$$

where σ is the Gaussian standard deviation and R is the truncation radius. If $d_{i,m,n} > R$, the contribution is set to zero. The density value at each grid cell is then obtained by accumulating the Gaussian contributions from all trajectory points:

$$D_{m,n} = \sum_{i=1}^{N} \mathbf{1}(d_{i,m,n} \le R)\, w_{i,m,n} \tag{4.5}$$

This formulation converts the sparse trajectory line into a continuous density field, where larger values indicate stronger influence from nearby trajectory segments. Compared with sparse trajectory line, the Gaussian density map provides smoother spatial guidance and allows the model to perceive not only where the trajectory is located, but also how its influence decays with distance. Additionally, to further incorporate flight-state information, the Gaussian diffusion range was adaptively modified using aircraft height and speed. The height $\widetilde{h}_i$ and speed $\widetilde{v}_i$ of each trajectory point were first normalized as:

$$\widetilde{h}_i = 1 - \frac{h_i - h_{\min}}{h_{\max} - h_{\min}}, \qquad \widetilde{v}_i = \frac{v_i - v_{\min}}{v_{\max} - v_{\min}} \tag{4.6}$$

The adaptive influence coefficient was then computed with an interaction term between low altitude and speed as:

$$\alpha_i = 1 + \widetilde{h}_i + \widetilde{v}_i + \widetilde{h}_i \widetilde{v}_i \tag{4.7}$$

With this adaptive formulation, low-altitude and high-speed trajectory segments are assigned to broader spatial influence regions. This reflects the physical assumption that aircraft operating closer to the ground and at higher speeds are more likely to contribute strongly to ground-level noise exposure. The interaction term further enhances the influence of trajectory points where low altitude and high speed occur simultaneously. After applying the adaptive correction, the final density map is computed as:

$$D_{m,n} = \sum_{i=1}^{N} \mathbf{1}(d_{i,m,n} \leq R_i) \exp\left[-\frac{1}{2}\left(\frac{d_{i,m,n}}{\sigma_0 \alpha_i}\right)^2\right] \tag{4.8}$$

In the present model, two density maps are generated at different scales: $\sigma_{01} = 1200\,\mathrm{m}$, $R_{01} = 1200\,\mathrm{m}$ and $\sigma_{02} = 600\,\mathrm{m}$, $R_{02} = 600\,\mathrm{m}$. This allows the network to capture both local trajectory-near effects and broader noise-influence patterns.

4.2.2 U-Net architecture with attention mechanisms

U-Net is a specific convolutional neural network initially used for biomedical image segmentation [65]. In this paper, the standard architecture of U-Net has been modified with attention mechanisms to make it more suitable for noise field prediction tasks. As shown in Fig 4.3, structurally, the proposed model adopts a classical encoder-decoder architecture, comprising an encoding path enhanced with SE attention [66], a bottleneck module incorporating spatial attention [67], and a corresponding decoding path. First, SE attention is applied before all input channels are fed into the U-Net. Specifically, for each input channel, global average pooling is first performed and then passed through a two-layer fully connected network to learn channel-wise weights, which are subsequently multiplied back to the original input channels. The SE module enables the model to more efficiently identify and emphasize the most informative feature channels during training, thereby facilitating feature extraction and improving model convergence. The encoder contains three down sampling stages. The initial number of feature channels is set to 32 and increased in the encoder to enhance the representation capacity for complex spatial patterns. Each stage is composed of a convolutional block followed by a 2×2 max-pooling layer. Within each convolutional block, two successive 3×3 convolutional layers are used, and each convolution is followed by batch normalization and ReLU activation. A spatial attention mechanism used at the bottleneck of the current U-Net model. Specifically, after three down sampling operations, the resulting feature map is subjected to both average pooling and max pooling along the channel dimension. The pooled feature maps are then concatenated to generate a spatial attention map. This spatial attention map is subsequently used to perform residual enhancement at each spatial location across all bottleneck feature channels. In this way, the model can emphasize spatially informative regions within the compressed information, thereby strengthening its spatial representation capability.

The decoder mirrors the encoder and comprises three up sampling blocks. In each block, transposed convolution is first used to increase spatial resolution, after which the up sampled feature maps are concatenated with the corresponding encoder features through skip connections. This skip-connection mechanism preserves low-level spatial details that may otherwise be lost during repeated down sampling. When minor mismatches in spatial dimensions occur, bilinear interpolation is used to align the feature maps before concatenation.

Finally, a 1×1 convolutional layer is applied to project the decoded features onto a single output channel, the predicted EPNL field. By combining the spatial reconstruction capability of U-Net with the SE and spatial attention, the proposed SE-U-Net is able to model complex nonlinear relationships among heterogeneous input variables while maintaining strong sensitivity to localized spatial structures.

4.3 Loss Function and Training Strategy

The model was optimized using a masked mean squared error loss with an additional boundary-aware weighting mechanism. Since target noise maps may contain padded regions, the loss was not computed over the entire rectangular grid. Instead, a binary mask was used to restrict the optimization to valid target pixels. The $\widehat{Y}_{i,j}$ denote the predicted EPNL value at grid cell, and $Y_{i,j}$ denote the corresponding CHOICE value. The binary mask is denoted as $M_{i,j}$, where $M_{i,j} = 1$ indicates a valid target pixel and $M_{i,j} = 0$ indicates a padded pixel. The basic masked MSE loss is defined as:

$$L_{\text{mask}} = \frac{\sum_{i,j} M_{i,j} \left(\widehat{Y}_{i,j} - Y_{i,j} \right)^2}{\sum_{i,j} M_{i,j}} \tag{4.9}$$

This formulation ensures that only physically meaningful target regions contribute to the training objective. Pixels outside the valid target mask do not affect the gradient update, which is particularly important when different flight cases have different spatial extents which are padded to a common size during batch training.

Due to the computational domain size limitation of the CHOICE model, the noise field calculation results are close to 20 dB but not zero at some computational domain boundaries. Therefore, the target result obtained using nearest neighbor interpolation for the model training may contain errors at the outer edges. Accounting for uncertainty near the boundary of the valid target region, a boundary-aware weighting mechanism was introduced. A sequence of boundary rings from the outer edge toward the interior. Each ring was assigned a predefined weight, with lower weights near the outer boundary and higher weights toward the interior region. In the current implementation, the ring weights are $[0.1, 0.3, 0.5, 0.7, 0.9]$, while the remaining inner valid region is assigned a weight of 1.0. The final boundary-weighted masked MSE is then written as:

$$L = \frac{\sum_{i,j} M_{i,j} E_{i,j} \left(\widehat{Y}_{i,j} - Y_{i,j} \right)^2}{\sum_{i,j} M_{i,j} E_{i,j}} \tag{4.10}$$

Here, $E_{i,j}$ down-weights pixels close to the boundary of the valid region, while preserving their contribution to the loss. All valid pixels involved in optimization, but boundary pixels contribute less strongly according to their ring weights. This strategy encourages the model to primarily learn the physically more reliable interior noise field, rather than overfitting to boundary errors introduced by interpolation. Consequently, the predictive capability of the model may be reduced near the noise boundary. However, these outer boundary regions usually correspond to low noise areas and are therefore not the primary focus in aircraft noise prediction.

Chapter 5

Summary of papers

5.1 Paper 1

Adapting turbofan noise modelling tool using neural networks
Chenzhao Li, Evangelia Maria Thoma, Xin Zhao
GPPS Conferences and Events 2025

5.1.1 Summary and discussion

In this paper machine learning models are developed to reduce the cost of turbofan noise prediction in system-level multidisciplinary design and optimization. The reference data were generated by coupling the engine performance code GESTPAN with CHOICE for an A320 class aircraft during approach. Seven engine design-point parameters were varied: fan pressure ratio, low-pressure compressor pressure ratio, specific thrust, thrust, Mach number, altitude, and deviation from International Standard Atmosphere conditions. One parameter was changed at a time around its nominal value, producing 705 design points. The models use these design parameters to predict the Effective Perceived Noise Level of the fan inlet, fan discharge, low-pressure compressor, combustor, low-pressure turbine, and jet, together with the total engine noise.

The first model is a deep neural network with three hidden layers of 64 nodes, ReLU activation, and a dropout rate of 0.3. The network is trained with the Adam optimizer for 2000 epochs, and five-fold cross-validation is used to make more effective use of the relatively small dataset. A K-nearest-neighbours model with three neighbours, Euclidean distance, and distance-based weighting is also constructed. The two models are then combined in a stacking architecture in which the DNN and KNN predictions are treated as inputs to a support-vector-regression meta-learner with a Gaussian kernel. This combination is intended to retain the DNN's ability to represent smooth global nonlinear trends while using the local approximation capability of KNN to describe abrupt variations. Twenty percent of the data were reserved for testing. All evaluated models achieved RMSE values below 0.3 dB for every engine component and for total engine noise. The largest DNN error was approximately 0.29 dB for the low-pressure compressor, whereas the stacking model reduced the corresponding RMSE to 0.17 dB. For the fan inlet, fan discharge, low-pressure compressor, and combustor, most predictions were within ±0.5 dB of the CHOICE values. Somewhat larger errors remained for the low-pressure turbine, jet, and total noise, but the stacking model generally showed better convergence than the DNN. Sensitivity studies of altitude and Mach number further demonstrated that both models reproduce the overall noise trends. The stacking model was more accurate at the discrete changes caused by changes in compressor or turbine stage count, where the smoother DNN response produced larger errors. The adapted model reduced the reported prediction time from several minutes for the original workflow to a few seconds, which is a substantial advantage when thousands of noise evaluations are required in an optimization loop.

The results show that a hybrid global-local learning strategy is useful when the underlying engine-sizing process contains both smooth responses and discrete configuration changes. At the same time, the detailed comparison indicates that much of the stacking model's improvement originates from KNN, and little difference between KNN and stacking is observed for several components. The dataset is also small and was generated by changing one design parameter at a time. It does not fully represent coupled variations in the multidimensional engine design space, which are expected in an actual MDO study. In addition, a distance-based method such as KNN has limited extrapolation capability outside the sampled ranges. The model is trained against CHOICE and consequently inherits the validity range and modelling assumptions of the semi-empirical source models. A larger space-filling dataset with simultaneous parameter variations, explicit out-of-domain checks, validation for other engine architectures and flight conditions, and integration into a complete aircraft-engine MDO framework are therefore important next steps.

5.1.2 Division of work

Chenzhao Li: Conceptualization, modelling, simulation, post-processing, data visualization, manuscript writing
Evangelia Maria Thoma: Consultation on noise code, manuscript reviewing
Xin Zhao: Conceptualization, manuscript writing, manuscript reviewing

5.2 Paper 2

Aircraft Trajectory Noise Modeling with Physics Informed Multi-Channel Attention U-Net
Chenzhao Li, Shuai Li, Xin Zhao

5.2.1 Summary and discussion

In this paper a Density-Guided Physics-Informed Attention U-Net (DGPIA U-Net) is developed for rapid prediction of two-dimensional aircraft noise fields along take-off trajectories. The purpose is to reduce the computational cost of trajectory-dependent noise assessment so that noise can be included in multidisciplinary aircraft and air-traffic-system studies involving many aircraft and operational procedures. The training data were generated with the Chalmers Noise Code (CHOICE) for an A320 class aircraft departing from Manchester Airport Runway 05R. Three departure routes, heading deviations from $-25°$ to $+25°$, and two noise-abatement departure procedures were combined to produce 606 noise cases. Each case was transformed to a trajectory-aligned 115×172 computational grid, and eleven trajectory-related physical variables were provided as model inputs.

The model introduces physical information at several levels. Sparse trajectory points are converted into continuous density maps by Gaussian kernel diffusion, with the kernel range adjusted according to aircraft height, speed, and their interaction. These maps provide a spatial prior describing where the trajectory is expected to influence the ground-noise field. An unsigned SDF channel describes the distance between each grid point and the trajectory, while a binary mask separates valid noise-map cells from padded regions. The U-Net backbone is supplemented with squeeze-and-excitation attention to reweight the heterogeneous input channels and spatial attention at the bottleneck to emphasize important regions of the noise field. Training uses a masked mean-square-error loss with reduced weights near uncertain interpolation boundaries, thereby directing the optimization towards the more reliable interior of each noise map.

The dataset was divided into training, validation, and test sets with a ratio of 8:1:1, and the reported results were averaged over five training runs with different random seeds. The model converged after approximately 200 epochs, with a total training time of about 12 hours on the reported CPU-based hardware. Once trained, the DGPIA U-Net produced noise fields at millisecond level, corresponding to a speed improvement of approximately two to three orders of magnitude relative to CHOICE. Across all test cases, the RMSE above 40 dB decreased from 0.58 dB for the standard U-Net to 0.36 dB for the DGPIA U-Net, an improvement of 37%. In high-noise areas with rapidly changing noise levels above 90 dB, the RMSE decreased from 1.14 to 0.87 dB, corresponding to an improvement of 23%. The progressive improvement from the standard U-Net to the attention U-Net and finally to the DGPIA U-Net indicates that channel and spatial attention and the density-guided physical prior provide complementary benefits.

The model performs most consistently in the main noise-contour region, while the largest errors occur near low-noise map boundaries and in high-noise regions with steep spatial gradients immediately after take-off. Part of the boundary error is a direct consequence of the loss formulation, which deliberately assigns less weight to uncertain outer cells. The remaining high-noise error indicates that the present spatial representation still has difficulty reproducing sharp changes associated with low altitude, high thrust, and source directivity. Furthermore, its demonstrated generalization is also limited to take-off cases for one A320 class aircraft and one runway configuration. Extension to landing trajectories, additional aircraft types and airports, and independent validation against measurements would be required before the model could be used as a general airport-noise predictor. Stronger physical constraints and improved attention mechanisms may also help resolve the remaining sharp-gradient errors.

5.2.2 Division of work

Chenzhao Li: Conceptualization, modelling, simulation, post-processing, data visualization, manuscript writing
Shuai Li: Consultation on U-Net modelling, manuscript reviewing
Xin Zhao: Conceptualization, manuscript writing, manuscript reviewing

Chapter 6

Conclusion

6.1 Concluding remarks

This thesis develops machine-learning-based aircraft noise prediction methods at two distinct scales: engine noise prediction during conceptual design and whole-aircraft noise prediction along flight trajectories. For turbofan design noise sensitivity, DNN predicts component and total EPNL with errors below 0.3 dB, and stacking with a local KNN learner improves behavior at discrete stage-count changes.The results show that single DNN model can reproduce CHOICE engine noise accurately within the sampled design domain. Local and global learners are complementary where the response contains both smooth trends and abrupt transitions. For trajectory noise assessment, DGPIA U-Net converts physical trajectory fields into two-dimensional EPNL contours at millisecond scale and substantially improves accuracy over a standard U-Net Sparse trajectories can be made compatible with convolutional field prediction through distance fields and adaptive Gaussian density guides.

The principal contribution of the thesis is therefore not a replacement for established aircraft-noise physics, but a framework for transferring information from conventional engineering models into computationally efficient surrogates. This progression provides a basis for including noise more directly in multidisciplinary aircraft design and operational studies involving many candidate configurations or trajectories.

6.2 Future work

Building on the machine-learning framework developed for aircraft-noise prediction, future research will extend the same data-driven methodology to another important component of aviation environmental performance: combustor emissions. Although aircraft noise and engine emissions arise from different physical processes, both are governed by highly nonlinear interactions among operating conditions, component design, and flight state. The experience gained in feature selection, surrogate modelling, sensitivity analysis, and uncertainty quantification for noise prediction therefore provides a valuable methodological foundation for developing rapid and reliable NOx prediction tools. The first stage of this work will establish a physics-informed database for conventional Jet-A and alternative fuels, including hydrogen, simplified sustainable aviation fuel surrogates, methane, methanol, ethanol, and selected fuel blends. Chemical-kinetic simulations will be performed over ranges of combustor inlet temperature and pressure, global and local equivalence ratio, residence time, and mixing conditions representative of aircraft engines. Rather than representing combustor architecture solely as a categorical variable, lean direct injection (LDI) and rich-burn/quick-quench/lean-burn (RQL) concepts will be described using physically meaningful parameters. For LDI combustors, these parameters will include local equivalence-ratio and temperature distributions, spray evaporation and mixing times, and recirculation-zone residence-time distributions. For RQL combustors, separate parameters will characterize the rich-burn zone, quench-zone mixing rate and unmixedness, and lean-burn-zone residence time.

Ultimately, this research will support a unified environmental assessment framework in which aircraft noise, NOx, direct CO_2 emissions, and lifecycle greenhouse-gas effects can be evaluated together during preliminary aircraft and engine design. This combined framework could enable faster comparison of propulsion technologies and clarify the trade-offs among acoustic performance, fuel sustainability, combustion efficiency, and pollutant emissions.

Bibliography

[1] S. Benz, J. Kuhlmann, S. Jeram, S. Bartels, B. Ohlenforst, and D. Schreckenberg. "Impact of Aircraft Noise on Health". In: *Aviation Noise Impact Management*. Ed. by L. Leylekian, A. Covrig, and A. Maximova. Cham: Springer International Publishing, 2022, pp. 173–195. DOI: 10.1007/978-3-030-91194-2_7 (cit. on p. 3).

[2] C. S. Kim, S. T. Grady, J. E. Hart, F. Laden, T. VoPham, D. D. Nguyen, J. E. Manson, P. James, J. P. Forman, and K. M. Rexrode. "Long-term aircraft noise exposure and risk of hypertension in the Nurses' Health Studies". In: *Environmental Research* 207 (2022), p. 112195 (cit. on p. 3).

[3] M. G. Smith, M. Cordoza, and M. Basner. "Environmental noise and effects on sleep: an update to the WHO systematic review and meta-analysis". In: *Environmental Health Perspectives* 130 (2022), p. 076001 (cit. on p. 3).

[4] O. Hahad, S. Rajagopalan, J. Lelieveld, M. Sørensen, M. Kuntic, A. Daiber, M. Basner, M. Nieuwenhuijsen, R. D. Brook, and T. Münzel. "Noise and Air Pollution as Risk Factors for Hypertension: Part II - Pathophysiologic Insight". In: *Hypertension* 80 (2023), pp. 1384–1392. DOI: 10.1161/HYPERTENSIONAHA.123.20617 (cit. on p. 3).

[5] S. J. Balk, R. E. Bochner, M. A. Ramdhanie, and B. K. Reilly. "Preventing excessive noise exposure in infants, children, and adolescents". In: *Pediatrics* 152 (2023), e2023063753 (cit. on p. 3).

[6] H.-G. Olbrich, M. Röösli, E. Herrmann, C. Maschke, K. Schadow, T. Hähnel, H.-J. Rupprecht, and M. Kaltenbach. "Aircraft noise exposure and risk for recurrent cardiovascular events after acute coronary syndrome: a prospective patient cohort study". In: *Environmental Research* 238 (2023), p. 117108 (cit. on p. 3).

[7] J. Park, P. A. Muennig, and Z. Zafari. "Projecting the economic burden of health impacts of aircraft noise: a case study of Baltimore Washington International Thurgood Marshall Airport". In: *Journal of Exposure Science & Environmental Epidemiology* 35 (2025), pp. 107–117 (cit. on p. 3).

[8] International Civil Aviation Organization. *The World of Air Transport in 2015 to 2024*. International Civil Aviation Organization. 2025. URL: https://www.icao.int/strategic-objectives/world-air-transport-2015%20to%202024 (visited on 07/29/2026) (cit. on p. 4).

[9] European Union Aviation Safety Agency, European Environment Agency, and EUROCONTROL. *European Aviation Environmental Report 2025*. Tech. rep. Figure 3.2: Evolution in certified aircraft noise levels over time. Cologne, Germany: European Union Aviation Safety Agency, 2025. URL: `https://www.easa.europa.eu/en/domains/environment/eaer` (visited on 08/05/2026) (cit. on p. 5).

[10] H. Yu and J. A. Mulder. "Arrival Trajectory Optimization for Passenger Aircraft using Genetic Algorithms". In: *11th AIAA Aviation Technology, Integration, and Operations (ATIO) Conference*. Virginia Beach, VA: American Institute of Aeronautics and Astronautics, 2011. DOI: `10.2514/6.2011-6804` (cit. on p. 4).

[11] S. Alam, M. H. Nguyen, H. A. Abbass, C. Lokan, M. Ellejmi, and S. Kirby. "A dynamic continuous descent approach methodology for low noise and emission". In: *29th Digital Avionics Systems Conference*. Pagination reproduced as printed in the source PDF. IEEE, 2010, 1–E. (Visited on 05/27/2026) (cit. on p. 4).

[12] S. J. Hebly and H. G. Visser. "Advanced noise abatement departure procedures: custom-optimised departure profiles". In: *The Aeronautical Journal* 119 (2015), pp. 647–661 (cit. on pp. 4, 23).

[13] A. Filippone. "Aircraft noise prediction". In: *Progress in Aerospace Sciences* 68 (2014), pp. 27–63. DOI: `10.1016/j.paerosci.2014.02.001` (cit. on pp. 5, 12).

[14] E. R. Boeker, E. Dinges, B. He, G. Fleming, C. J. Roof, P. J. Gerbi, A. S. Rapoza, and J. Hermann. *Integrated Noise Model (INM) Version 7.0 Technical Manual*. Tech. rep. 2008. URL: `https://rosap.ntl.bts.gov/view/dot/12188` (visited on 05/27/2026) (cit. on p. 5).

[15] J. B. Ollerhead, D. P. Rhodes, M. S. Viinikainen, D. J. Monkman, and A. C. Woodley. *The UK Civil Aircraft Noise Contour Model ANCON: Improvements in Version 2*. ERCD RD Report 9842. 1999 (cit. on p. 5).

[16] S. Pietrzko and R. Bütikofer. "FLULA - Swiss Aircraft Noise Prediction Program". In: *Proceedings of the Annual Conference of the Australian Acoustical Society: Innovation in Acoustics and Vibration*. Adelaide, Australia, 2002, pp. 13–15. (Visited on 05/27/2026) (cit. on p. 5).

[17] A. N. der AzB. *Anleitung zur Berechnung von Lärmschutzbereichen (AzB)*. Author string reproduced exactly as printed in the source PDF. 2007 (cit. on p. 5).

[18] L. Bertsch and U. Isermann. "Noise prediction toolbox used by the DLR aircraft noise working group". In: *INTER-NOISE and NOISE-CON Congress and Conference Proceedings*. Institute of Noise Control Engineering, 2013, pp. 805–813. (Visited on 05/27/2026) (cit. on p. 5).

[19] J. Raney. "Development of a New Computer System for Aircraft Noise Prediction". In: *2nd Aeroacoustics Conference*. Hampton, VA, USA: American Institute of Aeronautics and Astronautics, 1975. DOI: `10.2514/6.1975-536` (cit. on p. 6).

[20] R. E. Gillian. *Aircraft Noise Prediction Program User's Manual*. Tech. rep. 1982. URL: https://ntrs.nasa.gov/citations/19830007879 (visited on 05/27/2026) (cit. on p. 6).

[21] L. V. Lopes and C. L. Burley. *ANOPP2 User's Manual: Version 1.2*. Tech. rep. 2016. URL: https://ntrs.nasa.gov/citations/20160014858 (visited on 05/27/2026) (cit. on p. 6).

[22] L. Lopes and C. Burley. "Design of the Next Generation Aircraft Noise Prediction Program: ANOPP2". In: *17th AIAACEAS Aeroacoustics Conference, 32nd AIAA Aeroacoustics Conference*. Portland, Oregon: American Institute of Aeronautics and Astronautics, 2011. DOI: 10.2514/6.2011-2854 (cit. on p. 6).

[23] A. Filippone. *Flight Performance Software FLIGHT*. School of Mechanical, Aerospace and Civil Engineering, University of Manchester. Manchester, UK, 2015. URL: https://www.academia.edu/download/37489855/flight_manual.pdf (visited on 05/27/2026) (cit. on p. 6).

[24] A. Filippone. "Development of a New Aircraft Noise Prediction Program". In: *16th AIAA Aviation Technology, Integration, and Operations Conference*. Washington, DC: American Institute of Aeronautics and Astronautics, 2016. DOI: 10.2514/6.2016-3902 (cit. on p. 6).

[25] E. Maria Thoma, T. Grönstedt, E. Otero Sola, and X. Zhao. "Assessment of an Open-Source Aircraft Noise Prediction Model Using Approach Phase Measurements". In: *Journal of Aircraft* 61 (2024), pp. 745–760. DOI: 10.2514/1.C037332 (cit. on pp. 6, 9, 14).

[26] L. Bertsch. "Noise Prediction within Conceptual Aircraft Design". PhD thesis. Technische Universität Braunschweig, 2013. URL: https://elib.dlr.de/84386/ (visited on 05/27/2026) (cit. on p. 6).

[27] A. S. Tenney, M. N. Glauser, and J. Lewalle. "A Deep Learning Approach to Jet Noise Prediction". In: *2018 AIAA Aerospace Sciences Meeting*. Kissimmee, Florida: American Institute of Aeronautics and Astronautics, 2018. DOI: 10.2514/6.2018-1736 (cit. on p. 7).

[28] Y. Zhang, B. Chen, K. Zhao, X. Tang, X. Yang, and G. Hu. "Intelligent prediction of acoustic performance of landing gear using deep learning". In: *Physics of Fluids* 35 (2023), p. 076112. (Visited on 05/27/2026) (cit. on p. 7).

[29] Q. Zhang and W. Zhang. "A hybrid approach for reconstruction of transonic buffet aerodynamic noise: Integrating random forest and compressive sensing algorithm". In: *Aerospace Science and Technology* 152 (2024), p. 109379. DOI: 10.1016/j.ast.2024.109379 (cit. on p. 7).

[30] Q. Zhang, X. Wang, D. Yang, and W. Zhang. "Data-driven prediction of aerodynamic noise of transonic buffeting over an airfoil". In: *Engineering Analysis with Boundary Elements* 163 (2024), pp. 549–561. DOI: 10.1016/j.enganabound.2024.04.006 (cit. on p. 7).

[31] C. Wu and S. Redonnet. “A simple yet efficient data-driven model for the prediction of aircraft noise impact”. In: *Aerospace Science and Technology* 163 (2025), p. 110286. DOI: 10.1016/j.ast.2025.110286 (cit. on p. 7).

[32] S. Toraman, O. O. Dursun, and H. Aygun. “Prediction of noise of commercial aircraft based on itself specifications by using machine learning methods”. In: *Journal of Air Transport Management* 125 (2025), p. 102779 (cit. on p. 7).

[33] Tomas Grönstedt. *Development of methods for analysis and optimization of complex jet engine systems*. Chalmers Tekniska Hogskola (Sweden), 2000 (cit. on p. 9).

[34] Matthew Paul Allen. “Analysis and Synthesis of Aicraft Engine Fan Noise for Use in Psychoacoustic Studies”. PhD thesis. Virginia Tech, 2012 (cit. on pp. 9, 10).

[35] J. F. Groeneweg and E. J. Rice. “Aircraft Turbofan Noise”. In: *Journal of Turbomachinery* 109.1 (Jan. 1987), pp. 130–141. DOI: 10.1115/1.3262058 (cit. on p. 9).

[36] M. F. Heidmann. *Interim Prediction Method for Fan and Compressor Source Noise*. Technical Memorandum NASA-TM-X-71763. Cleveland, Ohio: NASA Lewis Research Center, June 1979 (cit. on pp. 9, 10).

[37] A. P. Dowling and Y. Mahmoudi. “Combustion Noise”. In: *Proceedings of the Combustion Institute* 35.1 (Jan. 2015), pp. 65–100. ISSN: 1540-7489. DOI: 10.1016/j.proci.2014.08.016 (cit. on p. 10).

[38] A. H. Marsh and G. L. Blankenship. *Review of Turbofan-Engine Combustion and Jet-Noise Research and Related Topics*. Technical Report FAA-RD80-16. Long Beach, California: DyTech Engineering, Inc., Jan. 1980 (cit. on pp. 10, 11).

[39] P. Gliebe, R. Mani, H. Shin, B. Mitchell, G. Ashford, S. Salamah, and S. Connell. *Aeroacoustic Prediction Codes*. Contractor Report NASA/CR-2000-210244. NASA Glenn Research Center, 2000 (cit. on p. 10).

[40] D. G. Dunn and N. A. Peart. *Aircraft Noise Source and Contour Estimation*. Contractor Report NASA-CR-114649. Seattle, Washington: NASA and Boeing Commercial Airplane Co., 1973 (cit. on pp. 10, 11).

[41] E. A. Krejsa and M. F. Valerino. *Interim Prediction Method for Turbine Noise*. Technical Memorandum NASA-TM-X-73566. Cleveland, Ohio: NASA Lewis Research Center, Nov. 1976 (cit. on p. 11).

[42] J. W. Russell. *An Empirical Method for Predicting the Mixing Noise Levels of Subsonic Circular and Coaxial Jets*. Tech. rep. NASA, 1984. URL: https://ntrs.nasa.gov/citations/19840010980 (visited on 05/27/2026) (cit. on p. 11).

[43] Michael James Lighthill. “On sound generated aerodynamically II. Turbulence as a source of sound”. In: *Proceedings of the Royal Society of London. Series A. Mathematical and Physical Sciences* 222.1148 (1954), pp. 1–32 (cit. on p. 11).

[44] Gerrit JJ Ruijgrok. “Elements of aviation acoustics”. In: *(No Title)* (2004) (cit. on p. 11).

[45] Roberto Merino-Martinez and Mirjam Snellen. “Implementation of tonal cavity noise estimations in landing gear noise prediction models”. In: *AIAA AVIATION 2020 FORUM*. 2020, p. 2578 (cit. on p. 12).

[46] Reto Pieren, Lothar Bertsch, Demian Lauper, and Beat Schäffer. “Improving future low-noise aircraft technologies using experimental perception-based evaluation of synthetic flyovers”. In: *Science of The Total Environment* 692 (2019), pp. 68–81 (cit. on p. 12).

[47] M. R. Fink. *Airframe Noise Prediction Method*. English. Technical Report FAA-RD-77-29. Washington, DC: Federal Aviation Administration, 1977 (cit. on p. 12).

[48] Martin R Fink. “Noise component method for airframe noise”. In: *INTER-NOISE and NOISE-CON Congress and Conference Proceedings*. Vol. 1977. 1. Institute of Noise Control Engineering. 1977, pp. 397–412 (cit. on p. 12).

[49] Werner Dobrzynski. “Almost 40 years of airframe noise research: what did we achieve?” In: *Journal of aircraft* 47.2 (2010), pp. 353–367 (cit. on p. 12).

[50] G. J. Bennett, J. Lai, G. O’Brien, D. Ragni, F. Avallone, and M. Pott-Pollenske. “Flow Control and Passive Low Noise Technologies for Landing Gear Noise Reduction”. In: *28th AIAA/CEAS Aeroacoustics 2022 Conference*. Aeroacoustics Conferences. American Institute of Aeronautics and Astronautics, June 2022. DOI: `10.2514/6.2022-2848` (cit. on p. 12).

[51] I. C. Dedoussi, T. P. Hynes, and H. A. Siller. “Investigating Landing Gear Noise Using Fly-Over Data: The Case of a Boeing 747-400”. In: *19th AIAA/CEAS Aeroacoustics Conference*. Berlin, Germany: American Institute of Aeronautics and Astronautics, May 2013. DOI: `10.2514/6.2013-2115` (cit. on p. 12).

[52] A. Hajczak, L. Sanders, and P. Druault. “Landing Gear Interwheel Tonal Noise Characterization with the Boundary Element Method”. In: *Journal of Sound and Vibration* 458 (Oct. 2019), pp. 44–61. ISSN: 0022-460X. DOI: `10.1016/j.jsv.2019.06.010` (cit. on p. 12).

[53] William E Zorumski. *Aircraft noise prediction program theoretical manual, part 1*. Tech. rep. 1982 (cit. on p. 13).

[54] JE Ffowcs Williams and David L Hawkings. “Sound generation by turbulence and surfaces in arbitrary motion”. In: *Philosophical Transactions for the Royal Society of London. Series A, Mathematical and Physical Sciences* (1969), pp. 321–342 (cit. on p. 13).

[55] Henry E Bass, Louis C Sutherland, Allen J Zuckerwar, David T Blackstock, and DM Hester. “Atmospheric absorption of sound: Further developments”. In: *The Journal of the Acoustical Society of America* 97.1 (1995), pp. 680–683 (cit. on pp. 13, 14).

[56] Tony FW Embleton. “Tutorial on sound propagation outdoors”. In: *The Journal of the Acoustical Society of America* 100.1 (1996), pp. 31–48 (cit. on pp. 13, 14).

[57] Yann LeCun, Yoshua Bengio, and Geoffrey Hinton. “Deep learning”. In: *nature* 521.7553 (2015), pp. 436–444 (cit. on p. 18).

[58] Pierre Baldi and Peter J Sadowski. “Understanding dropout”. In: *Advances in neural information processing systems* 26 (2013) (cit. on p. 19).

[59] Diederik P Kingma, Danilo J Rezende, Shakir Mohamed, and Max Welling. “Semi-supervised learning with deep generative models”. In: *Advances in neural information processing systems* 27 (2014) (cit. on p. 19).

[60] Martín Abadi, Paul Barham, Jianmin Chen, Zhifeng Chen, Andy Davis, Jeffrey Dean, Matthieu Devin, Sanjay Ghemawat, Geoffrey Irving, Michael Isard, et al. “{TensorFlow}: a system for {Large-Scale} machine learning”. In: *12th USENIX symposium on operating systems design and implementation (OSDI 16)*. 2016, pp. 265–283 (cit. on p. 19).

[61] Michael Steinbach and Pang-Ning Tan. “kNN: k-nearest neighbors”. In: *The top ten algorithms in data mining* (2009), pp. 165–176 (cit. on p. 20).

[62] David H Wolpert. “Stacked generalization”. In: *Neural networks* 5.2 (1992), pp. 241–259 (cit. on p. 20).

[63] Leo Breiman. “Bagging predictors”. In: *Machine learning* 24.2 (1996), pp. 123–140 (cit. on p. 20).

[64] Jerome H Friedman. “Greedy function approximation: a gradient boosting machine”. In: *Annals of statistics* (2001), pp. 1189–1232 (cit. on p. 20).

[65] O. Ronneberger, P. Fischer, and T. Brox. “U-Net: Convolutional Networks for Biomedical Image Segmentation”. In: *Medical Image Computing and Computer-Assisted Intervention - MICCAI 2015*. Ed. by N. Navab, J. Hornegger, W. M. Wells, and A. F. Frangi. Cham: Springer International Publishing, 2015, pp. 234–241. DOI: `10.1007/978-3-319-24574-4_28` (cit. on p. 28).

[66] J. Hu, L. Shen, and G. Sun. *Squeeze-and-Excitation Networks*. No publication year was given in the source PDF (cit. on p. 28).

[67] J. Park, S. Woo, J.-Y. Lee, and I. S. Kweon. *BAM: Bottleneck Attention Module*. 2018. DOI: `10.48550/arXiv.1807.06514` (cit. on p. 28).

Part II

Appended Papers

Proceedings of Global Power and Propulsion Society
ISSN-Nr: 2504-4400
GPPS Shanghai25
September 4-6, 2025
www.gpps.global

GPPS-TC-2025-014

Adapting turbofan noise modelling tool using neural networks

Chenzhao Li
chenzhao@chalmers.se
Chalmers University of Technology
Gothenburg, Sweden

Evangelia Maria Thoma
evangelia.maria.thoma@chalmers.se
Chalmers University of Technology
Gothenburg, Sweden

Xin Zhao
xin.zhao@chalmers.se
Chalmers University of Technology,
Gothenburg, Sweden

ABSTRACT

System-level multidisciplinary design and optimization (MDO) of turbofans, incorporating integrated noise and emissions predictions, can require substantial computational resources. Noise assessments typically consume significantly more compared to 1-dimensional simulations of turbofan performance and correlation-based emissions predictions, making them the bottleneck of the entire process. In this study, the use of neural networks in adapting an existing semi-empirical noise modelling tool for MDO applications is presented. The aim is to reduce the computation load while keeping the accuracy of the predictions sufficiently close to the original models. Deep neural networks (DNN) and its combination with K-nearest neighbors (KNN) make up stacking model have been applied for the purpose. The dataset for neural network training comes from the noise model developed by Chalmers Noise Code (CHOICE), an open-source framework with the capability to predict the source noise level, from individual airframe, engine components and the entire aircraft. For the aircraft approach phase, the neural network selects the important design parameters at the engine design point as inputs and outputs the noise of each engine component. Overall, the practical use of neural networks proves beneficial which could achieve noise prediction quickly and efficiently with high accuracy. The combined use of DNN and KNN could improve the accuracy of the trained models significantly.

INTRODUCTION

Since the introduction of turbofan engines in the 1950s, the commercial aviation industry has witnessed sustained and rapid growth. Alongside the rapid expansion of the aviation industry, noise pollution around airports has increasingly become a significant issue. The engine noise is considered to be one of the primary sources of jet aircraft noise, significantly affecting the airport staff and the people living or working in the vicinity (Zaporozhets and Tokarev, 1998; Mahashabde *et al.*, 2011; Zaporozhets, Tokarev and Attenborough, 2011; Delfs *et al.*, 2018). Modern prediction methods used in research for engine noise prediction are mainly based on semi-empirical or semi-analytical formulations, which are then transformed into far-field noise data through appropriate propagation models (Ventres, Theobald and Mark, 1982; Meyer and Envia, 1996; Dunn, Tweed and Farassat, 1999; Nark, Envia and Burley, 2009; Maria Thoma *et al.*, 2024). For turbofan engines, the major sources of noise components are compressor, fan inlet, fan discharge, combustor, turbine and jet (Matta, Sandusky and Doyle, 1977; Heidmann, 1979; Ribner, 1981; Mahan and Karchmer, 1991; Mendoza, Nance and Ahuja, 2008; Hultgren, 2010). During the early stages of an aircraft engine design, the performance parameters of these components under design conditions influence the magnitude of the above noise sources. Substantial computational resources and time are usually required for noise prediction based on semi-empirical or semi-analytical formulas due to the complexity of managing the entire engine design space under a multidisciplinary framework.

Machine learning methods, with their robust data processing capabilities, have been widely used in aeroacoustics prediction modelling (Revoredo, Mora-Camino and Slama, 2016; Tenney, Glauser and Lewalle, 2018; Akdeniz, Sogut and Turan, 2020; Li and Lee, 2020; Ikuta *et al.*, 2023; Redonnet *et al.*, 2024; Zhang *et al.*, 2024; Zhang, Yang and Zhang, 2024; Zhang and Zhang, 2024). They provide a new way to build an efficient and highly accurate engine noise prediction model. In this paper, machine learning methods are used to adapt an existing engine noise prediction model for a specific engine architecture across a wide range of design parameters. The aim is to create a fast-responding surrogated model to be used in system-level multidisciplinary design and optimization (MDO) of aircraft and engine design, providing reasonable noise predictions for various design options. To identify a suitable machine learning algorithm for adapting the existing engine noise prediction models, the performance of the Deep neural networks (DNN) algorithm, K-nearest neighbors (KNN) and the combined use of the two in predicting Effective Perceived Noise Level (EPNL) during the aircraft approach phase is compared.

DATASETS USED FOR THE MEACHING LEARNING MODEL DEVELOPMENT

The engine noise datasets used for machine learning model training were generated by the Chalmers Noise Code (CHOICE) (Maria Thoma *et al.*, 2024) which is an open-source framework with the capability of predicting the source noise level, for every frequency and longitudinal directivity, from individual airframe and engine components and the entire aircraft. The CHOICE noise estimation of aircraft engines was based on empirical and semi-empirical noise models found in published literature (Dunn and Peart, 1973; Fink, 1977; Fink, 1979; Heidmann, 1979; Russell, 1984; Kontos, Janardan and Gliebe, 1996; Sen *et al.*, 2004; Gliebe *et al.*, 2022). Every engine component was modelled separately, and the engine total noise was calculated as the sum of all the individual components.

The engine noise source estimation in CHOICE requires detailed engine performance parameters, which are estimated using the in-house code GESTPAN (Grönstedt, 2000). GESTPAN takes thrust, airspeed, altitude, and ambient conditions as input and generates several performance files for each of the engine components. The performance and dimension files for the engine were then input to CHOICE together with a trajectory file, and the engine noise was calculated for every point in the trajectory. The output from CHOICE was a sound pressure level matrix for every frequency and longitudinal directivity and for every trajectory point. This matrix was generated for every component separately, and the total noise was calculated by summing all the individual sources.

In this study, a case involving an A320-type aircraft was established. Turbofan design point parameters - Fan pressure ratio (FPR), Low-Pressure Compressor Pressure ratio (LPC PR), specific thrust, thrust, Mach number, deviation from International Standard Atmosphere (ΔISA), and altitude as listed in Table 1, have been varied around the nominal value within the specified range for this study. At the meantime overall pressure ratio, combustor outlet temperature and cooling flow fractions were fixed at design point. Specific thrust at design point was maintained for all cases except those with varying Specific Thrust. The thrust value at design point remained at the nominal value for all cases except those with varying thrust. A single key parameter was changed at a time, and changes in engine components and overall noise levels were stored and used as a dataset for subsequent machine learning training. The specified ranges for the selected parameters were defined to be able to demonstrate noticeable impact on noise levels while maintaining the parameters at reasonable levels. For example, a 2.5% change in design point FPR is relatively small compared to the changes of other parameters but can result in a 1 dB difference in engine total EPNL because of its significant impact on jet noise. The range for LPC PR variation, -15% to +15%, on the other hand, does not contribute to any clear difference in engine total noise but can activate the stage count change in LPC design and was initially considered as a good example to test KNN. After data generation, it has been found that most of the parameter variations have had stage count change in either LPC or LPT. The variation in design point ΔISA, as the only one which shows relatively linear relationship with the noise levels, was considered a good comparison case with the variations of other parameters in testing different machine learning models.

Table 1. Turbofan engine noise sensitivity parameters

Parameter	*Nominal Value*	*Range*
FPR	1.37 [-]	-2.5% to +2.5%
LPC PR	2.8 [-]	-15% to +15%
Specific Thrust	244.5 [kg/s]	-7% to +7%
Thrust	21000 [N]	-20% to +20%
Mach	0.78 [-]	-10% to +10%
Altitude	10668 [m]	-10% to +10%
ΔISA	10.0 [K]	-10 K to +10 K

*** Design point data if not specified**

MACHINE LEARNING MODELS

Deep Learning Model (DNN)

Deep Neural Network (DNN) is a machine learning model with multiple hidden layers between input and output. It processes data through interconnected neurons, applying activation functions and backpropagation to adjust weights, enabling complex pattern recognition and decision-making (LeCun, Bengio and Hinton, 2015; Goodfellow *et al.*, 2016). DNNs excel at handling complex data, recognizing patterns, and making accurate predictions. They improve with more data, support feature extraction, and perform well in regression tasks. Fig. 1 shows the configuration of the DNN model for predicting engine component noise and total noise, where the design point parameters as given in Table 1 were selected as inputs to train the DNN. A three-layer neural network model was used, with each hidden layer consisting of 64 nodes. The output includes six predicted engine component noise and total noise. The intermediate and output layers are fully connected. There are 705 design points used for training and testing.

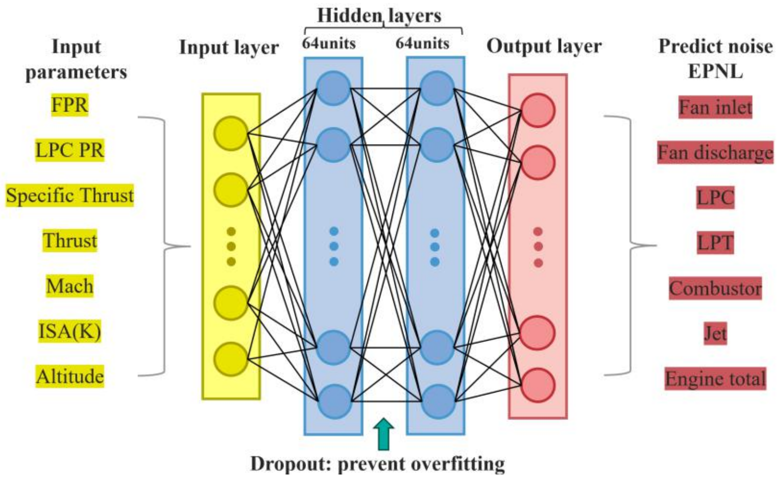

Fig.1 Schematic of Deep Learning Model

The rectified linear unit (ReLU) was used as the activation function. Dropout was applied to the output values of the first intermediate layer with a dropout rate of 0.3. Dropout is one of the most effective methods for preventing overfitting in neural networks (Baldi and Sadowski, 2013).The root-mean-square errors of the predicted engine noise EPNL for the six components and engine total (index *i*) with noise data amount (index *j*) are summarized to calculate the $RMSE_{total}$ shown as Eq. (1), where $E_{i,j}^{C}$ and $E_{i,j}^{P}$ are the CHOICE noise data and predicted noise data using NN.

$$RMSE_{total} = \sqrt{\frac{1}{560}\sum_{j=1}^{560}\frac{1}{7}\sum_{i=1}^{7}\left(E_{i,j}^{P} - E_{i,j}^{C}\right)^2} \qquad (1)$$

It is important to note that the raw database used here for training and testing the DNN is relatively small, compared to typical neural network applications. To minimize potential bias from the limited dataset, a 5-fold cross-validation method is employed. This technique ensures proper convergence during the training phase while using all data points to estimate network loss. As shown in Fig. 2, the entire dataset is first divided into two subsets according to the prescribed train-test split ratio. The first subset is used for DNN training, while the second is reserved for testing, following standard practice. However, the training subset is further divided into five non-overlapping sub-subsets. Four sub-subsets are used to train a specific DNN model, which is then evaluated using the fifth sub-subset. This process results in five independently trained and tested models, each following an 80%-20% train-test ratio. The best-performing fold is retained as the final DNN model and subsequently benchmarked against the unseen testing subset.

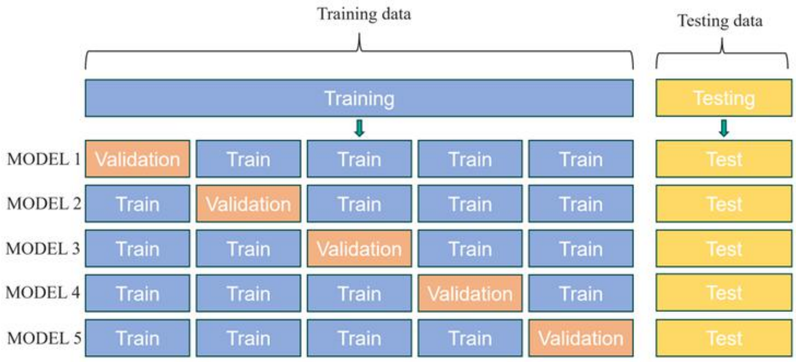

Fig.2 Sketch of the 5-fold cross-validation technique used in the DNN training.

The NN is trained to minimize the loss function $RMSE_{total}$ by using the Adam algorithm to update the weights (Kingma 2014). The backpropagation algorithm is used to calculate the gradient required by Adam. The number of epochs (number of times the weight coefficients are updated) is 2000. The model described above is implemented in Python with Keras library7 in Tensorflow backend (Abadi *et al.*, 2016).

Fig. 3 depicts the losses history of the DNN model, with illustration of the training phase and its convergence. As the training progresses, the loss function of the training dataset (blue line) decreases and becomes flat after 1500 epochs. The loss function for the testing dataset (red line) decreases and converges to approximately the same value as the blue line. There is no significant difference in the $RMSE_{total}$ between the training and test data, ranging from 0.1 to 0.2 dB. The results suggest that the DNN model achieve RMSE convergence in 2000 epochs.

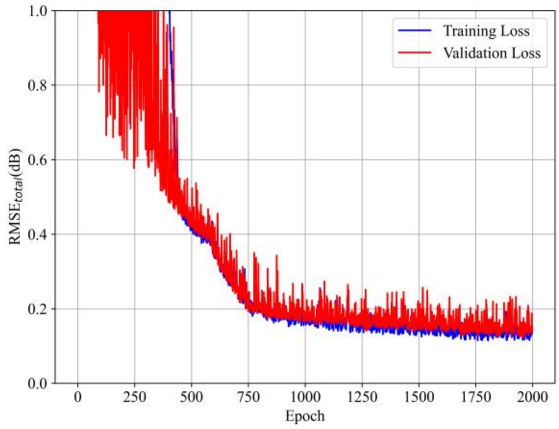

Fig.3 Learning curve of DNN

Stacking Algorithm (DNN-KNN)

KNN is a commonly used supervised learning algorithm (Guo *et al.*, 2003; Steinbach and Tan, 2009). Its primary aim is to calculate the distance between an object and its neighbors with known labels using Eq. 2:

$$d(x,y) = \left(\sum_{i=1}^{q} |\chi_i - y_i|^p \right)^{1/p} \qquad (2)$$

Where x is the object, y is its neighbor with known label; when p is 1 and 2, the distance is Manhattan distance and Euclidean distance, respectively. Based on the computed distances, the algorithm identifies the k nearest neighbors, where k is a user-defined hyperparameter that significantly influences the performance of model. Predictions are then made by averaging the target values of these neighbors. For weighted KNN, a distance-based weighting scheme assigns greater influence on closer neighbors, thereby improving prediction accuracy in certain cases. One of the main advantages of KNN regression is its simplicity and ability to model non-linear relationships without requiring complex feature transformations. Additionally, it adapts well to datasets with local patterns, as predictions are derived from immediate neighbors information. In this case, we choose the number of neighbors is 3, the weighting method is distance and the parameter p is set to 2.

Ensemble learning can enhance notably the generalization performance of models. Its basic idea is to accomplish learning tasks by combining multiple learners. According to combination strategies, ensemble learning can be classified into stacking (Wolpert, 1992), bagging (Breiman, 1996) and boosting (Friedman, 2001). Bagging and boosting directly put several weak learners together to form a strong learner. The output of a strong learner is determined by averaging or voting on the outputs of weak learners. Unlike bagging and boosting, stacking utilizes a meta-learner to gather a group of base learners. The core concept of stacking lies in constructing a multi-layer learning framework, where the predictions from multiple base learners are used as input features and further combined by a meta-learner to enhance the model's generalization performance. The stacking method typically involves two primary stages: training the base learners and constructing the meta-learner. In the first stage, different base learners are independently trained on the same dataset and generate their respective predictions. These base learners can include models with varying bias-variance characteristics, such as decision trees, support vector machines, and neural networks. In the second stage, the predictions produced by the trained base learners are treated as new features and fed into the meta-learner. The meta-learner is tasked with combing the outputs of multiple base models to generate a final prediction to better fit the target variable. In this research, DNN and KNN are selected as base learners. The Support Vector Regression (SVR) model with a Gaussian kernel is a powerful nonlinear regression technique well-suited for capturing complex relationships between input features and target variables. By implicitly mapping the input data into a high-dimensional feature space, the model enables linear regression in that space to approximate nonlinear patterns in the original input space. This approach offers strong generalization capabilities, making it particularly effective for modeling high-dimensional, small-sample datasets. In this study, SVR is employed as the meta-model, with the penalty parameter C set to 2000, epsilon $\varepsilon = 0.01$, and the Gaussian kernel selected as the kernel function. Its process is demonstrated in Figure 4. Advantage of stacking lies in its ability to effectively reduce the bias and variance of individual models, thereby improving the overall robustness and generalization capability of the combined model.

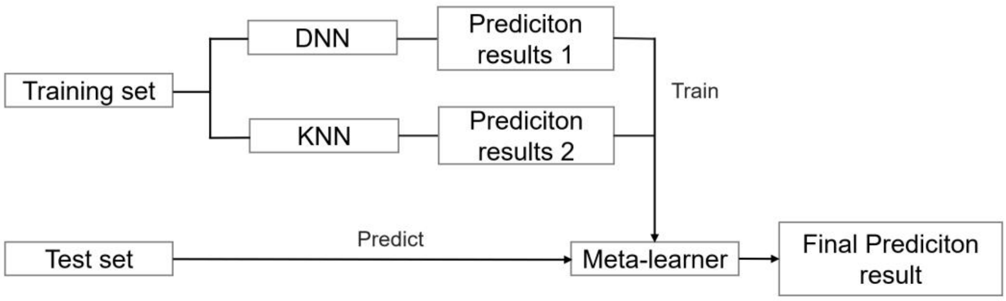

Fig.4 Diagram of the stacking model workflow

RESULTS AND DISCUSSION

Comparison of Machine Learning Algorithms in Noise Prediction

In this study, 20% of the total engine noise dataset was selected as a test set to evaluate the noise prediction performance of the DNN and stacking models. Fig. 5 illustrates the prediction performance of the three models on the test set for each engine component and the overall noise. The RMSE values of the three noise prediction models are less than 0.3 dB for each engine component and the overall noise. The highest RMSE value is approximately 0.29 dB for the LPC predicted by the DNN model. In comparison, the corresponding RMSE value for the stacking model is 0.17 dB, showing a significant reduction. Compared to the DNN and KNN models, the stacking model shows improvements in noise prediction for the LPC, LPT, and Jet components. In terms of noise prediction for the fan inlet, fan discharge, and combustor, the stacking model offers no substantial performance gain over KNN. Indeed, detailed comparison has shown that most of the benefits of the stacking model in the predictions are because of the combined use of KNN, while no substantial performance difference between the KNN and stacking models have been observed. Hence, also for clarity, the following analysis will focus on a comparison between the stacking and DNN models.

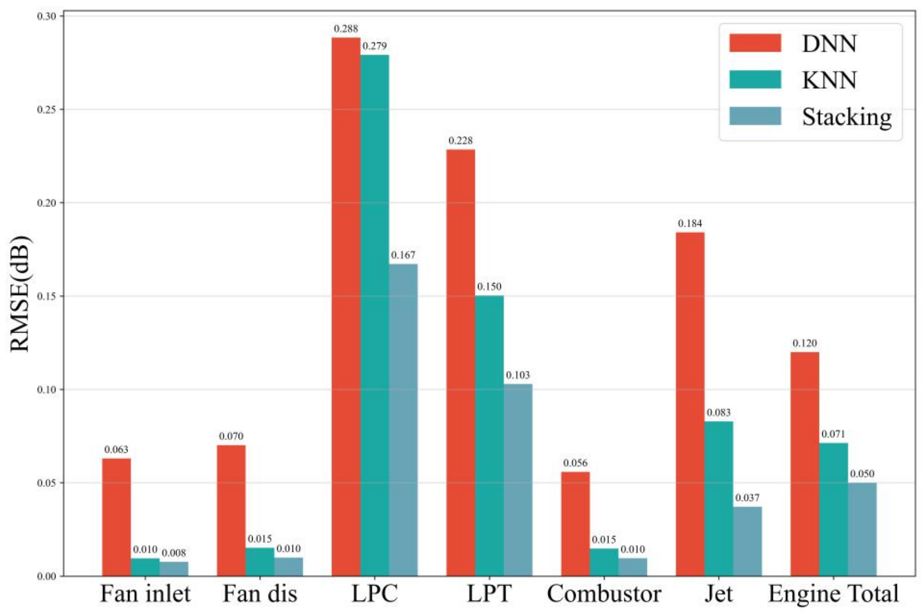

Fig. 5 The final loss function $RMSE_{total}$ values of testing dataset for each engine components and total.

The noise prediction results of stacking model and DNN model for each engine component are shown in Fig. 6. Both models demonstrate high accuracy in predicting the noise levels of the fan inlet, fan discharge, LPC, and combustor. The predicted values on the above engine components noise closely align with the CHOICE noise measurements, with error margins consistently within ±0.5 dB. Compared to the engine component noise mentioned above, the prediction errors of both models are slightly higher for the LPT, jet, and total engine noise. Both the DNN and stacking models exhibit some predictions with larger errors. However, overall, the stacking model demonstrates better convergence performance than the DNN model.

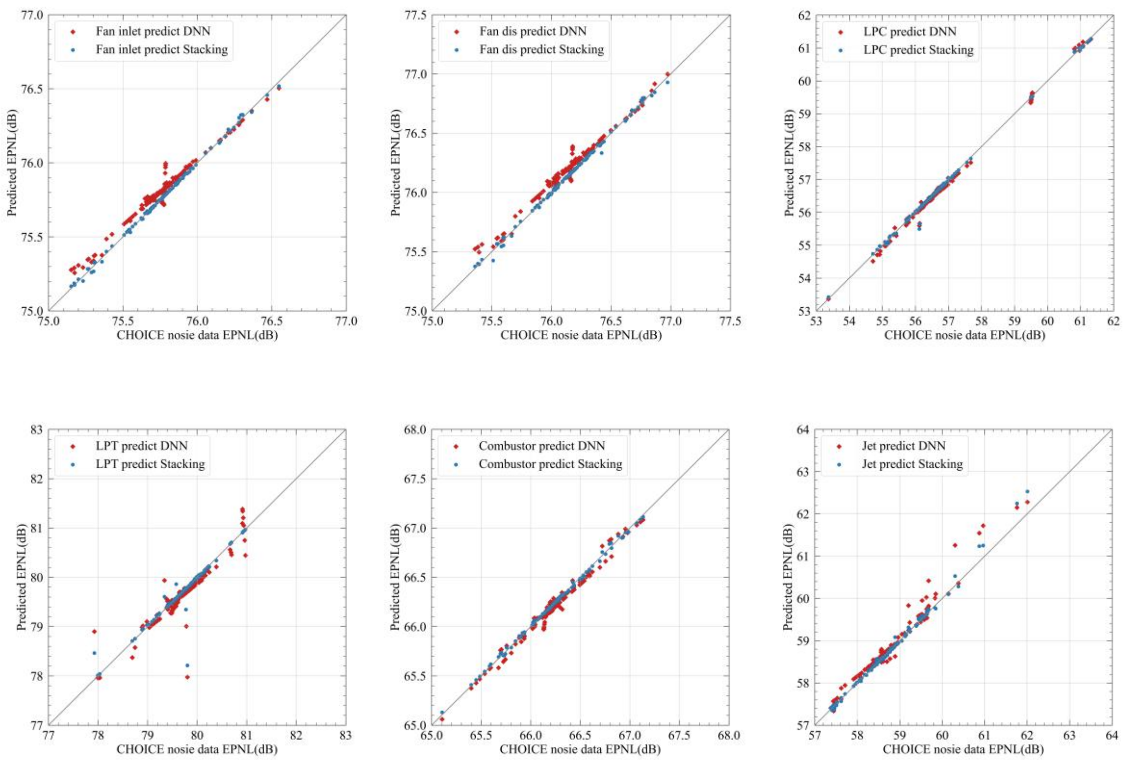

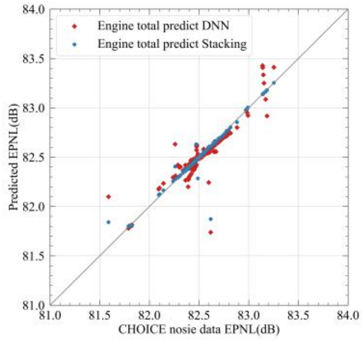

Fig.6 Comparison of all engine components EPNL prediction using DNN and Stacking Model

Engine Noise Predictions Sensitive Analysis

The sensitivities of key parameters on aircraft propulsion system noise assessment are investigated using an open-source aircraft noise prediction tool CHOICE as mentioned before. In addition, this section explores the performance of the two machine learning noise models compared to raw data when performing sensitivity analyses. Due to space limitations, altitude and Mach number were selected as the single variables for detailed analysis.

Figure 7 shows the noise variations of engine changes in altitude at the design point. Three different line styles were used to represent the CHOICE raw data, the DNN model predictions, and the stacking model predictions, respectively. The EPNL of fan inlet, fan discharge and combustor are almost unaffected by the variation of altitude. The LPC noise has an obvious step increase which is attributed to the increase in the number of compressor stages. Jet noise shows a downward trend due to the decrease in the mass flow rate decrease. As a result, Engine total noise remained as almost constant. Both the stacking model and the DNN model can predict the trend of EPNL variation. However, when faced with step changes, the stacking model predicts the trend more accurately than the DNN model, demonstrating higher overall accuracy.

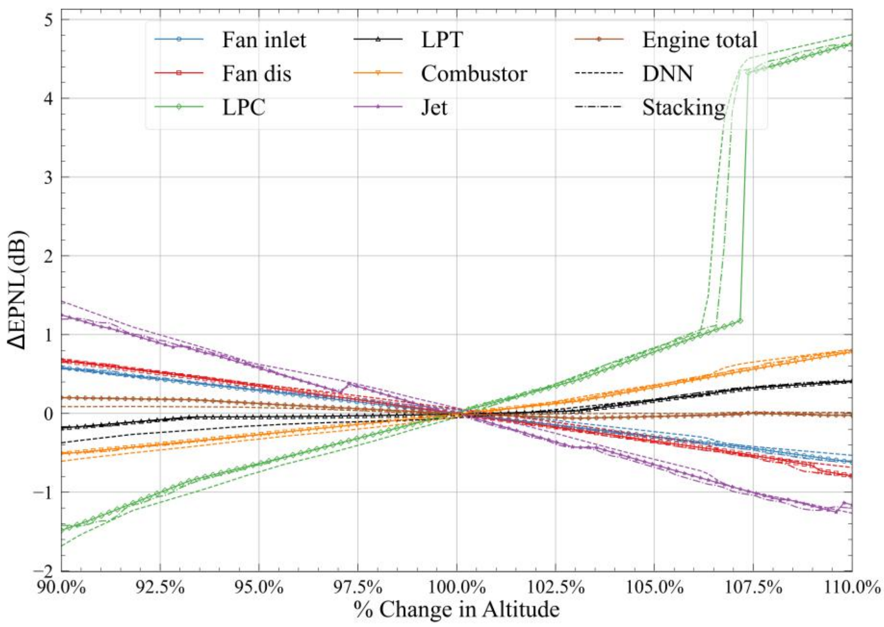

Fig.7 Variation of engine components and total noise EPNL for ±10% variation of altitude, relative to the baseline case

Figure 8 illustrates the noise variation for $\pm 10\%$ changes in flight Mach number. Fan and combustor noise showed a slight increase but remained almost constant. LPC noise showed a slight downward trend and LPT noise showed a clear step down but showed an increase after the step down occurred. Jet noise showed a clear drop followed by a gradual increase. Compared to the DNN model's more error-prone predictions, the stacking model's predictions align closely with the raw data, particularly in regions with step changes.

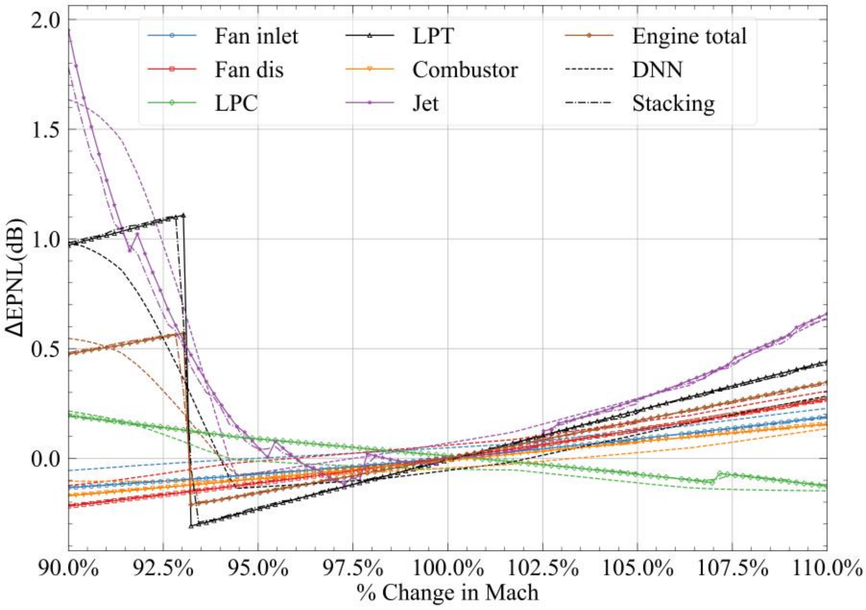

Fig.8 Variation of engine components and total noise EPNL for ±10% variation of Mach, relative to the baseline case.

The DNN model captures the global features and non-linear relationships of the data by fully utilizing the limited dataset through 5-fold cross-validation, demonstrating strong predictive capability. However, due to the limited amount of training data, the prediction accuracy of the DNN model decreases when step changes occur in the relationships between variables. In contrast, the KNN algorithm demonstrates better performance in these regions due to its inherent local approximation characteristics. KNN is a distance-based model, where predictions are based entirely on the distribution of neighboring points. The stacking model further enhances prediction accuracy by allowing the meta-function to perform a secondary integration of the DNN and KNN outputs, thereby achieving superior performance compared to either model alone.

CONCLUSIONS

In this paper, nonlinear aeroengine noise models with varying design parameters based on DNN and KNN algorithms are developed and applied to predict engine noise during the aircraft approach phase. The effect of variations in engine design point parameters on engine noise was investigated, and the performance of machine learning models was evaluated separately. In summary, the DNN and stacking models can accurately predict the noise generated by the engine during the approach phase. The RMSE values for each engine noise component on the test set are less than 0.3 dB. Compared to DNN model alone, the stacking model shows significant improvements in noise prediction for the LPC and LPT when handling step changes.

Compared to the original noise model which would take several minutes for noise prediction, the neural network adapted noise model has significantly reduced the computation time down to a few seconds while maintaining sufficient accuracy. The reduced prediction time offered by the deep neural network (DNN) is particularly valuable in the context of iterative design and optimization processes, where thousands of evaluations may be required to explore high-dimensional design spaces or perform real-time assessments. In such scenarios, cumulative time savings become substantial, making fast prediction a practical necessity rather than a convenience. However, it's worth noting that the training dataset used in this study is relatively small compared to typical machine learning applications. In future work, a more complete dataset will be utilized and the generated neural networks based noise model will be used in MDO framework for assessing its performance in engine and aircraft integrated design and optimization.

ACKNOWLEDGMENTS

This work has received funding from the Horizon Europe research and innovation programme under GA n° 101096275. This work is co-funded by UK Research and Innovation (UKRI) under the UK government's Horizon Europe funding guarantee n° 10068673.

REFERENCE

Abadi, M., Barham, P., Chen, J., Chen, Z., Davis, A., Dean, J., Devin, M., Ghemawat, S., Irving, G. and Isard, M. (2016) *12th USENIX symposium on operating systems design and implementation (OSDI 16)*.

Akdeniz, H.Y., Sogut, M.Z. and Turan, O. (2020) 'Prediction and simulation of aircraft noise in the international Eskisehir Hasan Polatkan airport (LTBY)', *Aircraft Engineering and Aerospace Technology*, 93(1), pp. 171-179. Available at: 10.1108/aeat-03-2020-0056

Baldi, P. and Sadowski, P.J. (2013) 'Understanding dropout', *Advances in neural information processing systems*, 26.

Breiman, L. (1996) 'Bagging predictors', *Machine learning*, 24, pp. 123-140.

Delfs, J., Bertsch, L., Zellmann, C., Rossian, L., Kian Far, E., Ring, T. and Langer, S.C. (2018) 'Aircraft noise assessment—From single components to large scenarios', *Energies*, 11(2), p. 429.

Dunn, D.G. and Peart, N. (1973) *Aircraft noise source and contour estimation*.

Dunn, M., Tweed, J. and Farassat, F. (1999) 'The application of a boundary integral equation method to the prediction of ducted fan engine noise', *Journal of sound and vibration*, 227(5), pp. 1019-1048.

Fink, M.R. (1977) 'Airframe noise prediction method', *Final Report*.

Fink, M.R. (1979) 'Noise component method for airframe noise', *Journal of aircraft*, 16(10), pp. 659-665.

Friedman, J.H. (2001) 'Greedy function approximation: a gradient boosting machine', *Annals of statistics*, pp. 1189-1232.

Gliebe, P., Mani, R., Connell, S., Salamah, S., Sober, J. and Coffin, R. (2022) *AST Critical Propulsion and Noise Reduction Technologies for Future Commercial Subsonic Engines Aeroacoustic Prediction Codes-Supplement: Code Descriptions and Users Guides*.

Goodfellow, I., Bengio, Y., Courville, A. and Bengio, Y. (2016) *Deep learning (1)*. MIT press Cambridge.

Grönstedt, T. (2000) *Development of methods for analysis and optimization of complex jet engine systems*. Chalmers Tekniska Hogskola (Sweden).

Guo, G., Wang, H., Bell, D., Bi, Y. and Greer, K. (2003) *On The Move to Meaningful Internet Systems 2003: CoopIS, DOA, and ODBASE: OTM Confederated International Conferences, CoopIS, DOA, and ODBASE 2003, Catania, Sicily, Italy, November 3-7, 2003. Proceedings*. Springer.

Heidmann, M. (1979) 'Interim prediction method for fan and compressor noise source', *NASA TX-71763 (June 1975)*.

Hultgren, L.S. (2010) *Core-Noise*.

Ikuta, Y., Imamura, T., Takaishi, T. and Kobayashi, T. (2023) 'Noise Prediction for Aircraft during Approach by Neural Network Using Sound Source Data Obtained from Microphone Array Measurement', *AIAA AVIATION 2023 Forum*. doi: 10.2514/6.2023-3927.

Kontos, K.B., Janardan, B. and Gliebe, P. (1996) *Improved NASA-ANOPP noise prediction computer code for advanced subsonic propulsion systems*.

LeCun, Y., Bengio, Y. and Hinton, G. (2015) 'Deep learning', *nature*, 521(7553), pp. 436-444.

Li, S. and Lee, S. (2020) 'A Machine Learning-Based Fast Prediction of Rotorcraft Broadband Noise', *Aiaa Aviation 2020 Forum*. doi: 10.2514/6.2020-2588.

Mahan, J.R. and Karchmer, A. (1991) 'Combustion and core noise', *Aeroacoustics of flight vehicles: theory and practice*, 1, pp. 483-517.

Mahashabde, A., Wolfe, P., Ashok, A., Dorbian, C., He, Q., Fan, A., Lukachko, S., Mozdzanowska, A., Wollersheim, C. and Barrett, S.R. (2011) 'Assessing the environmental impacts of aircraft noise and emissions', *Progress in Aerospace Sciences*, 47(1), pp. 15-52.

Maria Thoma, E., Grönstedt, T., Otero Sola, E. and Zhao, X. (2024) 'Assessment of an Open-Source Aircraft Noise Prediction Model Using Approach Phase Measurements', *Journal of Aircraft*, 61(3), pp. 745-760. Available at: 10.2514/1.C037332

Matta, R., Sandusky, G. and Doyle, V. (1977) *GE Core Engine Noise Investigation-Low Emmission Engines*. Department of Transportation, Federal Aviation Administration, Systems ….

Mendoza, J., Nance, D. and Ahuja, K. (2008) *14th AIAA/CEAS Aeroacoustics Conference (29th AIAA Aeroacoustics Conference)*.

Meyer, H.D. and Envia, E. (1996) *Aeroacoustic analysis of turbofan noise generation*.

Nark, D., Envia, E. and Burley, C. (2009) *15th AIAA/CEAS Aeroacoustics Conference (30th AIAA Aeroacoustics Conference)*.

Redonnet, S., Bose, T., Seth, A. and Li, L.K.B. (2024) 'Airfoil self-noise prediction using deep neural networks', *Engineering Analysis with Boundary Elements*, 159, pp. 180-191. Available at: 10.1016/j.enganabound.2023.11.024

Revoredo, T., Mora-Camino, F. and Slama, J. (2016) 'A two-step approach for the prediction of dynamic aircraft noise impact', *Aerospace Science and Technology*, 59, pp. 122-131. Available at: 10.1016/j.ast.2016.10.017

Ribner, H.S. (1981) 'Perspectives on jet noise', *AIAA journal*, 19(12), pp. 1513-1526.

Russell, J.W. (1984) *An empirical method for predicting the mixing noise levels of subsonic circular and coaxial jets*.NASA.

Sen, R., Hardy, B., Yamamoto, K., Guo, Y. and Miller, G. (2004) 'Airframe noise sub-component definition and model'.

Steinbach, M. and Tan, P.-N. (2009) 'kNN: k-nearest neighbors', in *The top ten algorithms in data mining*. Chapman and Hall/CRC, pp. 165-176.

Tenney, A.S., Glauser, M.N. and Lewalle, J. (2018) 'A Deep Learning Approach to Jet Noise Prediction', *2018 AIAA Aerospace Sciences Meeting*. doi: 10.2514/6.2018-1736.

Ventres, C., Theobald, M. and Mark, W. (1982) *Turbofan noise generation. volume 1: Analysis*.

Wolpert, D.H. (1992) 'Stacked generalization', *Neural networks*, 5(2), pp. 241-259.

Zaporozhets, O., Tokarev, V. and Attenborough, K. (2011) *Aircraft Noise: Assessment, prediction and control*. CRC Press.

Zaporozhets, O.I. and Tokarev, V.I. (1998) 'Aircraft noise modelling for environmental assessment around airports', *Applied Acoustics*, 55(2), pp. 99-127.

Zhang, Q., Wang, X., Yang, D. and Zhang, W. (2024) 'Data-driven prediction of aerodynamic noise of transonic buffeting over an airfoil', *Engineering Analysis with Boundary Elements*, 163, pp. 549-561. Available at: 10.1016/j.enganabound.2024.04.006

Zhang, Q., Yang, D. and Zhang, W. (2024) 'Optimal transonic buffet aerodynamic noise PSD predictions with Random Forest: Modeling methods and feature selection', *Aerospace Science and Technology*, 150 Available at: 10.1016/j.ast.2024.109245

Zhang, Q. and Zhang, W. (2024) 'A hybrid approach for reconstruction of transonic buffet aerodynamic noise: Integrating random forest and compressive sensing algorithm', *Aerospace Science and Technology*, 152 Available at: 10.1016/j.ast.2024.109379

APPENDIX A - COPYRIGHT/OPEN ACCESS

APPENDIX B - GPPS Presenter Policy and Paper Acceptance

According to GPPS's presenter attendance policy, a paper cannot be published or indexed and may not be cited as a published paper until at least one author pays the registration fee and attends the conference. The GPPS reserves the right to withdraw from its publications any paper that is not presented by an author of the paper at the appropriate conference. Any paper that is withdrawn may not be cited as a published paper.

Aircraft Trajectory Noise Modeling with Physics Informed Multi-Channel Attention U-Net

Chenzhao Li[1], Shuai Li[1], Xin Zhao[1,*]

[1] Department of Mechanical Engineering, Chalmers University of Technology, 41296 Gothenburg, Sweden

ARTICLE INFO

Article history:
Received
Received in revised form
Accepted
Available online

Keywords:

Aircraft Trajectory Noise Prediction;
Deep Neural Network; Attention UNet;

ABSTRACT

Conventional best practice and physics-based noise prediction methods exhibit limitations in computational efficiency and input data requirements when applied to multidisciplinary integrated design of future aircraft and real-time trajectory-level noise assessment. To address this challenge, this study proposes a Density-Guided Physics-Informed Attention U-Net (DGPIA U-Net) for rapid predicting two-dimensional aircraft noise fields. The proposed framework uses U-Net architecture as its backbone and introduces density-guided physics-informed maps generated through adaptive Gaussian kernel diffusion to transform sparse trajectory information into continuous spatial influence fields. Furthermore, squeeze-and-excitation channel attention and bottleneck spatial attention are incorporated to enhance the weighting of heterogeneous physical variables and improve spatial feature representation. The model is trained and evaluated using 606 take-off noise cases generated by a semi-empirical aircraft noise prediction code for an A320-like aircraft departing from Manchester Airport Runway under different routes. These routes were constructed by varying heading deviations and noise abatement departure procedures. Comprehensive evaluations demonstrate that the proposed DGPIA U-Net accurately reconstructs EPNL noise contours while achieving prediction speeds approximately 2–3 orders of magnitude faster than CHOICE. Compared with the standard U-Net, DGPIA U-Net improves RMSE by 37% in regions above 40 dB and by 23% in regions above 90 dB. These results indicate that the proposed model can efficiently and accurately predict trajectory-dependent aircraft noise fields under various departure conditions.

1. Introduction

With the continued expansion of the aviation industry, aircraft noise pollution in areas surrounding airports has become increasingly prominent and has emerged as an important research topic in the field of environmental health. A substantial body of research has shown that aircraft noise has kinds of effects on both psychological and physiological human health[1]. Long-term exposure to high levels of aircraft noise may lead to sleep disturbance, high risk hypertension, reduced attention, and impaired learning efficiency[2–4]. These effects are often more obvious in

* *Corresponding author.*
E-mail address: xin.zhao@chalmers.se

vulnerable populations, including children, older adults, and individuals susceptible to cardiovascular disease and pregnant women leading to low birth weight[5–7]. Aircraft noise management is therefore critical for lowering noise exposure in communities near the airport. To include noise pollution related public health concerns in the development of sustainable airport operations, the assessment and prediction of aircraft noise from departures and arrivals is essential.

Noise prediction method based on flight trajectories and aircraft performance makes it possible to estimate, prior to flight execution, the local airport noise impacts associated with different operations. Such predictive capability is valuable for trajectory optimization, for example by avoiding flying over densely populated areas[8], designing continuous descent operations to reduce thrust requirement and noise[9], and customizing optimized noise abatement departure procedures[10]. This provides a foundation for multi-objective flight optimization that simultaneously accounts for operational efficiency and environmental impacts. Research on aircraft noise prediction methods can generally be classified into two major categories: (1) best practice methods and (2) theoretical methods[11].

The best practice approach can be traced back to 1978, when the Federal Aviation Administration (FAA) introduced the Integrated Noise Model (INM)[12], a program that has since been widely used by airports and regulatory authorities around the world. This computational tool provides a relatively simple framework for estimating aircraft noise in the vicinity of airports and assessing its impact on surrounding communities with only a small set of input parameters. Specifically, the method relies on extensive empirical formulations, such as flyover measurement data and other experimental observations, to calculate the noise level at a given receiver location based on noise–power–distance (NPD) data, engine thrust and atmospheric conditions. Similar approaches have also been adopted in several other countries, including the ANCON model in the United Kingdom[13], FLULA in Switzerland[14], and the SIMUL and AzB codes in Germany[15,16]. These models are based on NPD databases combined with different sound-propagation attenuation models or statistical approaches to perform noise prediction. The IMPACT developed by EURONCONTROL used aircraft noise and performance (ANP) database for noise modelling purposes. ANP was collected by EUROCONTROL and the U.S. Federal Aviation Administration (FAA) and then verified by the FAA/U. S [MISS the reference]. The NPD/ANP databases themselves benefit from large volumes of historical data, including radar trajectory records and real-time ground microphone measurements of noise exposure levels. Consequently, best practice methods are inherently constrained by the substantial financial and logistical resources required to establish and maintain a comprehensive database infrastructure.

Theoretical methods build physical modeling of noise generation and propagation. The development of theoretical aircraft noise prediction can be traced back to the early 1970s, when FAA and NASA started to predict the noise generated by single flyover events. One of the earliest computational tools developed for this purpose was ANOPP (Aircraft Noise Prediction Program), established at NASA Langley[17,18]. In this framework, aircraft flight dynamics were coupled with semi-empirical models describing the generation and propagation of noise from various sources, including the fan, compressor, jet exhaust, wings, and landing gear. The propagation module accounted for physical effects on the received noise, such as spherical spreading, atmospheric attenuation, and ground reflection. Subsequently, the second-generation framework, ANOPP2, introduced substantial advancements, partially incorporating computationally intensive high-fidelity methods[19,20]. Most source and propagation models have since been investigated and developed independently. Correspondingly, each model typically requires a large number of input parameters and huge computational source to ensure adequate computational accuracy. This approach, which predicts aircraft noise by combining individual discrete noise sources with empirical or semi-empirical formulations, has subsequently achieved substantial progress. Filippone, Marily etc. developed integrated aircraft noise-prediction frameworks FLIGHT and CHOICE that require moderate computational demand while maintaining relatively high predictive accuracy, based on publicly available semi-empirical methods[21–23]. Nevertheless, the prediction of trajectory-dependent aircraft noise still requires considerable computational resources, including the time for computing detailed aircraft and engine performance data input. In addition, the German Aerospace Center (DLR) developed the PANAM code as a tool for aircraft noise design and assessment, with a particular emphasis on comparative noise evaluation across different aircraft configurations[24]. To provide rapid solutions and efficient analysis capability, PANAM accounts only for the dominant noise contributions in the overall aircraft noise prediction. Engine noise is represented solely by jet and fan noise components. As a result, the computational efficiency is improved, but at the expense of prediction accuracy.

In recent years, with the rapid advancement of artificial intelligence, many people focus on the application of machine learning to aircraft noise prediction. This technique applies such as artificial neural networks, random forests, and convolutional neural networks (CNN), machine-learning-based methods to extract informative physical features, achieving fast and accurate prediction. As the first to apply machine learning to the prediction of aeroacoustics, Tenney et al. quantified the effects of feature space, learning rate, and network architecture on model performance, demonstrated the high prediction accuracy of a deep neural network (DNN) predicting jet noise for far-field overall sound pressure level[25]. Subsequently, an increasing number of researchers have attempted to integrate physical information with machine-learning models, establishing new methodologies for aircraft noise study. Based on experimental measurements, Zhang et al. developed a noise spectral deep learning (NSDL) approach to predict landing-gear aerodynamic noise[26]. In this framework, an encoder was used to extract the dominant characteristics of the noise spectrum, while a multi-layer perception (MLP) was employed to establish the mapping between these features and flow parameters such as velocity and angle of attack. In a series of subsequent studies, Zhang and co-workers used high-fidelity computational fluid dynamics (CFD) results as the database for machine learning, and achieved accurate prediction of airfoil aerodynamic noise by means of random forest and compressed sensing algorithms[27,28]. These studies focus on applying machine learning techniques in the prediction of component level noise sources from high fidelity simulations and experiments, to reduce the demand of large number of simulations and tests. At overall aircraft level, Wu and Redonnet extracted a wide range of aircraft airframe structural and flight performance parameters as inputs and developed a simplified whole-aircraft noise prediction model using a multivariate linear regression-based machine learning approach. The model demonstrated high predictive accuracy; however, its outputs were limited to two specific noise monitoring locations[29]. Suat Toraman and co-workers employed random forest and long short-term memory (LSTM) approaches to develop aircraft noise prediction models at the approach, sideline, and cutback certification points[30]. Using publicly available noise databases for Airbus and Boeing aircraft, they extracted practical operational parameters, such as aircraft weight and engine thrust, as model inputs. Although the model demonstrated relatively high predictive accuracy, its outputs were limited to noise estimates at only three certification points, and lack of noise impact over the area covered by the flight trajectory which is more crucial for realistic flight operation.

In summary, the integration of machine learning with physical information has achieved promising progress in the prediction of individual aircraft noise sources, such as jet noise, airfoil noise, and landing-gear noise. However, the prediction of trajectory-dependent noise for the whole aircraft deploying machine learning techniques is still missing. Significant limitations exist in traditional best practice methods and theoretical methods that highly detailed aircraft and propulsion data input are required as well as relatively high computational cost. Even minutes of computation for noise, in multidisciplinary integrated design of future aircraft and air traffic system combining hundreds of aircraft and near-airport operational procedures, is a bottle neck for real-time and large-scale air traffic applications. Therefore, this study focuses on developing a physics-informed machine learning framework for whole aircraft trajectory noise prediction in milliseconds level. First, based on the ordinary physics feature input extracted, the density guided map using Gaussian kernel diffusion and physical information was introduced to convert the sparse trajectory physics information to a continuous spatial influence map, enabling robust learning of noise propagation. Second, the U-Net network is trained to transform field inputs embedded with physical information into noise field outputs. Building upon the standard U-Net architecture, squeeze-and-excitation attention (SE) mechanism was applied to adaptively adjust the weights of multiple input physical quantities during training, facilitating faster convergence. In addition, spatial attention mechanism was used to perform residual enhancement at each spatial location across all bottleneck feature channels, strengthening model spatial representation capability.

2. Method

2.1 Data generation and process

The trajectory aircraft noise mapping datasets used for machine learning model training were generated by the Chalmers Noise Code (CHOICE) which is an open-source framework with the capability of predicting the source noise level, for every frequency and longitudinal directivity, from individual airframe and engine components and the entire aircraft[23]. The CHOICE noise estimation of aircraft trajectory was based on empirical and semi-empirical noise models found in published literature[31–34]. CHOICE computes the Effective Perceived Noise Level (EPNL) in the vicinity of the flight trajectory based on the input trajectory coordinates and the corresponding flight-state parameters at each trajectory point, including physical variables such as airspeed, climb rate, and engine thrust.

In this study, the departure procedure of an A320-like aircraft from Runway 05R at Manchester Airport was selected as study case. By varying the post-liftoff horizontal flight trajectory and the vertical climb profiles associated with different departure procedures, a noise database covering a range of flight trajectories was established. In the horizontal plane, three officially published departure procedures for Runway 05R at Manchester Airport—ASMIM, LISTO2Z, and DESIG1Z—were considered, and the flight heading after liftoff was changed. The heading deviation ranged from −25° to +25°, with an increment of 0.5° for each variation, the parameter variations as shown in table 1. In the vertical plane, two different noise abatement departure procedures (NADP)[10], NADP1 and NADP2 were adopted. The main difference between them lies in their noise control objectives. NADP1 is primarily intended to mitigate noise in areas close to the airport, as the aircraft usually maintain a steeper climb for a longer period and low air speed after takeoff, thereby reducing noise exposure near the runway. In contrast, NADP2 is mainly aimed at reducing noise in areas farther from the airport, as it generally initiates acceleration and configuration cleanup earlier, which helps lower the noise impact in regions located farther along the departure path. In accordance with the official guidance, the flight altitude was constrained to 5,000 ft. All trajectory noise results were generated using CHOICE. Based on different horizontal trajectories and two distinct vertical climb procedures, a total of 606 trajectory noise files were produced to serve as the database for the model, the 3D diagram of trajectories database as shown in Fig 1.

Table 1
Summary of datasets

Parameter	Value
Runway 05R take off procedure	ASMIM, LISTO2S, DESIG1S
NADP operation	NADP1, NADP2
Heading deviation angle α	−25° ~ +25°, Δ α=0.5°
Total take off procedure cases	606

For each flight case, the raw trajectory data and the corresponding EPNL results were first converted into a trajectory-aligned two-dimensional computational grid. The grid was constructed using the first and last trajectory points as the longitudinal reference axis, while the transverse direction was defined as the normal direction to the flight path, and the grid extent was adaptively determined to cover the effective EPNL results field. Because of the differences in each takeoff route, the noise mapping size generated by CHOICE varies. Therefore, before training begins, padding was

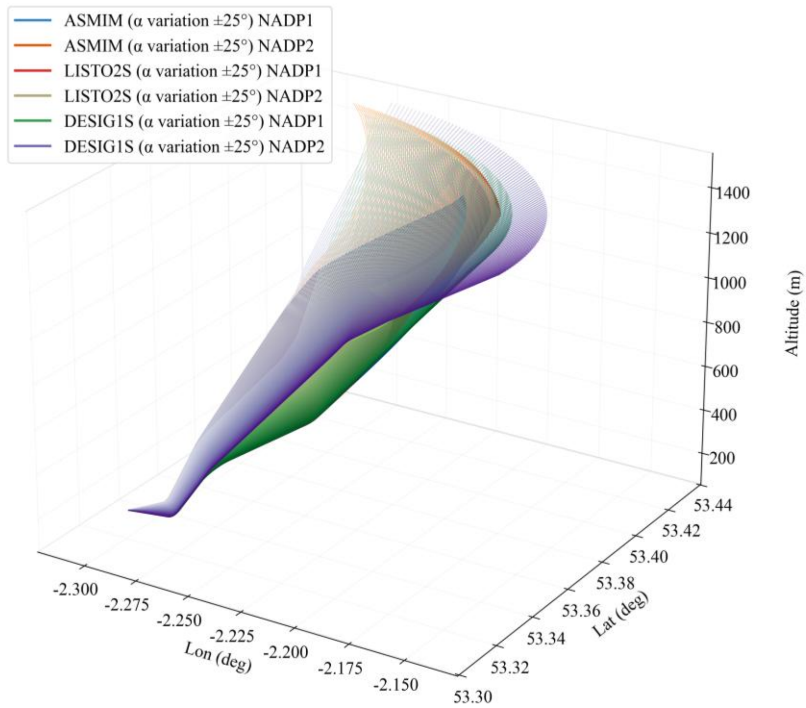

Fig. 1. 3D diagram of trajectories database

used to unify all labeled results to the maximum noise mapping size. The two-dimensional field size of the input and output is 115×172. The model input consisted of heterogeneous physical and spatial feature maps. Eleven trajectory-related physics variables were used as input channel, including time, true air speed, ground speed, Mach number, height, distance, flaps angle, slats angle, landing gear state, airfoil angle of attack and aircraft climb rate. Before being passed to the neural network, each continuous input channel was standardized using training-set statistics. For a given channel c , the global mean μ_c and standard deviation σ_c were computed by aggregating all valid grid values from the training cases. The normalized input was then obtained as Eq. (1):

$$\widehat{X_c}(i,j) = \frac{X_c(i,j)-\mu_c}{\sigma_c} \tag{1}$$

This operation maps heterogeneous physical quantities, such as trajectory-referenced distance, speed, Mach number, altitude and aircraft configuration variables, onto a comparable dimensionless scale. Signed Distance Functions (SDF)provide spatial distance field with trajectory and computational grid, as shown in Fig.2. The trajectory was first projected from geographic coordinates into a local Cartesian coordinate system. The flight path was then represented as a two-dimensional polyline composed of consecutive trajectory points. For each grid cell, the SDF value was computed as the shortest Euclidean distance from the grid point to the trajectory polyline:

$$D_{SDF(i,j)} = \min_k \left|\left|G(i,j) - Q_k\right|\right| \tag{2}$$

Where $G(i,j)$ denotes the Cartesian coordinate of the grid cell (i,j), and Q_k is the closest projected point on the k -th trajectory segment. In the current model, the unsigned form of the SDF is used. Therefore, $D_{SDF(i,j)} \geq 0$, and the channel encodes the distance magnitude from each grid cell to the nearest point on the flight trajectory. In addition, a binary mask map indicates whether a grid point is valid targe or padding. Providing this mask as an input to the model facilitates the construction of the loss function, enabling the model to focus more on the valid regions.

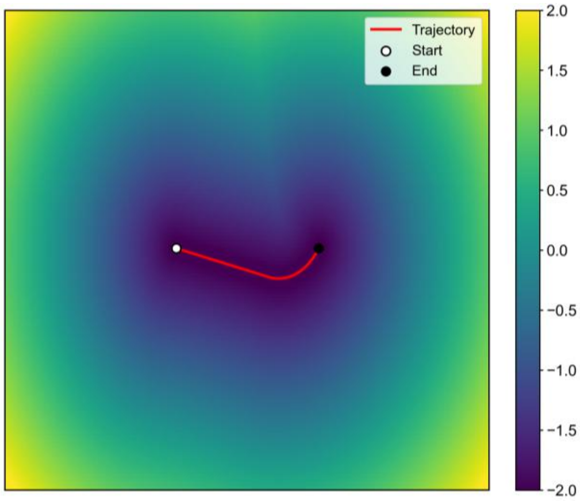

Fig. 2. The schematic diagram of SDF on the computational grid

2.2 Density-Guided Physics-Informed Attention U-Net (DGPIA U-Net)

As shown in Fig.3, Density-Guided Physics-Informed Attention U-Net (DGPIA U-Net) model is designed to reconstruct the two-dimensional distribution of effective perceived noise level (EPNL) from multi-channel input features. Model comprises two key components: a) multi density guided map, b) the U-Net network with attention mechanisms. Density-guided maps are introduced as physics-informed spatial prior inputs by using adaptive Gaussian kernels. Multi-scale density maps are generated by projecting trajectory points onto the grid using adaptive Gaussian kernels modulated by flight height, speed, and their interaction. They provide physics-informed spatial priors that indicate where trajectory-induced noise influence is stronger. The standard U-Net is used as the main encoder-decoder architecture for EPNL field reconstruction. The encoder progressively extracts multi-level features from the channels input feature maps through convolutional blocks and downsampling operations. Then the decoder restores the spatial resolution through upsampling layers and skip connections. The final 1×1 convolution maps the decoded feature representation to a single-channel EPNL prediction. Attention mechanisms include channel SE attention, Bottleneck spatial attention. They help the model focus on important physical variables, feature channels, and spatial regions relevant to EPNL prediction. The details of the above components are provided in Section 2.2.1 to 2.2.2

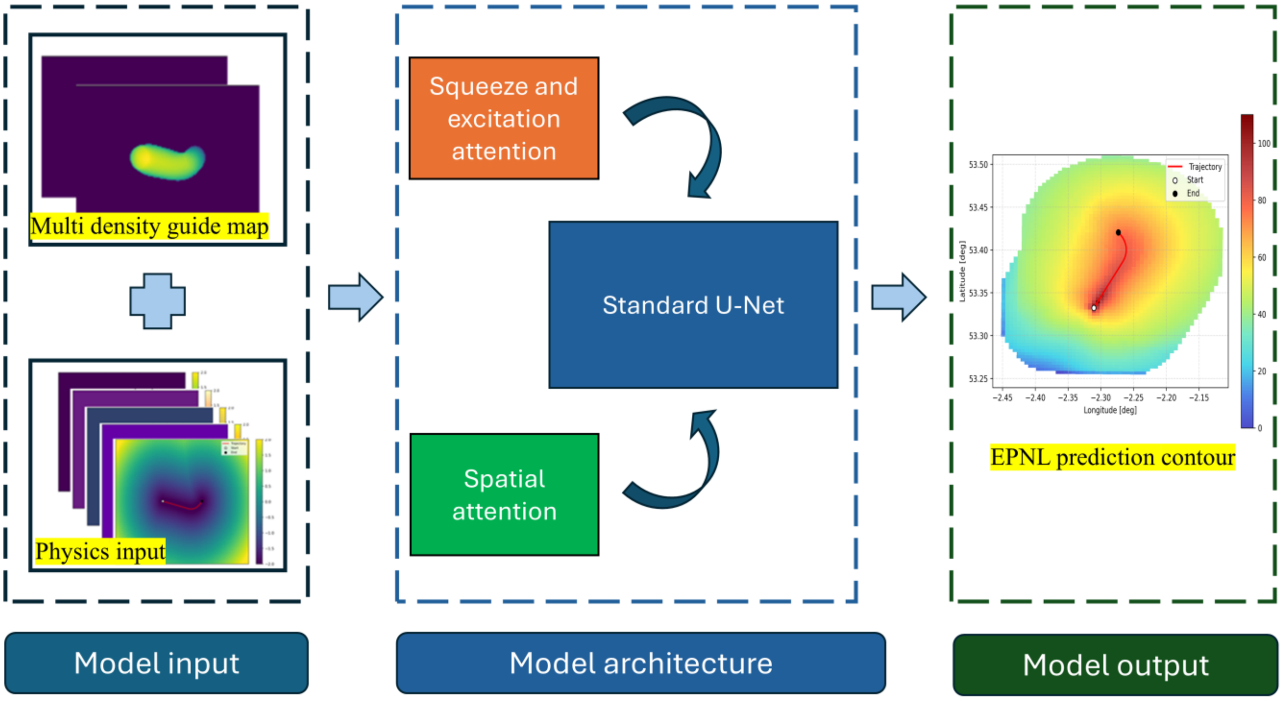

Fig. 3. Density-Guided Physics-Informed Attention U-Net (DGPIA U-Net) model framework

2.2.1 Density guided map based on Gaussian kernel diffusion and physical information

In the present model, the density map used as a physics-informed prior input that transforms discrete flight-trajectory points into a continuous two-dimensional influence field. The original trajectory consists of a sequence of discrete points, each point containing the aircraft physical state at a given time instant, including altitude, speed and other variables. Compared with the output of a two-dimensional noise field, the original trajectory physical information serve as model input is sparse. Therefore, the density guide map was applied to construct a continuous spatial influence map through Gaussian diffusion. Specifically, for a trajectory point $p_i = (x_i, y_i)$ and a grid cell $g_{m,n} = (x_{m,n}, y_{m,n})$, their Euclidean distance is defined as Eq. (3):

$$d_{i,m,n} = ||g_{m,n} - p_i||_2 \quad (3)$$

The Gaussian contribution from the i-th trajectory point to the grid cell $(m, n)$is calculated as Eq. (4):

$$w_{i,m,n} = \exp\left[-\frac{1}{2}\left(\frac{d_{i,m,n}}{\sigma}\right)^2\right],\ d_{i,m,n} \le R \quad (4)$$

where σ is the Gaussian standard deviation and R is the truncation radius. If $d_{i,m,n} > \mathrm{R}$, the contribution is set to zero. The density value at each grid cell is then obtained by accumulating the Gaussian contributions from all trajectory points:

$$D_{m,n} = \sum_{i=1}^{N} 1\left(d_{i,m,n} \leq R\right) w_{i,m,n} \tag{5}$$

This formulation converts the sparse trajectory line into a continuous density field, where larger values indicate stronger influence from nearby trajectory segments. Compared with sparse trajectory line, the Gaussian density map provides smoother spatial guidance and allows the model to perceive not only where the trajectory is located, but also how its influence decays with distance. Additionally, to further incorporate flight-state information, the Gaussian diffusion range was adaptively modified using aircraft height and speed. The height $\widetilde{h_i}$ and speed $\widetilde{v_i}$ of each trajectory point were first normalized as:

$$\widetilde{h_i} = 1 - \frac{h_i - h_{min}}{h_{max} - h_{min}} \ , \ \widetilde{v_i} = \frac{v_i - v_{min}}{v_{max} - v_{min}} \tag{6}$$

The adaptive influence coefficient was then computed with an interaction term between low altitude and speed as:

$$\alpha_i = 1 + \widetilde{h_i} + \widetilde{v_i} + \widetilde{h_i}\widetilde{v_i} \tag{7}$$

The Gaussian standard deviation and truncation radius for each trajectory point were then adjusted as:

$$\sigma_i = \sigma_0 \alpha_i, \ R_i = R_0 \alpha_i \tag{8}$$

where σ_0 and R_0 are the base Gaussian standard deviation and radius. With this adaptive formulation, low-altitude and high-speed trajectory segments are assigned to broader spatial influence regions. This reflects the physical assumption that aircraft operating closer to the ground and at higher speeds are more likely to contribute strongly to ground-level noise exposure. The interaction term further enhances the influence of trajectory points where low altitude and high speed occur simultaneously. After applying the adaptive correction, the final density map is computed as:

$$D_{m,n} = \sum_{i=1}^{N} 1\left(d_{i,m,n} \leq R_i\right) \exp\left[-\frac{1}{2}\left(\frac{d_{i,m,n}}{\sigma_i}\right)^2\right] \tag{9}$$

In the present model, two density maps are generated at different scales: $\sigma_{01} = 1200m, R_{01} = 1200m$ and $\sigma_{02} = 600m, R_{02} = 600m$. This allows the network to capture both local trajectory-near effects and broader noise-influence patterns.

2.2.2 U-Net architecture with attention mechanisms

U-Net is a specific convolutional neural network initially used for biomedical image segmentation [35]. In this paper, the standard architecture of U-Net has been modified with attention mechanisms to make it more suitable for noise field prediction tasks. As shown in figure 4, structurally, the proposed model adopts a classical encoder–decoder architecture, comprising an encoding path enhanced with SE attention[36], a bottleneck module incorporating spatial attention[37], and a corresponding decoding path. First, SE attention is applied before all input channels are fed into the U-Net. Specifically, for each input channel, global average pooling is first performed and then passed through a two-layer fully connected network to learn channel-wise weights, which are subsequently multiplied back to the original input channels. The SE module enables the model to more efficiently identify and emphasize the most informative feature channels during training, thereby facilitating feature extraction and improving model convergence. The encoder contains three down sampling stages. The initial number of feature channels is set to 32 and increased in the encoder to enhance the representation capacity for complex spatial patterns. Each stage is composed of a convolutional block followed by a 2×2 max-pooling layer. Within each convolutional block, two successive 3×3 convolutional layers are used, and each convolution is followed by batch normalization and ReLU activation.

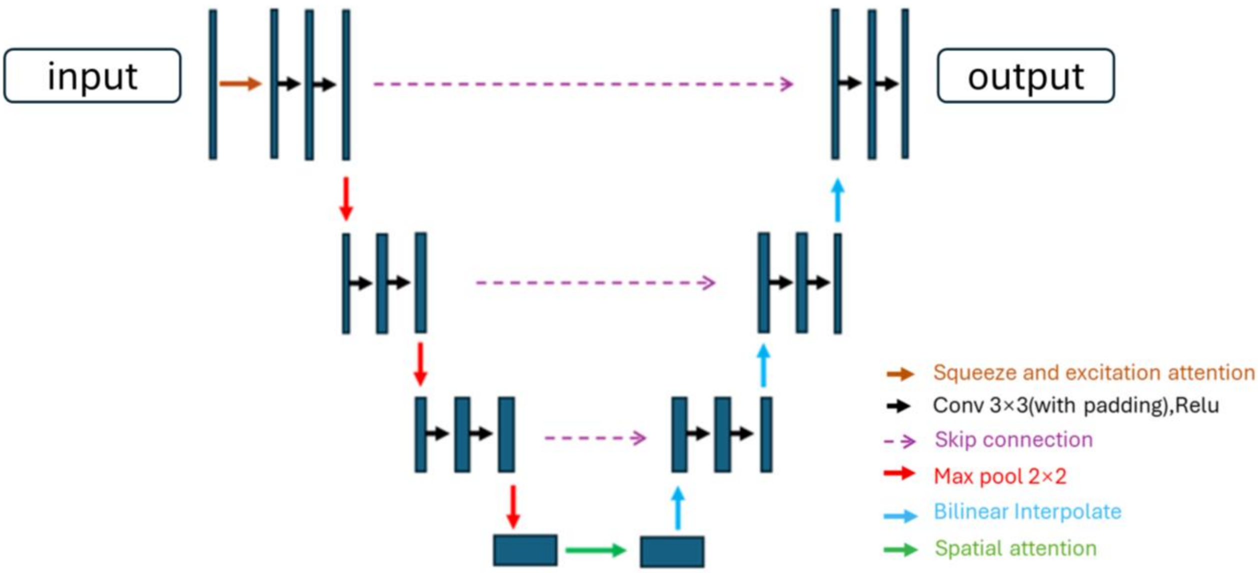

Fig. 4. U-Net architecture with attention mechanisms

A spatial attention mechanism used at the bottleneck of the current U-Net model. Specifically, after three down sampling operations, the resulting feature map is subjected to both average pooling and max pooling along the channel dimension. The pooled feature maps are then concatenated to generate a spatial attention map. This spatial attention map is subsequently used to perform residual enhancement at each spatial location across all bottleneck feature channels. In this way, the model can emphasize spatially informative regions within the compressed information, thereby strengthening its spatial representation capability.

The decoder mirrors the encoder and comprises three up sampling blocks. In each block, transposed convolution is first used to increase spatial resolution, after which the up sampled feature maps are concatenated with the corresponding encoder features through skip connections. This skip-connection mechanism preserves low-level spatial details that may otherwise be lost during repeated down sampling. When minor mismatches in spatial dimensions occur, bilinear interpolation is used to align the feature maps before concatenation.

Finally, a 1×1 convolutional layer is applied to project the decoded features onto a single output channel, the predicted EPNL field. By combining the spatial reconstruction capability of U-Net with the SE and spatial attention, the proposed SE-U-Net is able to model complex nonlinear relationships among heterogeneous input variables while maintaining strong sensitivity to localized spatial structures.

2.2.3 Data-Driven loss function

The model was optimized using a masked mean squared error loss with an additional boundary-aware weighting mechanism. Since target noise maps may contain padded regions, the loss was not computed over the entire rectangular grid. Instead, a binary mask was used to restrict the optimization to valid target pixels. The $\hat{Y}_{i,j}$ denote the predicted EPNL value at grid cell, and $Y_{i,j}$ denote the corresponding CHOICE value. The binary mask is denoted as $M_{i,j}$, where $M_{i,j} = 1$ indicates a valid target pixel and $M_{i,j} = 0$ indicates a padded pixel. The basic masked MSE loss is defined as:

$$L_{mask} = \frac{\sum_{i,j} M_{i,j}\left(\hat{Y}_{i,j} - Y_{i,j}\right)^2}{\sum_{i,j} M_{i,j}} \tag{10}$$

This formulation ensures that only physically meaningful target regions contribute to the training objective. Pixels outside the valid target mask do not affect the gradient update, which is particularly important when different flight cases have different spatial extents which are padded to a common size during batch training.

Due to the computational domain size limitation of the CHOICE model, the noise field calculation results are close to 20 dB but not zero at some computational domain boundaries. Therefore, the target result obtained using nearest neighbor interpolation for the model training may contain errors at the outer edges. Accounting for uncertainty near the boundary of the valid target region, a boundary-aware weighting mechanism was introduced. A sequence of boundary rings from the outer edge toward the interior. Each ring was assigned a predefined weight, with lower weights near the outer boundary and higher weights toward the interior region. In the current implementation, the ring weights are [0.1,0.3,0.5,0.7,0.9], while the remaining inner valid region is assigned a weight of 1.0. The final boundary-weighted masked MSE is then written as:

$$L = \frac{\sum_{i,j} M_{i,j} E_{i,j}\left(\hat{Y}_{i,j} - Y_{i,j}\right)^2}{\sum_{i,j} M_{i,j} E_{i,j}} \tag{11}$$

Here, $E_{i,j}$ down-weights pixels close to the boundary of the valid region, while preserving their contribution to the loss. All valid pixels involved in optimization, but boundary pixels contribute less strongly according to their ring weights. This strategy encourages the model to primarily learn the physically more reliable interior noise field, rather than overfitting to boundary errors introduced by interpolation. Consequently, the predictive capability of the model may be reduced near the noise boundary. However, these outer boundary regions usually correspond to low-noise areas and are therefore not the primary focus in aircraft noise prediction.

3. Results

3.1 DGPIA U-Net model simulation and analysis of results

The dataset was divided into training, validation and test sets with ratio of 8:1:1. The model was trained using the Adam optimizer developed by the PyTorch Machine Learning Library[38], with an initial learning rate of 0.001 and learning rate decay factor of 0.5. When the validation loss failed to improve by 0.001 for 25 consecutive epochs, the learning rate was reduced to half of its value, with a minimum learning rate of 5×10^{-5}. To avoid overfitting, an early-stopping method was employed, which was triggered when the validation loss remained effectively unchanged for 100 consecutive epochs. All reported results represent the average outcomes from five independent training runs with different random seeds, ensuring statistical reliability and reproducibility of findings.

Fig. 5 illustrates the iteration process of the loss function during the training and validation of the model, which achieved convergence at approximately the 200th iteration. The total training time was approximately 12 h on a hardware environment equipped with a 13th Gen Intel(R) Core (TM) i7-1365U CPU, 32 GB RAM. Once trained, the DGPIA U-Net model achieved noise-field prediction speeds in milliseconds level that were 2–3 orders of magnitude faster than those of CHOICE, while maintaining high predictive accuracy.

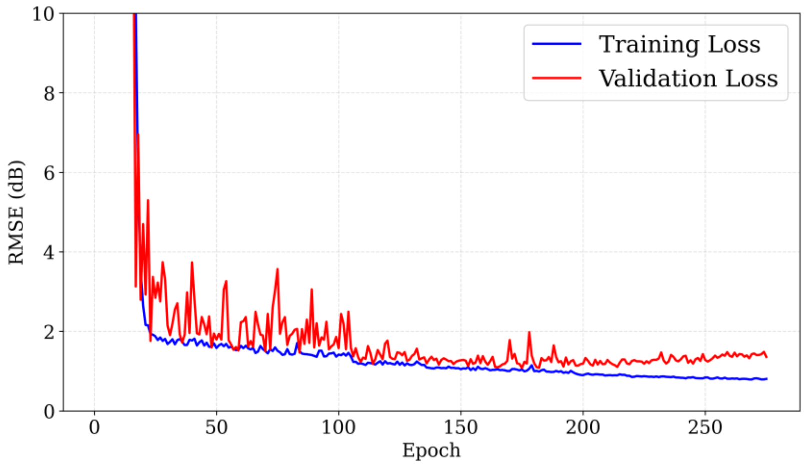

Fig. 5. Learning curve of DGPIA U-Net model

The DGPIA model was applied for experimental validation through the test set to show the noise field prediction capability. The following Figure 6 presents the contour diagrams of the CHOICE, DGPIA model prediction, and errors results for takeoff procedure from EGCC Runway 05R ASMIM heading deviation -10° with NADP1 operation. The RMSE and MAE value of model is 0.85dB and 0.42dB. The noise contour predicted by the model is basically the same as CHOICE. A more detailed error distribution reveals that errors occur primarily near the outer edge regions with low noise levels, as well as in the high-noise region around the center. As discussed previously, the loss function adopted during model training incorporates a boundary-weighting strategy, which weakens the model's predictive capability near the outer boundaries to some extent. Therefore, additional error analyses were conducted for regions where the noise level exceeded 40 dB and 50 dB, respectively. For the region above 40 dB, a limited number of high-error areas can still be observed near the prediction boundary. However, when the threshold is increased to 50 dB, the boundary-related high-error regions disappear completely. Figure 7 shows zoomed-in contour maps of the high-noise region, including the CHOICE reference results, DGPIA model predictions, and errors. The comparison indicates that relatively large prediction errors are primarily concentrated in regions with steep spatial gradients in the noise contours after take-off. The steep spatial gradients in the EPNL contours are mainly associated with the initial climb phase, during which the aircraft operates at low altitude and high thrust, leading to rapid variations in the dominant noise sources. Moreover, aircraft engine noise is characterized by pronounced directivity, with jet noise and fan noise exhibiting stronger radiation towards the rear of the aircraft[11,39,40].

Figure 8 shows the prediction accuracy of different models for this test case. As shown in Fig. 8(a), in regions with EPNL thresholds above 40 dB, all three models achieve RMSE values below 1 dB. Among them, the DGPIA model obtains the lowest RMSE of 0.32 dB, whereas the standard U-Net exhibits the highest RMSE of 0.61 dB. As the EPNL threshold increases, all three models reach their minimum RMSE in regions above 50 dB. Beyond this threshold, the RMSE gradually increases and reaches its maximum in regions above 90 dB and 100 dB. Specifically, the RMSE of the DGPIA model exceeds 0.7 dB, while that of the Attention U-Net exceeds 1.2 dB, and the standard U-Net reaches values above 2 dB. A similar trend is observed for MAE as shown in Fig.8(b). The lowest MAE values are obtained in regions above 50 dB, followed by a gradual increase as the EPNL threshold rises, with peak MAE values occurring in regions above 90 dB and 100 dB. These results indicate that, when prediction errors in low-noise boundary regions below 40 dB are excluded, the models generally achieve good predictive accuracy and generalization capability in the main noise-contour region. However, their performance in high-noise regions remains limited. Predictive accuracy improves progressively from the standard U-Net to the Attention U-Net and further to the DGPIA model. This improvement can be attributed to the synergistic effect of the SE attention and spatial attention mechanisms. Specifically, the SE attention mechanism enhances the model's sensitivity to the relative importance of multi-channel physical inputs, while the spatial attention mechanism improves its ability to capture high-noise regions and steep noise-gradient variations. Furthermore, the introduction of the Gaussian-diffused guide density map, constructed from velocity and altitude information, provides the model with physics-informed prior knowledge that is analogous to the mechanism of far-field sound pressure estimation. This further enhances the model's capability to predict the spatial distribution of the noise field.

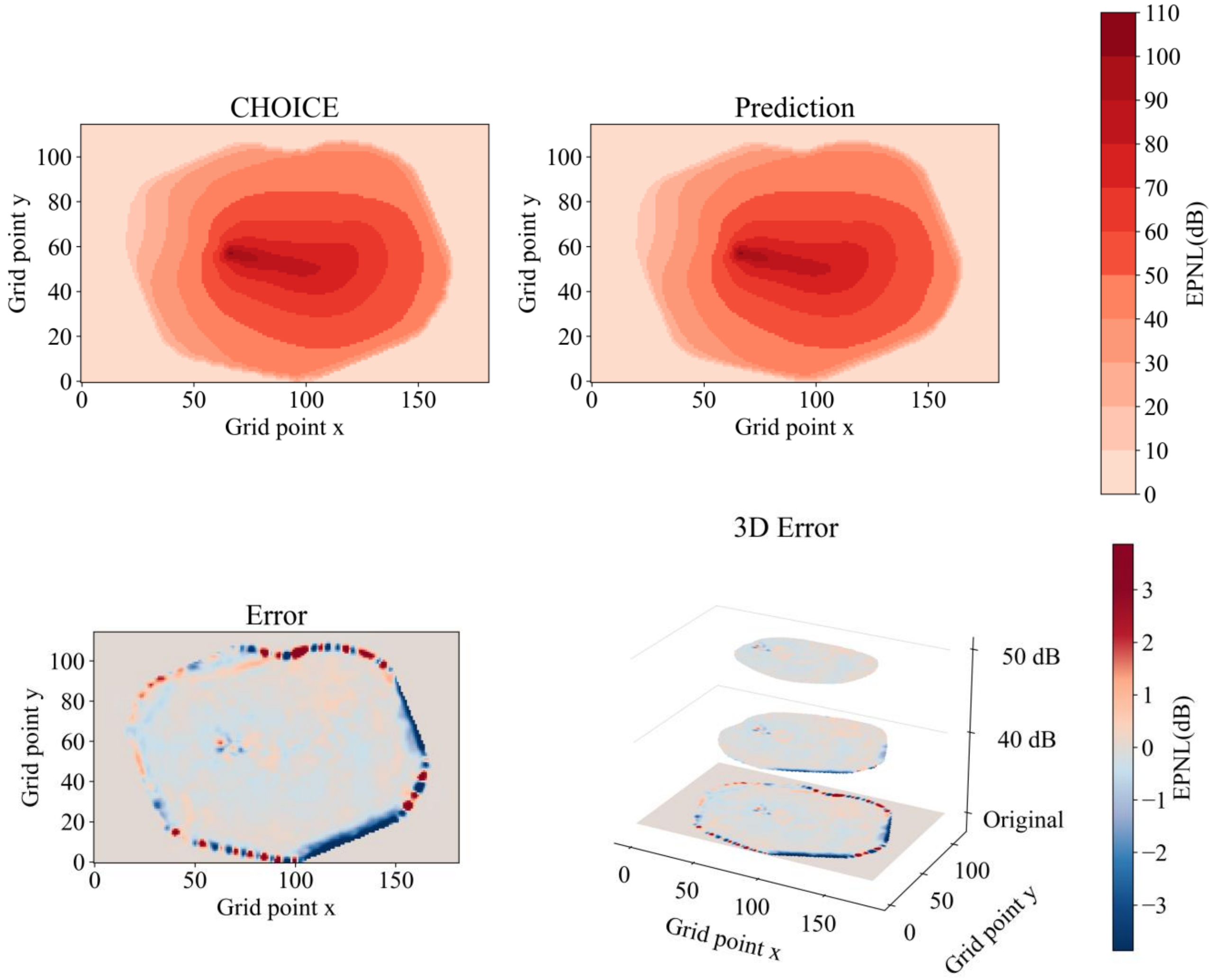

Fig. 6. The contour diagrams of the CHOICE, DGPIA model prediction, and errors result for takeoff procedure from EGCC Runway 05R ASMIM heading deviation -10° with NADP1 operation

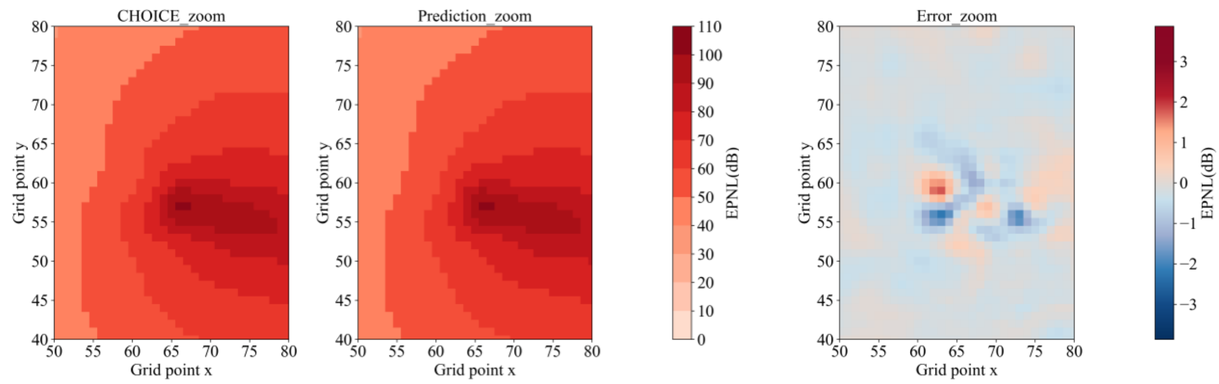

Fig. 7. Zoomed-in contour diagrams of the CHOICE and errors result for takeoff procedure from EGCC Runway 05R ASMIM heading deviation -10° with NADP1 operation

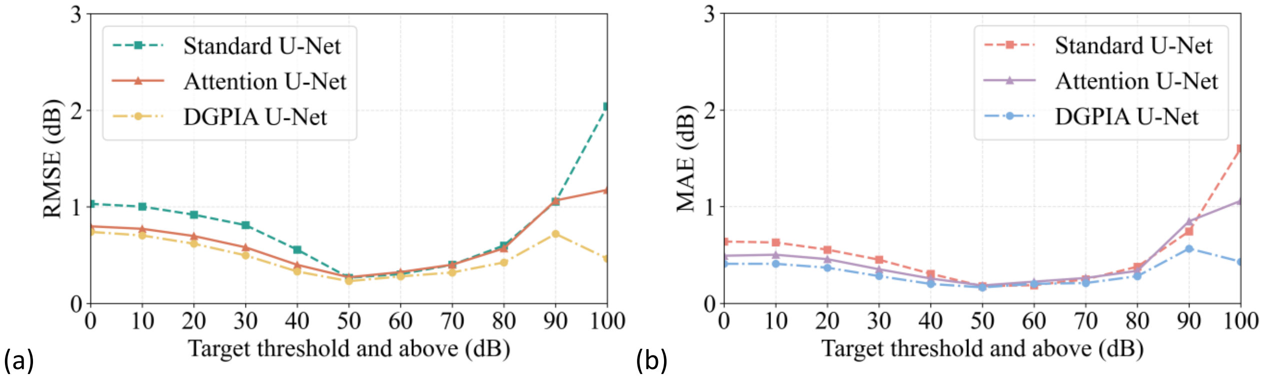

Fig. 8. The prediction accuracy of different models for takeoff procedure from EGCC Runway 05R ASMIM heading deviation -10° with NADP1 operation: (a) RMSE value (b) MAE value

Figures 9-10 evaluate the DGPIA model performance of noise field prediction capability for the aircraft takeoff from EGCC Runway 05R from DESIG1S heading deviation +18° with NADP2 operation. Similarly, relatively large prediction errors are observed near the low-noise peripheral regions, whereas the model achieves higher predictive accuracy in regions where the noise level exceeds 40 dB and 50 dB. In addition, a certain decrease in prediction accuracy can be observed in the high-noise region after aircraft take-off. Fig.11 compares the prediction accuracy of different models for the test case. As shown in Fig. 11(a), all three models achieve relatively low RMSE values in the threshold range of 40–60 dB, indicating good predictive performance in the main noise-contour region. However, the RMSE increases progressively at higher target thresholds, particularly above 80 dB, suggesting that prediction errors become more pronounced in high-noise regions. Figure 11(b) shows a similar trend for MAE. The MAE values remain low and relatively stable between 40 and 70 dB, whereas a clear increase is observed when the threshold exceeds 80 dB. Among the three models, DGPIA U-Net consistently achieves the lowest RMSE and MAE over most threshold ranges, especially in the high-noise region. In addition, the model maintains robust predictive performance across test cases with varying departure routes, heading deviations, and noise abatement operations. This indicates that the DGPIA U-Net model has strong generalization capability under diverse take-off operating conditions.

The following figure 12 presents a comprehensive study comparing the prediction accuracy of different models for all test cases. The results demonstrate a clear performance hierarchy: DGPIA U-Net achieves highest accuracy across all noise level areas. Compared with the conventional U-Net baseline, DGPIA U-Net demonstrates a significant improvement, reducing the RMSE by 37% for noise levels above 40 dB, from 0.58 dB to 0.36 dB, and by 23% for noise levels above 90 dB, from 1.14 dB to 0.87 dB. The RMSE results indicate that DGPIA U-Net effectively suppresses large errors, leading to global consistency in noise field prediction. In terms of MAE accuracy evaluation, compared with U-Net baseline, the DGPIA U-Net model achieves a 27% improvement in regions above 40 dB, from 0.30 dB to 0.21 dB and a 22% improvement in regions above 90 dB, from 0.81 dB to 0.63 dB. The MAE results show that DGPIA U-Net improves point- wise accuracy. By examining the overall trends of the three curves, it can be observed that the model performance improves progressively from the

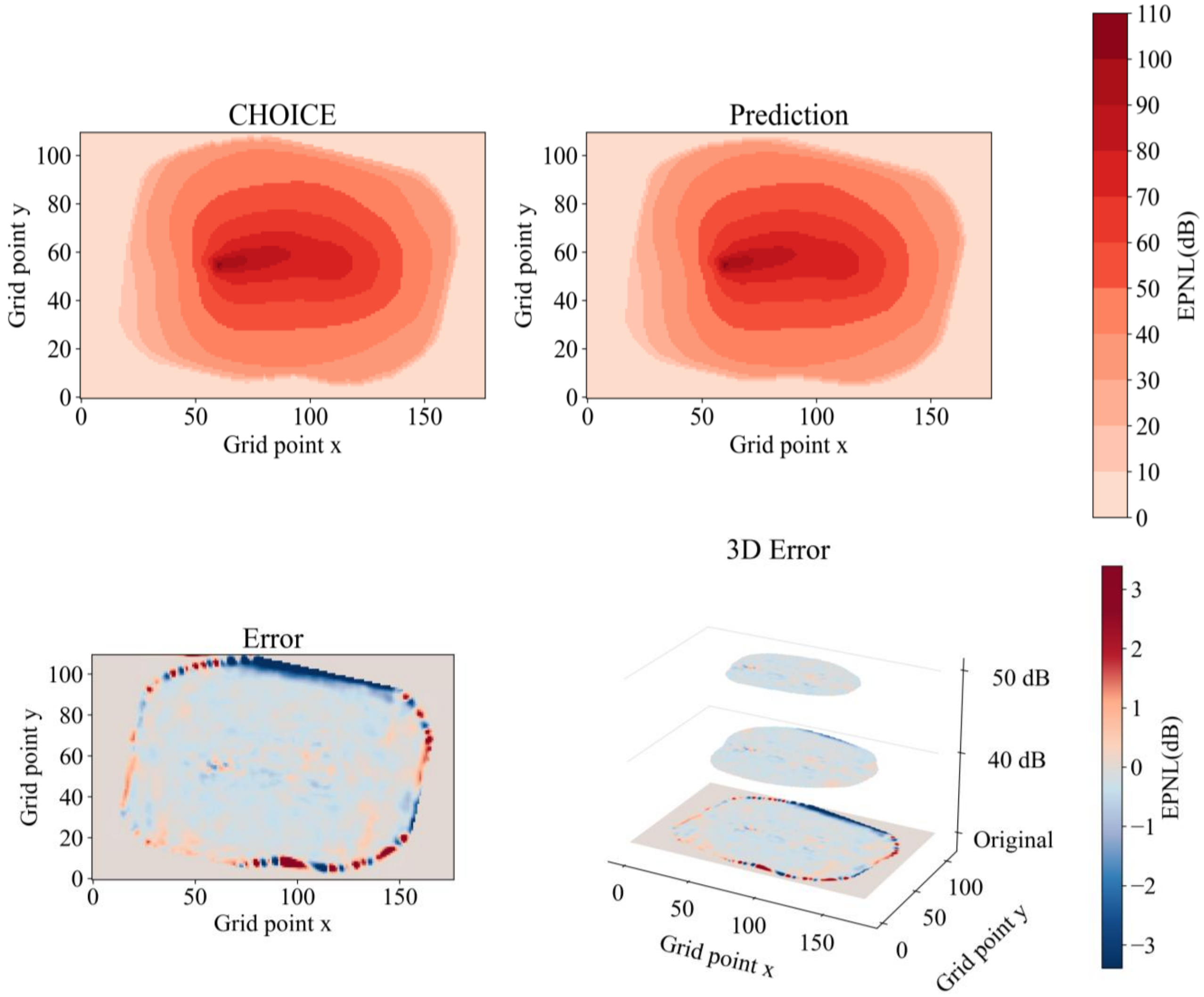

Fig. 9. The contour diagrams of the CHOICE, DGPIA model prediction, and errors result for takeoff procedure from EGCC Runway 05R DESIG1S heading deviation +18° with NADP2 operation

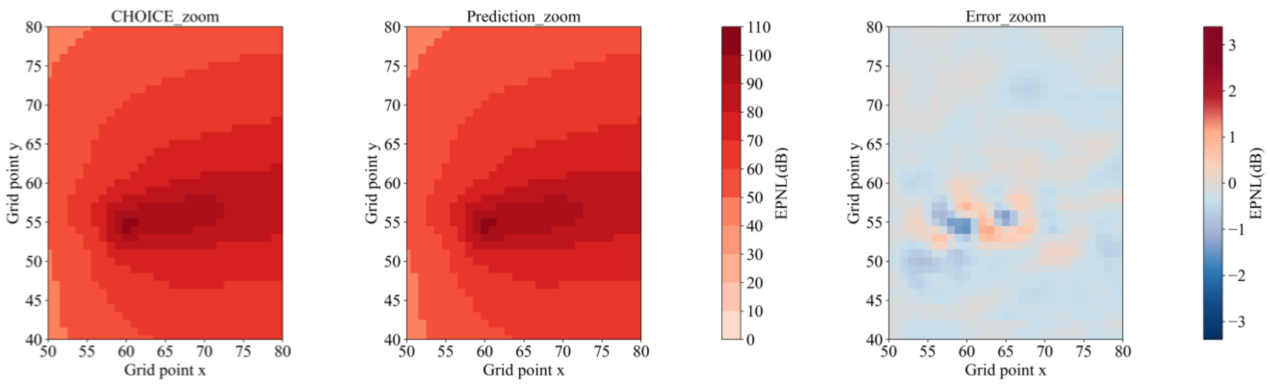

Fig. 10. Zoomed-in contour diagrams of the CHOICE and errors result for takeoff procedure from EGCC Runway 05R DESIG1S heading deviation +18° with NADP2 operation

standard U-Net to the Attention U-Net, and further to the DGPIA U-Net. This indicates that the attention mechanism and the density-map-guided mechanism proposed in this study can produce a cumulative effect, progressively enhancing the model's predictive accuracy and generalization capability. However, the model still shows certain limitations in predicting high-noise regions where the noise gradient changes rapidly after aircraft takeoff.

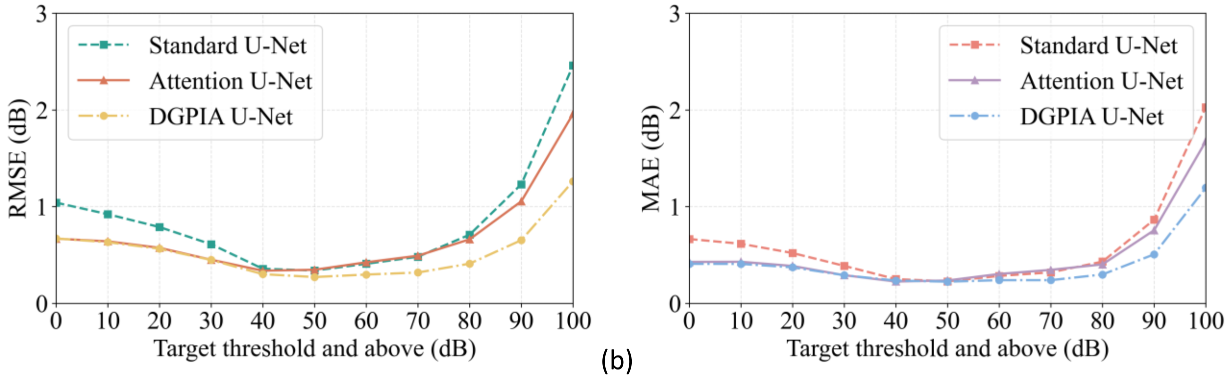

(a) (b)

Fig. 11. The prediction accuracy of different models for takeoff procedure from EGCC Runway 05R DESIG1S heading deviation +18° with NADP2 operation: (a) RMSE value (b) MAE value

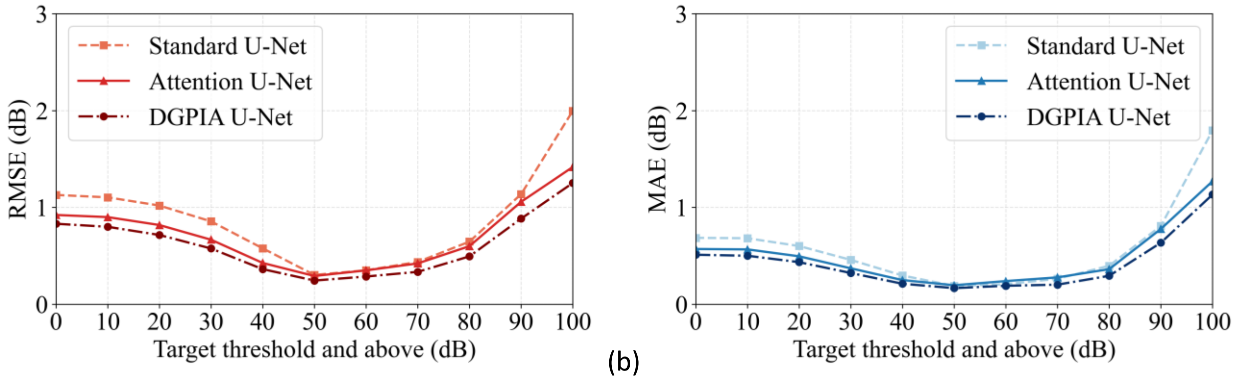

(a) (b)

Fig. 12. The prediction accuracy of different models for all test cases: (a) RMSE value (b) MAE value

4. Conclusions

Traditional best practice and theoretical approaches still exhibit significant limitations when applied to whole aircraft noise trajectory prediction. These limitations include the requirement for highly detailed aircraft and propulsion-system input data, as well as relatively high computational costs. Multidisciplinary integrated design frameworks for aircraft and air traffic systems, where hundreds of aircraft and airport-adjacent operational procedures may need to be evaluated, noise calculations can take several minutes. This computational burden becomes a critical bottleneck for real-time and large-scale air traffic applications. To address these problems, this study develops a Density-Guided Physics-Informed Attention U-Net (DGPIA U-Net) model that enables accurate aircraft noise trajectory prediction at the millisecond scale. Comprehensive validation of aircraft take-off procedure at EGCC airport runway 05R different operations demonstrate two key conclusions:

(1) The model maintains robust predictive performance across test cases with varying departure routes, heading deviations, and noise abatement operations indicates that the strong generalization capability under diverse take-off operating conditions. Compared with the standard U-Net model, the DGPIA U-Net model achieves higher predictive accuracy and stronger generalization capability in two-dimensional noise-field prediction. Specifically, the DGPIA U-Net consistently outperforms the baseline U-Net in terms of both RMSE and MAE at different take-off procedures. In the region above 40 dB, the RMSE and MAE are improved by 37% and 27%, respectively. The improvement in model performance mainly stems from two aspects. First, density-guided maps based on Gaussian kernel diffusion and physical information are introduced to provide the model with physics-informed prior knowledge that is analogous to the mechanism of far-field sound pressure estimation. Second, SE and spatial attention mechanisms are incorporated to enhance the model's ability to adaptively reweight multiple input variables and to capture spatial details, respectively.

(2) Compared with traditional best practice and theoretical approaches, the proposed model offers a millisecond-level computational advantage once training is completed. This enables real-time noise prediction for large-scale air traffic scenarios and provides useful insights into future air traffic noise optimization problems.

Nevertheless, the current framework presents limitations. First, in the high-noise region during the take-off phase, the model still shows limited capability in capturing sharp noise-gradient variations. Second, both the training and testing datasets used in this study are based on takeoff procedures, while landing-procedure noise is not considered. Third, the current model is limited to an A320-like aircraft, and its generalization capability across different aircraft types remains to be further validated. Future work will focus on incorporating stronger physics-informed constraints and improving the spatial attention mechanism to better capture local regions with sharp noise-gradient variations. In addition, the model will be extended to broader application scenarios, including both take-off and landing noise prediction for multiple aircraft types.

Acknowledgement
This work has received funding from the Horizon Europe research and innovation programme under GA n° 101096275. This work is co-funded by UK Research and Innovation (UKRI) under the UK government's Horizon Europe funding guarantee n° 10068673.

References

[1] S. Benz, J. Kuhlmann, S. Jeram, S. Bartels, B. Ohlenforst, D. Schreckenberg, Impact of Aircraft Noise on Health, in: L. Leylekian, A. Covrig, A. Maximova (Eds.), Aviat. Noise Impact Manag., Springer International Publishing, Cham, 2022: pp. 173–195. https://doi.org/10.1007/978-3-030-91194-2_7.

[2] C.S. Kim, S.T. Grady, J.E. Hart, F. Laden, T. VoPham, D.D. Nguyen, J.E. Manson, P. James, J.P. Forman, K.M. Rexrode, Long-term aircraft noise exposure and risk of hypertension in the Nurses' Health Studies, Environ. Res. 207 (2022) 112195.

[3] M.G. Smith, M. Cordoza, M. Basner, Environmental noise and effects on sleep: an update to the WHO systematic review and meta-analysis, Environ. Health Perspect. 130 (2022) 076001.

[4] O. Hahad, S. Rajagopalan, J. Lelieveld, M. Sørensen, M. Kuntic, A. Daiber, M. Basner, M. Nieuwenhuijsen, R.D. Brook, T. Münzel, Noise and Air Pollution as Risk Factors for Hypertension: Part

II—Pathophysiologic Insight, Hypertension 80 (2023) 1384–1392. https://doi.org/10.1161/HYPERTENSIONAHA.123.20617.
[5] S.J. Balk, R.E. Bochner, M.A. Ramdhanie, B.K. Reilly, Preventing excessive noise exposure in infants, children, and adolescents, Pediatrics 152 (2023) e2023063753.
[6] H.-G. Olbrich, M. Röösli, E. Herrmann, C. Maschke, K. Schadow, T. Hähnel, H.-J. Rupprecht, M. Kaltenbach, Aircraft noise exposure and risk for recurrent cardiovascular events after acute coronary syndrome: a prospective patient cohort study, Environ. Res. 238 (2023) 117108.
[7] J. Park, P.A. Muennig, Z. Zafari, Projecting the economic burden of health impacts of aircraft noise: a case study of Baltimore Washington International Thurgood Marshall Airport, J. Expo. Sci. Environ. Epidemiol. 35 (2025) 107–117.
[8] H. Yu, J.A. Mulder, Arrival Trajectory Optimization for Passenger Aircraft using Genetic Algorithms, in: 11th AIAA Aviat. Technol. Integr. Oper. ATIO Conf., American Institute of Aeronautics and Astronautics, Virginia Beach, VA, 2011. https://doi.org/10.2514/6.2011-6804.
[9] S. Alam, M.H. Nguyen, H.A. Abbass, C. Lokan, M. Ellejmi, S. Kirby, A dynamic continuous descent approach methodology for low noise and emission, in: 29th Digit. Avion. Syst. Conf., IEEE, 2010: pp. 1-E. https://ieeexplore.ieee.org/abstract/document/5655502/ (accessed May 27, 2026).
[10] S.J. Hebly, H.G. Visser, Advanced noise abatement departure procedures: custom-optimised departure profiles, Aeronaut. J. 119 (2015) 647–661.
[11] A. Filippone, Aircraft noise prediction, Prog. Aerosp. Sci. 68 (2014) 27–63. https://doi.org/10.1016/j.paerosci.2014.02.001.
[12] E.R. Boeker, E. Dinges, B. He, G. Fleming, C.J. Roof, P.J. Gerbi, A.S. Rapoza, J. Hermann, Integrated noise model (INM) version 7.0 technical manual, (2008). https://rosap.ntl.bts.gov/view/dot/12188 (accessed May 27, 2026).
[13] J.B. Ollerhead, D.P. Rhodes, M.S. Viinikainen, D.J. Monkman, A.C. Woodley, The UK civil aircraft noise contour model ANCON: Improvements in Version 2, ERCD RD Rep. 9842 (1999).
[14] S. Pietrzko, R. Bütikofer, FLULA-Swiss aircraft noise prediction program, in: Proc. Innov. Acoust. Vib. Annu. Conf. Aust. Acoust. Soc. Adel. Aust., 2002: pp. 13–15. https://www.acoustics.asn.au/conference_proceedings/AAS2002/AAS2002/PDF/AUTHOR/AC020035.PDF (accessed May 27, 2026).
[15] A.N. der AzB, Anleitung zur Berechnung von Lärmschutzbereichen (AzB), (2007).
[16] L. Bertsch, U. Isermann, Noise prediction toolbox used by the DLR aircraft noise working group, in: INTER-NOISE NOISE-CON Congr. Conf. Proc., Institute of Noise Control Engineering, 2013: pp. 805–813. https://ince.publisher.ingentaconnect.com/contentone/ince/incecp/2013/00000247/00000008/art00093?crawler=true&mimetype=application/pdf (accessed May 27, 2026).
[17] J. Raney, Development of a new computer system for aircraft noise prediction, in: 2nd Aeroacoustics Conf., American Institute of Aeronautics and Astronautics, Hampton,VA,U.S.A., 1975. https://doi.org/10.2514/6.1975-536.
[18] R.E. Gillian, Aircraft noise prediction program user's manual, 1982. https://ntrs.nasa.gov/citations/19830007879 (accessed May 27, 2026).
[19] L.V. Lopes, C.L. Burley, ANOPP2 user's manual: version 1.2, 2016. https://ntrs.nasa.gov/citations/20160014858 (accessed May 27, 2026).
[20] L. Lopes, C. Burley, Design of the Next Generation Aircraft Noise Prediction Program: ANOPP2, in: 17th AIAACEAS Aeroacoustics Conf. 32nd AIAA Aeroacoustics Conf., American Institute of Aeronautics and Astronautics, Portland, Oregon, 2011. https://doi.org/10.2514/6.2011-2854.
[21] A. Filippone, Flight Performance Software FLIGHT, Manch. UK Sch. Mech. Aerosp. Civ. Eng. Univ. Manch. (2015). https://www.academia.edu/download/37489855/flight_manual.pdf (accessed May 27, 2026).
[22] A. Filippone, Development of a New Aircraft Noise Prediction Program, in: 16th AIAA Aviat. Technol. Integr. Oper. Conf., American Institute of Aeronautics and Astronautics, Washington, D.C., 2016. https://doi.org/10.2514/6.2016-3902.

[23] E. Maria Thoma, T. Grönstedt, E. Otero Sola, X. Zhao, Assessment of an Open-Source Aircraft Noise Prediction Model Using Approach Phase Measurements, J. Aircr. 61 (2024) 745–760. https://doi.org/10.2514/1.C037332.

[24] L. Bertsch, Noise prediction within conceptual aircraft design, PhD Thesis, Technische Universität Braunschweig, 2013. https://elib.dlr.de/84386/ (accessed May 27, 2026).

[25] A.S. Tenney, M.N. Glauser, J. Lewalle, A Deep Learning Approach to Jet Noise Prediction, in: 2018 AIAA Aerosp. Sci. Meet., American Institute of Aeronautics and Astronautics, Kissimmee, Florida, 2018. https://doi.org/10.2514/6.2018-1736.

[26] Y. Zhang, B. Chen, K. Zhao, X. Tang, X. Yang, G. Hu, Intelligent prediction of acoustic performance of landing gear using deep learning, Phys. Fluids 35 (2023). https://pubs.aip.org/aip/pof/article/35/7/076112/2902078 (accessed May 27, 2026).

[27] Q. Zhang, W. Zhang, A hybrid approach for reconstruction of transonic buffet aerodynamic noise: Integrating random forest and compressive sensing algorithm, Aerosp. Sci. Technol. 152 (2024) 109379. https://doi.org/10.1016/j.ast.2024.109379.

[28] Q. Zhang, X. Wang, D. Yang, W. Zhang, Data-driven prediction of aerodynamic noise of transonic buffeting over an airfoil, Eng. Anal. Bound. Elem. 163 (2024) 549–561. https://doi.org/10.1016/j.enganabound.2024.04.006.

[29] C. Wu, S. Redonnet, A simple yet efficient data-driven model for the prediction of aircraft noise impact, Aerosp. Sci. Technol. 163 (2025) 110286. https://doi.org/10.1016/j.ast.2025.110286.

[30] S. Toraman, O.O. Dursun, H. Aygun, Prediction of noise of commercial aircraft based on itself specifications by using machine learning methods, J. Air Transp. Manag. 125 (2025) 102779.

[31] M.R. Fink, Noise Component Method for Airframe Noise, J. Aircr. 16 (1979) 659–665. https://doi.org/10.2514/3.58586.

[32] Y. Guo, C.L. Burley, R.H. Thomas, Landing Gear Noise Prediction and Analysis for Tube-And-Wing and Hybrid-Wing-Body Aircraft, in: 54th AIAA Aerosp. Sci. Meet., American Institute of Aeronautics and Astronautics, San Diego, California, USA, 2016. https://doi.org/10.2514/6.2016-1273.

[33] M.F. Heidmann, Interim prediction method for fan and compressor source noise, 1975. https://ntrs.nasa.gov/citations/19750017876 (accessed May 27, 2026).

[34] J.W. Russell, An empirical method for predicting the mixing noise levels of subsonic circular and coaxial jets, NASA, 1984. https://ntrs.nasa.gov/citations/19840010980 (accessed May 27, 2026).

[35] O. Ronneberger, P. Fischer, T. Brox, U-Net: Convolutional Networks for Biomedical Image Segmentation, in: N. Navab, J. Hornegger, W.M. Wells, A.F. Frangi (Eds.), Med. Image Comput. Comput.-Assist. Interv. – MICCAI 2015, Springer International Publishing, Cham, 2015: pp. 234–241. https://doi.org/10.1007/978-3-319-24574-4_28.

[36] J. Hu, L. Shen, G. Sun, Squeeze-and-Excitation Networks, (n.d.).

[37] J. Park, S. Woo, J.-Y. Lee, I.S. Kweon, BAM: Bottleneck Attention Module, (2018). https://doi.org/10.48550/arXiv.1807.06514.

[38] Z. Zhang, Improved adam optimizer for deep neural networks, in: 2018 IEEEACM 26th Int. Symp. Qual. Serv. IWQoS, Ieee, 2018: pp. 1–2. https://ieeexplore.ieee.org/abstract/document/8624183/ (accessed May 27, 2026).

[39] K. Viswanathan, Progress in prediction of jet noise and quantification of aircraft/engine noise components, Int. J. Aeroacoustics 17 (2018) 339–379. https://doi.org/10.1177/1475472X18778279.

[40] Y. Özyörük, B.J. Tester, Application of frequency-domain linearized Euler solutions to the prediction of aft fan tones and comparison with experimental measurements on model scale turbofan exhaust nozzles, J. Sound Vib. 330 (2011) 3846–3858.